醫學博士 學位論文

Effect of metabolic substrates on intracellular Ca^{2+} homeostasis and contractility in cardiac myocytes of healthy and hypertensive rats

대사 물질에 의한 정상과 고혈압 백서 심장 세포의 칼슘 및 수축성 조절에 대한 연구

2017年 06月

서울大學校 大學院

醫科學科 醫科學專攻

赵 载 豪

대사 물질에 의한 정상과 고혈압 백서 심장 세포의 칼슘 및 수축성 조절에 대한 연구

Effect of metabolic substrates on intracellular Ca^{2+} homeostasis and contractility in cardiac myocytes of healthy and hypertensive rats

지도교수 장 은 화

이 논문을 의학박사 학위논문으로 제출함
2017년 06월

서울대학교 대학원
의과학과 의과학전공
赵 载 豪

赵载豪의 의학박사 학위논문을 인준함
2017년 06월

위 원 장 김성준 (인)

부위원장 장은화 (인)

위 원 오세일 (인)

위 원 조주연 (인)

위 원 염재범 (인)

Effect of metabolic substrates on intracellular Ca^{2+} homeostasis and contractility in cardiac myocytes of healthy and hypertensive rats

by
Zai Hao Zhao M.D.

A thesis submitted to the Department of Biomedical Sciences in partial fulfillment of the requirements for the Degree of Doctor of Philosophy in Biomedical Sciences at Seoul National University College of Medicine

June, 2017

Approved by Thesis Committee:

Professor _____Chairman

Professor _____Vice chairman

Professor _____

Professor _____

Professor _____

Abstract

Metabolism is an important precondition of contractile function in cardiac myocyte. Until recently, glucose has been used as the source for myocyte ATP in majority of physiological experiments. In fact, fatty acids are the predominant metabolic substrates in healthy heart and such metabolism is altered in the myocardium under pathological stress. Accordingly, I aimed to test the effects of metabolic substrates' supplementation (including glucose, fatty acids and other metabolic substrates, termed NF) on intracellular Ca^{2+} handling, myofilament Ca^{2+} sensitivity and contraction in left ventricular (LV) myocytes from normal and angiotensin II (Ang II)-induced hypertensive rats (HTN).

My results showed that NF significantly increased myocyte contraction and facilitated relaxation from normal heart. Similar to NF, supplementation of 3 fatty acids (linoleic acid, oleic acid and palmitic acid) also increased sarcomere shortening. However, inhibition of beta-oxidation process with carnitine palmitotransferase-1 (CPT-1) inhibitor, ranolazine, did not affect myocyte contraction increment in NF, indicating that glucose and fatty acid-dependent metabolism complement with each other in supporting cardiac contraction. In addition, NF increased the amplitudes of diastolic and systolic Ca^{2+} transients ($[Ca^{2+}]_i$), abbreviated time constant of $[Ca^{2+}]_i$ decay (tau), but prolonged the peak duration of $[Ca^{2+}]_i$. Ca^{2+} content in the sarcoplasmic reticulum (SR) was increased by NF. Whole-cell patch-clamp experiments revealed that NF increased Ca^{2+} influx via L-type Ca^{2+} channels (LTCC, I_{Ca}-integral) and prolonged the action potential duration (APD). Furthermore, NF induced myofilament Ca^{2+} desensitization, which is responsible for NF-induced changes in $[Ca^{2+}]_i$ handling. NF reduced intracellular pH ($[pH]_i$). Buffering $[pH]_i$ with HCO_3^-/CO_2 attenuated Δ $[pH]_i$ and reversed myofilament Ca^{2+} desensitization and Ca^{2+} transient in NF in normal heart. Collectively, NF stimulates myocyte contraction by increasing Ca^{2+} influx through LTCCs and Ca^{2+} release from

the SR. Myofilament Ca^{2+} desensitization (via reducing $[pH]_i$) contributes, at least in part, to NF-induced greater $[Ca^{2+}]_i$. In LV myocytes from HTN rats, where myofilament Ca^{2+} sensitivity was reduced and $[Ca^{2+}]_i$ was greater, NF increased myocyte contraction and $[Ca^{2+}]_i$ handling, reduced myofilament Ca^{2+} sensitivity further, despite that Ca^{2+} influx via LTCC was reduced.

β-adrenergic stimulation with isoprenaline (ISO) significantly increased myocyte contraction in NF in both groups. In addition, ISO induced delayed-aftercontraction (DAC) and spontaneous Ca^{2+} transients (sCa) in NF and the frequency of DAC was ~3 fold higher in HTN. Biochemical experiments indicated that tyrosine phosphorylation of insulin receptor (IR), IR substrate-1 and endothelial NOS (eNOS) phosphorylation (eNOS-Ser^{1177}) were blunted by NF in normal heart. In HTN, the insulin and eNOS-dependent signaling was reduced before NF application. Accordingly, insulin did not affect NF-enhancement of sarcomere shortening in basal or with ISO in both groups. Furthermore, NOS inhibition with L-NAME (1mM, 30 min ~ 1hr) failed to affect myocyte responses to NF in either group. These results suggest that insulin and eNOS-dependent signaling were impaired in LV myocyte with metabolic substrates' supplementation.

Notably, NOS inhibition with L-NAME increased DAC and sCa by ISO in normal heart but reduced these parameters in HTN. Such effects were mimicked by nNOS inhibitor, SMTC, suggesting the role of nNOS. β-1AR blockers nebivolol and cordycepin, two NO-potentiating chemicals, significantly decreased diastolic and peak amplitudes of Ca^{2+} transients with NF+ISO in both groups and abolished ISO-induced SCs in NF. KB-R7943, a Na^{+}-Ca^{2+} exchanger inhibitor, abolished DAC in LV myocytes from sham and HTN.

Taken together, supplementation of myocardial favourable metabolic substrates affects Ca^{2+}

handling and excitation-contraction coupling. Notably, myofilament Ca^{2+}desensitization contributes to the regulation of intracellular $[Ca^{2+}]_i$ homeostasis, an unrecognized regulation of myocyte $[Ca^{2+}]_i$ and contraction. Impaired insulin/NO signaling is involved in arrhthmogenesis in NF under beta-adrenergic stimulation. In particular, nNOS exerts contrasting effects on DAC with NF in normal and HTN rat hearts.

Some of the results are published in *J Vis Exp* and *Pflugers Arch* (Zhao ZH et al., 2016; Zhao ZH et al., 2016). **Student number: 2014-30872**

Keywords: Metabolic substrate, insulin, eNOS, nNOS, nitric oxides, contraction, intracellular Ca^{2+} transient, myofilament Ca^{2+} sensitivity, hypertension, arrhythmias

Contents

List of tables and figures

Part III: Metabolic substrate is affecting the LV myocyte contraction and $[Ca^{2+}]_i$ by regulating myofilament Ca^{2+} sensitivity in Ang II-induced hypertensive rat heart.

Part IV: Metabolic substrate' regulation of cardiac contraction and the roles of eNOS and nNOS in LV myocytes from sham and hypertensive rat heart.

List of abbreviations

ATP = adenosine-5'-triphosphate

CPT-1 = carnitine palmitoyltransferase 1

eNOS = endothelial nitric oxide synthase

FA=fatty acid

FS = fractional shortening

HF = heart failure

HP = hypertension

LV = left ventricular

NCX= sodium/calcium exchanger

nNOS = neuronal nitric oxide synthase

NO = nitric oxide

NOS = nitric oxide synthase

RyR = ryanodine receptor

SERCA = Ca^{2+} ATPase in sarcoplasmic reticulum

SR= sarcoplasmic reticulum

$[Ca^{2+}]_i$ = intracellular calcium concentration

4-AP = 4 – aminopyridine

AP = action potential

NCX = sodium-calcium exchanger

NT = normal Tyrode solution

NF = NT solution containing fatty acids

DAC = delay after contraction

Chemicals of abbreviations

Ang II =angiotensin II

BDM = 2,3-butanedione monoxime

L-NAME = Nω-nitro-L-arginine methyl ester hydrochloride

PA = palmitic acid

OA = oleic acid

LA = linoleic acid

SMTC = S-methyl-L-thiocitrulline acetate salt

Rano = Ranolazine

KB-R7943 = 2-[2-[4-(4-Nitrobenzyloxy)phenyl]ethyl]isothiourea mesylate

ISO = isoprenaline

CODY = cordycepin

Introduction

The heart is an omnivorous organ that relies on both FAs and carbohydrates to produce myocardial ATP. Constant supply of ATP through cardiac metabolism is essential to maintain the normal functions of the heart (Lopaschuk GD et al, 2010; Shipp JC et al, 1961). In healthy heart, FA-dependent beta-oxidation accounts for 70–90 % of myocardial ATP and the remaining amount is produced through carbohydrate metabolism (such as glucose oxidation and glycolysis) (Lopaschuk GD et al, 2010). However, during disease progression (hypertrophy and early stage heart failure), glucose oxidation and glycolysis become the predominant sources of cellular ATP, indicating a metabolic shift from FAs to glucose utilization (Lopaschuk GD et al, 2010). At the end stage of heart failure, both glucose metabolism and beta-oxidation are dysregulated, resulting in energy deficiency and impaired myocardial contraction (Lopaschuk GD et al, 2010). Until recently, glucose has been used as the sole metabolic substrate in most of cardiac physiological studies (despite the importance of FAs in cardiac metabolism). Accordingly, I aim to evaluate the impact of metabolic substrates' supplementation on the mechanisms mediating cardiac contractility in normal rat hearts and in those under stress.

Cardiac excitation-contraction (E-C) coupling is the fundamental scheme for analyzing mechanical properties of the myocardium, *i.e.*, the contractile function of the heart (Bers, D.M., et al, 2002; Eisner, D.A., et al, 2000). E-C coupling is initiated by membrane depolarization secondary to the activity of sarcolemmal ion channels (*e.g.*, the voltage-gated Na^+ channel, which can be measured via patch-clamp techniques). Subsequent activation of LTCCs and Ca^{2+} influx via LTCCs trigger the bulk of Ca^{2+} release through RyRs, increasing the cytosolic Ca^{2+} concertation from the nanomolar (nM) to micromolar (μM) level. Such an increase in cytosolic Ca^{2+} promotes Ca^{2+} binding to troponin C (TnC) in thin filaments and elicits conformational changes of the filament complex to facilitate the actin-myosine interaction and attains myocardial

contraction (Palmiter, K.A., et al, 1997). Conversely, the cytosolic Ca^{2+} is re-uptake back into the SR through SERCA2a or is extruded out of the myocyte via the Na^{+}/Ca^{2+} exchanger, resulting in the dissociation of actin-myosin and myocyte relaxation (Bers, D.M., et al, 2002; Eisner, D.A., et al, 2000; Palmiter, K.A., et al, 1997). In this scheme, the activity of SERCA2a is generally considered to determine the speed of myocardial relaxation because it accounts for 70-90 % of cytosolic Ca^{2+} removal in most mammalian heart cells (Bers, D.M., et al, 2002). As such, abnormal Ca^{2+} handling by LTCC, RyR and SERCA2a, etc. has been considered the primary mechanisms for impaired contractility and relaxation in diseased heart (Bers, D.M., et al, 2002; Eisner, D.A., et al, 2000; Palmiter, K.A., et al, 1997; Missiaen, L., et al, 2000).

In reality, free cytosolic Ca^{2+} that functions as the messenger in E-C coupling accounts for around 1% of total intracellular Ca^{2+} and the majority of Ca^{2+} is bound to intracellular Ca^{2+} buffers (Trafford, A.W., et al, 1999; Berlin, J.R., et al, 1994). This is due to the fact that various Ca^{2+} buffers are abundant in cardiac myocytes, e.g., membrane phospholipids, ATP, phosphocreatine, calmodulin, parvalbumin, myofibril TnC, myosin, SERCA2a, and calsequestrin in the SR (Trafford, A.W., et al, 1999; Berlin, J.R., et al, 1994; Robertson, S.P., et al, 1981). Among them, SERCA2a and TnC are the predominant Ca^{2+} buffers (Trafford, A.W., et al, 1999; Berlin, J.R., et al, 1994; Robertson, S.P., et al, 1981). Furthermore, Ca^{2+} binding to its buffers is dynamic processes during twitch (e.g., 30-50% of Ca^{2+} binds to TnC and dissociate from it during Ca^{2+} transients) (Robertson, S.P., et al, 1981) and the changes in Ca^{2+} binding cause additional “release” of free Ca^{2+} to cytosol, results in alterations of the intracellular Ca^{2+} concentration. Consequently, perturbation of intracellular Ca^{2+} level induces abnormal myofilament movements, which are the precursors of contractile dysfunction and arrhythmias (Schobert, T., et al, 2012; Briton, S.J., et al, 2014). Many factors (both physiological and pathological) can be the sources of post-transcriptional modifications of

myofilament proteins, which influence myofilament Ca^{2+} buffering and myofilament Ca^{2+} sensitivity (Schober, T., et al, 2012; Briston, S.J., et al, 2014; Patel, B.G, et al, 2013). Recently, it was reported that mutations in myofilament proteins increase the Ca^{2+} binding affinity and intracellular Ca^{2+} handling, triggering pause-dependent potentiation of Ca^{2+} transients, abnormal Ca^{2+} release, and arrhythmias (Schober, T., et al, 2012). In line with this concept, we have also shown that myofilament Ca^{2+} desensitization in hypertensive rat hearts is involved in increasing diastolic and systolic intracellular Ca^{2+} level (Jin CZ et al., 2013), which may have the vulnerability of the LTCC to Ca^{2+}-dependent inactivation (Wang, Y., et al, 2015). Hence, myofilament Ca^{2+}sensitivity is an "active" regulator of intracellular Ca^{2+} homeostasis and myocyte contractile function.

Therefore, in **Part I**, I describe a protocol that assesses the changes of myofilament Ca^{2+} sensitivity in isolated cardiac myocytes. Comprehensive analysis of intracellular Ca^{2+} profile, myofilament Ca^{2+} sensitivity and contraction will unearth novel mechanisms underlying myocardial mechanics.

Free fatty acids (FFAs) and glucose are the primary substrates of myocardial energy metabolism but the substrate preferences in the healthy myocardium are flexible depending on circulating metabolites. Under normal conditions, a minimum of 60% of the ATP is derived from oxidation of free FAs and with only about 30% of its energy coming from glycolysis and GTP formation in the tricarboxylic acid (TCA) cycle through glucose oxidation (Gary D et al., 2010). Uptake of FFAs is primarily determined by the circulating FFA concentrations, which can vary significantly depending on whether the individual is fed or fasted, under metabolic or ischemic stress or suffers from diabetes. Free FAs can be taken up by passive diffusion across the myocardial cell membrane or by transport proteins (e.g. CD36). Once inside the cardiomyocyte, free FAs enter the mitochondria by CTP-1 and undergo beta-oxidation. The

products, acetyl-CoA, $FADH_2$ and NADH enter the Krebs cycle and produce large amount of ATP. Even though the principal energy sources of the heart are lipids, maintenance of glucose metabolism is important for cardiac structure and function (Gray S et al., 2011). Glucose mainly enters myocardial cells via the glucose transporters, GLUT1 and GLUT4 which approximately account for 40% and 60% of cardiac glucose transporters. Despite its limited contribution to energy production, glycolysis remains an important mechanism in transmembrane ions transfer. Two major ion pumps, the sodium pump (Na^+/K^+-ATPase) and the SERCA, both utilize glycolytic ATP to maintain cellular integrity, especially under O_2 deficient conditions (Opie LH. et al., 2002). In over-nutrient conditions, such as insulin resistance and diabetes, the rate of glucose uptake is reduced while that of circulating free FAs is increased: leading the heart to utilize even more FAs for its energy needs (Dirkx E et al., 2011; Steinbusch LK et al., 2011). Recent research suggests that obesity causes cardiac insulin resistance primarily by inhibiting cardiac glucose oxidation whereas glucose uptake and glycolysis is unaltered (Zhang L et al., 2011; Ussher JR et al., 2009). Patients with type 2 diabetes have elevated circulating FAs and derive most of their myocardial energy demands from increased beta-oxidation of FAs. By contrast, glucose oxidation is reduced even in the presence of hyperglycemia (Boudina S et al., 2007). This inability of the diabetic heart to oxidize glucose is associated with increased myocardial oxygen consumption, since oxidation of glucose results in greater ATP production per mole of oxygen consumed than oxidation of FAs. It is also associated with decreased left ventricular mechanical efficiency. The earliest changes observed in the hearts of obese rodents are reduced content and translocation of the insulin dependent GLUT4 in the myocardial sarcolemma. This results in reduced rates of glucose uptake and subsequently in reduced glycolysis and glucose oxidation. By contrast, FA uptake facilitated by CD36 translocated to the membrane is increased leading to increased fatty acid oxidation (Coort SLM et al., 2004). The proposed mechanisms of myocardial insulin resistance include dyslipidemias and

lipotoxity, mitochondrial dysfunction, inflammation and endoplasmic reticulum stress (Gray S et al., 2011). Despite increased FFA oxidation, FFA uptake frequently excesses the mitochondrial oxidative capacity and any excess FAs taken up results in intracellular accumulation of lipid derived metabolites. Accumulation of lipids and lipid intermediates in the heart has been demonstrated to be associated with systolic and diastolic dysfunction (Boudina S et al., 2007). Generation of FA-associated reactive oxygen species leads to uncoupling of mitochondria, which reduces mitochondrial ATP production. This mitochondrial uncoupling contributes to increased oxygen consumption and demand without a concomitant increase in ATP production, which results in decreased cardiac efficiency (Boudina S. et al., 2009; Laskowski KR. Et al., 2008).

Therefore, in **Part II, III**, I investigated the effects of metabolic substrate supplementation (fatty acids: palmitic acid, linoleic acid, and oleic acid; glucose; pyruvate; and lactate, termed NT solution with fatty acids, NF) on myocyte contraction, relaxation, intracellular Ca^{2+} handling, and myofilament Ca^{2+} sensitivity in LV myocytes from normal and HTN rats.

Over-nutrition or metabolic syndrome has also been associated with a variety of cardiovascular diseases including type 2 diabetes, hypertension, cardiac arrhythmias (sudden cardiac death), stroke and heart failure (Whaley-Connell A et al, 2011). For example, intravenous injection of long-chain saturated fatty acids into anaesthetized healthy dogs *in vivo* induced ventricular arrhythmias (Soloff LA et al, 1970). In contrast, inhibition of lipolysis from adipose tissue by a nicotinic acid analogue reduced the incidence of ventricular arrhythmias (Rowe MJ et al, 1975). Furthermore, supplementation of FAs to isolated rat hearts *in vitro* reduced LV contractility and slowed heart rate (Opie LH et al, 1970). So far, oxidative stress, systematic inflammation or FA-induced lipotoxicity are suggested to link the adverse myocardial function and cardiovascular

remodeling (Vigouroux C et al, 2011; Boden G et al, 2013). The mechanistic insights, however, remain unclear.

Insulin is essential in the uptake of metabolic substrates and cardiac metabolism and insulin resistance is a malignant condition that predisposes endothelial and muscle dysfunction, inflammation and oxidative stress (Whaley-Connell A et al, 2011; Boden G et al, 2013; Pulakat L et al, 2011; Yu Q et al, 2011). In normal myocardium, stimulation of insulin receptors (tyrosine kinase phosphorylation of insulin receptor β-subunit, IR, or insulin receptor substrate-1, IRS-1) activates phosphatidylinositol 3-kinase (PI3K)-Akt-eNOS or MAPK pathways (Montagnani M et al, 2002; Turner N et al, 2014; Johnson AM et al, 2013). Therefore, eNOS plays an important role as a transfer medium in cardiomyocyte metabolism.

In the heart, three NOS isoforms are present: neuronal NOS (nNOS, NOS1), endothelial NOS (eNOS, NOS3), and inducible NOS (iNOS, NOS2). Under normal circumstances, NO exerts several functions in the myocardium, such as acceleration of relaxation (Paulus WJ et al., 2004; Seddon M et al., 2007). This effect is attributed to cGMP-dependent, protein kinase G (PKG)-mediated phosphorylation of troponin I, leading to a reduction in myofilament Ca^{2+} sensitivity (Paulus WJ et al., 1995; Shah AH et al., 1994; Layland J et al., 2002). Myocardial eNOS is mostly localized at the sarcolemmal and T-tubular caveolae, sites where caveolin-3 is also localized and where several signal transduction pathways have been shown to be modulated by NO (Shaul PW et al., 2002). Sarcolemma-bound eNOS inhibited the L-type Ca^{2+} channel and attenuated the β-adrenergic receptor-stimulated increase in myocardial contractility (Yurok R et al., 2000; Shaula PW et al., 2002). A higher rate of ouabain-induced ventricular arrhythmias was found in ventricular myocytes isolated from mice lacking a functional eNOS gene (Kubota et al., 2000). Application of a NO donor, *S*-nitrosoacetylcysteine, diminished the drug-induced arrhythmias in these preparations (Kubota et al., 2000). Furthermore, in isolated guinea pig

heart, pre-treatment with sodium nitroprusside and l-arginine reduced the incidence of digoxin-induced ventricular arrhythmia (Altug S et al., 1999). Sodium nitroprusside, but not l-arginine, was also found to suppress digoxin-induced ventricular arrhythmias in intact guinea pig heart (Altug S et al., 1999). Recently, we have reported that eNOS protein expression is down-regulated in hypertensive myocardium.

Different from eNOS, myocardial nNOS is normally localized at the SR membrane, where it influences the activity of calcium-handling (Xu KY et al., 1999; Sears CE et al., 2003). Myocardial nNOS stimulates SR Ca^{2+} release and reuptake, facilitates Ca^{2+}-induced Ca^{2+} release, and potentiates cardiac force-frequency responses (Khan et al., 2003; Danson EJ et al., 2005), probably by S-nitrosylation of calcium-handling proteins. eNOS has been found to be uncoupled in the myocardium of a mice model of transverse aortic constriction (TAC)-induced pressure overload and eNOS produces superoxide rather than NO (Taklmoto E et al., 2005; Kuzkaya N et al., 2003; Xia Y et al., 1996), and becomes responsible for cardiac oxidative stress, left ventricular (LV) hypertrophy and dysfunction (Taklmoto E et al., 2005; Kuzkaya N et al., 2003; Xia Y et al., 1996). In addition, eNOS is known to be an "endogenous beta-blocker" by restoring the sympatho-vagal balance, promoting vasodilatation and neoangiogenesis (Masslon et al., 2007) and protects the heart under pathological stress. In contrast, nNOS protein expression and activity are up-regulated in diseased heart, including hypertension, which is responsible for greater diastolic and systolic Ca^{2+} levels secondary to myofilament Ca^{2+} desensitization (Jin CZ et al, 2013). In healthy heart, nNOS inhibits L-type Ca^{2+} channel activity and intracellular Ca^{2+} release and modulates cardiac contraction (Sears CE et al, 2003). nNOS gene disruption increased Ca^{2+} current and prolonged the slow time constant of inactivation of the calcium current significantly, leading to an increased Ca^{2+} influx and a greater calcium load in SR of nNOS-deficient cardiomyocyte (Sears CE et al., 2003). The contractile response to β-

adrenergic stimulation was greatly enhanced in nNOS-deficient cardiomyocytes as well as in cardiomycytes from wild-type mice treated with a specific nNOS inhibitor, vinyl-L-N-5(1-imino-3-butenyl)-L-ornithine (Ashley EA et al., 2002). nNOS inhibits xanthine oxidoreductase (XOD) activity, both enzymes co-localizing in the SR. Thus, in $nNOS^{-/-}$ mice XOD-mediated production of reactive oxygen species (ROS) is increased, leading to depression of myocardial excitation-contraction coupling (Khan SA et al., 2004). nNOS deletion or inhibition leads to increased Ca^{2+} current through the L-type Ca^{2+} channels and reduction in SERCA activity, leading to increase of contraction and impairment of relaxation (Seddon M et al., 2007). The roles of nNOS in regulating myocyte contraction and intracellular Ca^{2+} level in the presence of metabolic substrates are unknown.

A variety of pathological conditions can increase risk for development of ventricular arrhythmias in humans including diabetes, obesity, myocardial infarction (MI), and heart failure. Many of these diseases' common factors are sympathetic dysfunction. Norepinephrine released from sympathetic nerves activates cardiac β-AR to modulate myocyte repolarization and contractility. Sympathetic stimulation of cardiac β_1-adrenergic receptors (β-AR) induces positive inotropic and chronotropic effects, the most effective mechanism to acutely increase the output of the heart. Activation of cardiac β-AR modulates myocytes repolarization by altering transmembrane currents and Ca^{2+} homeostasis (Thomas D et al., 2004; Cutler MJ et al., 2011; Bers DM et al., 2008). β-adrenergic stimulated cAMP leads to phosphorylation of proteins involved in excitation-contraction coupling including phospholamban, L-type Ca^{2+} channels, and ryanodine receptors (RyR), resulting in increased sarcoplasmic reticulum (SR) Ca^{2+}-ATPase (SERCA) activity and an increase in SR Ca^{2+} content.(Bers DM et al., 2002). Thus, during sympathetic stimulation more Ca^{2+} is released from the SR (Shannon TR et al., 2000) to activate the myofilaments, increasing contractility, but spontaneous Ca^{2+} release from

the SR also become more likely (Valdivia HH et al., 1995; Marx SO et al., 2000). The increased cytosolic and SR Ca^{2+} levels that occur during sympathetic activation can lead to SR Ca^{2+} overload, which may result in spontaneous opening of RyRs and Ca^{2+} release that is not in response to an action potential. This leads to Ca^{2+} extrusion from the cytosol via the Na^{+}/Ca^{2+} exchanger (NCX) (Pogwizd SM et al., 2001). NCX is electrogenic, extruding one Ca^{2+} ion (2+) in exchange for 3 Na^{+} ions (3+), which produces a net inward current. If the inward current is large enough, the membrane depolarizes and a triggered action potential may occur. So during sympathetic activation is likely due to delayed afterdepolarizations (DADs) (Pogwizd SM et al., 2004), which are membrane depolarizations occurring during phase 4 of the action potential. Therefore, the positive inotropic effects of sympathetic stimulation that allow myocytes to meet increased cardiac demands are accompanied by increased risk for pathological arrhythmias.

Therefore, in **Part IV**, I investigated the effects of metabolic substrate supplementation on β-adrenergic regulation of myocyte function from normal and HTN rat hearts.

Materials & Methods

Animals

Sprague-Dawley rats (8-12 wks. old, male) were used in this study. In some experiments, rats were subjected to Ang II infusion subcutaneously using osmotic minipumps for 4 wks. Those animals were paired with a sham-operated group. Briefly, rats (of 8 wks. old, male) were anesthetized with isoflurane (2.5 %). An osmotic minipump (rats, Alzet model 2004) containing Ang II (200μl, 6mM, infusion rate 125ng/min/kg) was implanted in the midscapular region under sterile condition. Sham-operated animals underwent the same surgical procedure, except for no pump insertion. Blood pressures were measured by Non-Invasive Blood Pressure System, tail-cuff method (CODA, Torrington, CT, USA). Rats were warmed at 37 ^{o}C for 15 min before measurement; each value used in analysis was the mean of ten estimates.

The study protocol was in accordance with the Guide for the Care and Use of Laboratory Animals published by the US National Institutes of Health (NIH Publication No. 85-23, revised 1996), and also conforms to the Institutional Animal Care and Use Committee (IACUC) in Seoul National University (IACUC approval No.: SNU-101213-1; SNU-110629-5).

Isolated left ventricular myocytes

Rats were anesthetized with pentobarbital sodium (30 mg/kg, i.p.), pinned out and the thorax was rapidly opened up. The heart was exposed and the thymus gland removed to expose the aorta. A suture was looped around the aorta and then an incision was made in the aorta into which a cannula (made from a blunted 19G needle) filled with Ca^{2+} free isolation solution (in mM: NaCl 135, KCl 5.4, $MgCl_2$ 3.5, Glucose 5, HEPES 5, Na_2HPO_4 0.4, Taurine 20; pH titrated to 7.40 using NaOH) was inserted. The suture was tightened in order to secure the cannula and

the heart was removed from the chest cavity. The cannulated heart was then secured to the Langendorff perfusion system (Fig. 2) taking care not to introduce any bubbles into the coronary circulation, as this is known to affect the efficiency of the isolation procedure.

The heart was perfused with Ca^{2+}-free isolation solution, which was aerated with 100% oxygen and maintained at 37 ^{o}C, for 10 min and then with a primary enzyme solution [containing 1mg/ml of collagenase type II (Worthington biochemical Co., Lakewood, NJ, USA)], 0.1mg/ml of protease, 1.67mg/ml bovine serum albumin (BSA) and 50 μM Ca^{2+} in isolation solution]. Which was also aerated with 100% oxygen and maintained at 37 ^{o}C, for 8 min. At the end of this period, the heart was removed from the perfusion system and the needle, suture, aorta and any extraneous tissue removed so that the heart could be accurately weighed. Once weighed, the atria and the right ventricles were carefully dissected away and the LV was dissected into smaller pieces and put in a 50 ml Erlenmeyer flask with 10 ml of secondary enzyme solution (containing 1mg/ml collagenase, 1.67 mg/ml BSA and 50 μM Ca^{2+} in isolation solution).

The flask was shaken at 80 rev/min for a period of 10 min in a 37 ^{o}C water bath, after which it was taken out and the LV tissue allowed to settle, and then the supernatant solution filtered into a centrifuge tube. A further 10 ml of the secondary enzyme solution was added to the remaining LV tissue which was again shaken at 80 rev/min for a further 10 min. 10 ml of 1% BSA in isolation solution was added to the supernatant in the centrifuge tube which was then centrifuge at 600 rpm for 2 min. After this, the supernatant was removed and the pellet containing the LV myocytes was resuspended in storage solution (in mM: NaCl 120, KCl 5.4, $MgSO_4$ 5, Taurine 20, HEPES 10, Na-pyruvate 5, Glucose 5.5, $CaCl_2$ 0.2, mannitol 29; pH titrated to 7.40 using NaOH). The yield of rod shaped LV myocytes ranged from 50 to 80% of the total number of cells isolated. The myocyte suspension was stored at room temperature and

cells were used within 8 hours of isolation.

Measurement of LV myocyte contraction

The recording bath was made up of a Perspex-sided chamber with a microscope coverslip floor, mounted on the stage of a high-resolution inverted microscope (Diaphot 200, Nikon, JP) supported on a pneumatic anti-vibration table. HEPES-buffered perfusion solution (in mM; NaCl 141.4, KCl 4, NaH_2PO_4 0.33, HEPES 10, Glucose 5, mannitol 14.5, $CaCl_2$ 1.8, $MgCl_2$ 1; pH titrated to 7.40 using NaOH) perfused by a speed entered from the left hand side of the bath after being heated to 36 ± 1 ^oC by passage through a thermostatically controlled heater situated at the entrance to the perfusion bath. The solution was subsequently removed by suction from the right hand side of the bath ensuring a constant and adjustable flow of the perfusion solution across the recording bath chamber.

A suspension of LV myocytes in storage solution was placed in the recording bath and the cells allowed to settle to the bottom of the bath. Once settled, perfusion solution was perfused at a constant rate (2 ml/min) and the temperate maintained at 36 ± 1 ^oC.

LV myocytes were stimulated with electrodes placed in the bath and connected to a digital stimulator (Medical Systems Corp, Greenvale, NY, USA). Stimulation voltage was maintained at 10 V and frequency was maintained at 2 Hz.

Changes in cell sarcomere length were displayed on the computer by the acquisition program (IonOptix Corp, Milton, MA, USA, Fig. 3). And recordings were stored on-line for subsequent off-line analysis. Measurements from at least 10 steady state contractions were averaged for each cell.

Measurement of $[Ca^{2+}]_i$ transients & myofilament Ca^{2+} sensitivity

Fura-2 fluorescence was monitored from LV myocytes pre-incubated in perfusion solution containing 2 μM acetoxymethyl ester of Fura-2 (1 mM stock solution was prepared in anhydrous DMSO) and 250 μM Ca^{2+} for 15 min at room temperature and in the dark. After this period, the solution containing Fura-2 was removed and the LV myocytes were washed in perfusion solution containing 500 μM Ca^{2+} for 10 min after which the cells were finally washed in 500 μM Ca^{2+} perfusion solution before being used. Myocytes thus loaded with Fura-2 were placed on the perfusion chamber, perfused with HEPES-buffered perfusion solution (1.8 mM Ca^{2+}) and field-stimulated at 2 Hz.

Light collection was restricted to the myocytes by an adjustable aperture and background fluorescence was subtracted for each excitation wavelength. The Fura-2 fluorescence ratio (i.e. the ratio of the photon live count detected by the excitation at 360 nm compared with that at 380 nm) was used to estimate $[Ca^{2+}]_i$ .The amplitude of the time constant of decay (ms) was calculated by fitting an exponential curve to the transient.

In some cells, sarcomere shortening and Fura-2 ratio were recorded simultaneously. Myofilament Ca^{2+} sensitivity was assessed from phase-plane diagrams of Fura-2 ratio versus sarcomere length by measuring the gradient of the Fura-2- sarcomere length trajectory during late relaxation of the twitch contraction. The position of the trajectory reflects the relative myofilament response to Ca^{2+}.

Measurements from at least 10 steady state contractions were averaged for each myocyte for each stage of the experimental protocols. All experiments were carried out at 36 ± 1˚C and field-stimulated at 2 Hz.

Electrophysiological recording

1. Measurement of L-type Ca^{2+} current using whole-cell voltage clamp technique

The cell were transferred to a small chamber (0.2ml) on the stage of an inverted microscope (Nikon), and perfused continuously with NT solution at 35-37℃.

A patch pipette (glass microelectrode) with a resistance of 1.5-2.8MΩ was used to obtain a GigaΩ seal. It was pulled from borosilicate glass capillaries (TW150F-3, WPI) using a micropipette puller (Model PP-830, NARISHIE, Japan) by 2 step protocol (step1, 64.3℃; step 2, 49.5℃.

Isolated myocyte was patched in the whole cell configuration and the currents were recorded using an Axopatch200A amplifier (Axon Instruments). L-type calcium channel currents (I_{Ca}) were recorded 5-8 minutes after patch rupture for the current to stabilize, steady-state I_{Ca} was assessed during a step to 0mV at a stimulation frequency of 0.1 Hz (Holding at -40 mV "Single pulse"). Then, I_{Ca} was elicited by 200ms step depolarization from a holding potential of -40mV to test potentials ranging from -60 to +50 mV (Fig. 7 "step pulse").

For each myocyte, the current was normalized to current density (in pA/pF), and the cell membrane capacitance (C_m) was measured by the voltage-clamp ramp method (-10 mV hyperpolarizing ramp pulse immediately followed by a 10 mV depolarizing ramp of the same duration (100ms) from a holding potential of -40 mV). C_m can be read directly in the membrane test window of Clampex 10.1.

Extracellular solution for Ica recordings are (in mM): NaCl 141.4, KCl 4, NaH_2PO_4 0.33, $MgCl_2$ 1, $CaCl_2$ 1.8, glucose 10, HEPES 10, pH 7.4 NaOH. The pippet solution designed for Ca^{2+} current recording only contained (in mM): CsCl 110, TEA-Cl 20, NaCl 10, HEPES 10, $MgCl_2$ 1, Mg-ATP 5, EGTA 10, pH 7.2 CsOH, osmolarity 298 mOsm. Each solution was

delivered to the recording chamber by gravity flow.

The inactivation time constant of LTCC was best fit by a double exponential (Clampfit, Axonpatch, 200A, Axon Instruments) curve to the I_{Ca} trace elicited by the 15th sweep (-20mV) of "Step pulse", and fast *tau* was used for comparisons between sham and HP rats.

Ca^{2+} influx via LTCC was also compared by calculation integral of I_{Ca} trace elicited by the 7th sweep (0mV) of "Step pulse". I calculated the integral of net inward current during initial 40ms.

2. Measurement of action potential using current clamp technique.

The action potential profile of the myocyte was recorded with current clamp technique in NT and in NF (sampling rate: 10 kHz) at 35-36 ℃ (Axon Instruments, 200A). The pipette (resistance 1-2 MΩ) solution contains (in mM) 110 K-aspartate, 30 KCl, 5 NaCl, 10 HEPES, 0.1 EGTA, 5 MgATP, 5 creatine phosphate, and 0.05 cAMP adjusted to pH 7.2.

3. Measurement of intracellular Ca^{2+} and calculation of SR content using whole-cell voltage-clamp

Cells were voltage-clamped using the whole-cell patch-clamp technique and stimulated with 50 ms duration pulses from -40 to +10 mV from a holding potential of -60 mV at frequency of 0.5 Hz using Axonpatch 2A and pCLAMP software. K^+ currents were blocked by the addition of 4-aminopyridine (5 mM) and $BaCl_2$ (0.1 mM). Electrodes (2-3 MΩ resistance) were filled with (in mM): $CsCl_2$, 120; TEA-Cl, 20; HEPES, 10; Na_2ATP, 5; CsEGTA, 0.02; pH=7.2 with CsOH. All experiments were performed at 37 ℃.

The Ca^{2+} indicator Fura-5F, pentapotassium salt (Invitrogen, UK; 100μM) was loaded via

the patch pippete and a 475 nm light-emitting diode (Cairn Research Instruments, UK) used to excite the fluorophore. The ratio values were normalized to the diastolic value and are expressed as R/R_{res}, where R_{rest} is the ratio at diastolic Ca^{2+}.

SR Ca^{2+} content was measured by applying 5 mM caffeine to release Ca^{2+} from the SR. Measurements were made of both the amplitude of the resulting cytoplasmic Ca^{2+} transient and the integral of the accompanying Na-Ca exchange (NCX) current. The integral of this current gives a measure of the amount of Ca^{2+} release from the SR that is pumped out of the cell by NCX.

Immunoblotting

Immunoblots were performed in rat LV myocyte lysates using specific antibodies against eNOS (NOS3, BD Transduction Laboratories), and its phosphorylated fraction (Ser^{1177}, Upstate). LV myocytes after incubated with NF or appropriate treatments for 10 min were lysed in lysis buffer contained (mmol/L) 50 Tris-HCl (pH 7.4), 100 NaCl, 1% Triton X-100, 50 NaF, 5 EDTA, 40 β-glycerophosphate, 0.2 ortho-vanadate, 0.001 aprotinine and 0.1 leupeptine. The samples were snap frozen in liquid N_2 until performance for the immunoblotting. Blots were developed using ECL Plus Western blotting detection reagents (Amersham Bioscience). To evaluate the phosphorylated fractions of eNOS, membranes were stripped of antibodies using Restore Western Blot Stripping Buffer (Pierce Chemical). The relative densities were calculated by normalizing of each blot with GAPDH

Immunoprecipitation

For immunoprecipitation, LV myocytes were lysed in lysis buffer (50mM Tris-HCl, pH 8.0, 280mM NaCl, 0.2mM EGTA, 1mM DTT, 100mM NaF, 1mM PMSF, 0.2mM NaVO3, 0.5%

NP-40, 10% Glycerol) freshly supplemented with phosphatase and protease inhibitors. Briefly, 0.5 or 2 mg of total lysate was incubated overnight at 4 °C with IRβ (#3025; Cell Signaling) or IRS-1 (sc-559; Santa Cruz Biotechnology) antibody. These primary antibodies had been captured by Protein A agarose (#16-125; Millipore). The immunoprecipitated protein-beads complex was subjected to Western blotting for p-Tyr IR β (#3026) or p-IRS-1 (Tyr612; sc-17195-R).

Metabolomics

The concentrations of three fatty acids were quantified by a 7890B series gas chromatography coupled with a 7000B series triple quadrupole mass spectrometer (Agilent Technologies, Santa Clara, CA, USA). The serum concentration of each fatty acids were quantified using previously described protocols with minor modifications (Yi et al., 2007). Briefly, 200 μL of plasma were diluted with 100 μL of PBS and 20 μL of (100 μL/mL) internal standard was spiked. 2 mL of 5% H_2SO_4 in MeOH was added to the prepared samples and incubated in water bath at 70 °C for 30 mins to be reacted. Afterwards, the prepared samples were extracted twice by using 2 mL of hexane. The supernatants were evaporated under N_2 evaporator and dried samples were reconstituted in 100 μL of hexane for further analysis.

Chemicals

Angiotensin II (Ang II, Sigma) was used to induce hypertension. L-NAME (1mM, Sigma) and SMTC (100 nM, Sigma) was used to target eNOS and nNOS activity, respectively. Isoproterenol (ISO, 10-50 nM) was used to stimulate amplitude of LV myocyte contraction. Insulin (10 nM, sigma) was used to stimulate intracellular metabolism, NAC (1mM, sigma) was used to reduce intracellular oxidation. Ranolazine (10μM, Sigma) was used to inhibit the

activity of CPT-1. Caffeine (5mM, sigma) is the agonist of the cardiac ryanodine receptor (RyR2) Ca^{2+} release channel. Nebivolol (10 nM, 1μM, Sigma) was used to block the β−1-adrenoceptor and activate the β-3 adrenoceptor. Cordycepin (50 μM, 100 μM, Sigma) was used to block the adrenergic receptor. KB-R7943 (100 μM, Sigma) was used to inhibite the Na^{+}-Ca^{2+} exchanger (NCX).

Chemical compositions in NT and fatty acid- containing NF solution

Metabolic substrates (oleic acid 200 μM, palmitic acid 100 μM, linoleic acid 100 μM, lactate 1mM, pyruvate 100 μM and carnitine 50 μM) were supplemented to the normal Tyrode solution (NT, in mM: NaCl 141.4, KCl 4, NaH_2PO_4 0.33, $MgCl_2$ 1, HEPES 10, Glucose 5.5, $CaCl_2$ 1.8). The composition and the concentrations of metabolic substrates are modified from rodent's blood sample results (Khairallah M et al., 2004).

Fatty acids (oleic acid, palmitic acid, linoleic acid) were dissolved in 1.35 mM (0.09 g/ml) BSA in NT solution at 70 ℃ for 3 h to make respective stock solutions (10mM). The composition and the concentrations of metabolic substrates are modified from blood sample results of normal subjects (Maya Khairallah et al., 2003).

Statistics

Data are expressed as means ± s.e. or as relative to control (100%) and n indicates the number of cells used. For all comparisons, cells were obtained from a minimum of three hearts per treatment group per protocol. Data were analyzed using one way ANOVA or student's unpaired *t* test. A value of $P < 0.05$ was considered to be statistically significant.

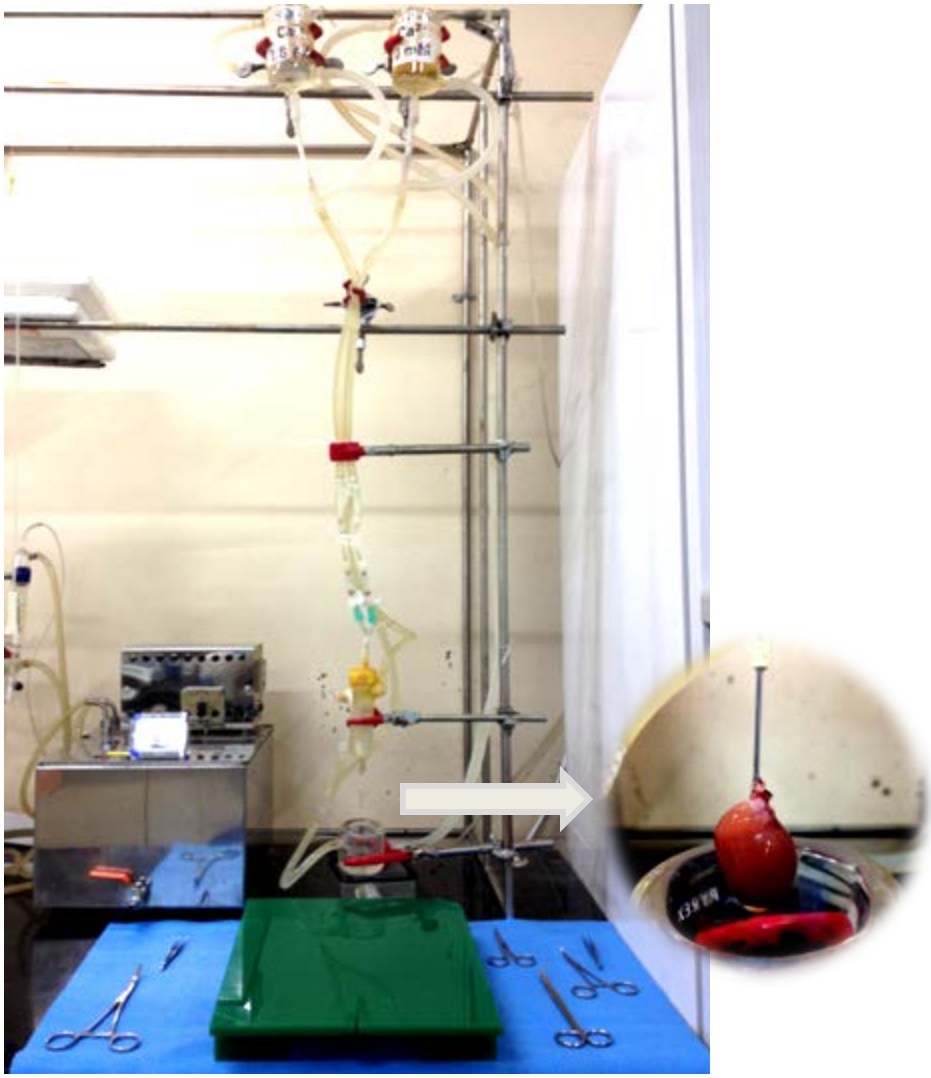

Figure 1. Langendorff perfusion system

Above is the Langendorff perfusion system used to perfuse isolation solution to the heart cannulated *via* aorta (inset, magnified picture with mounted heart on the perfusion system).

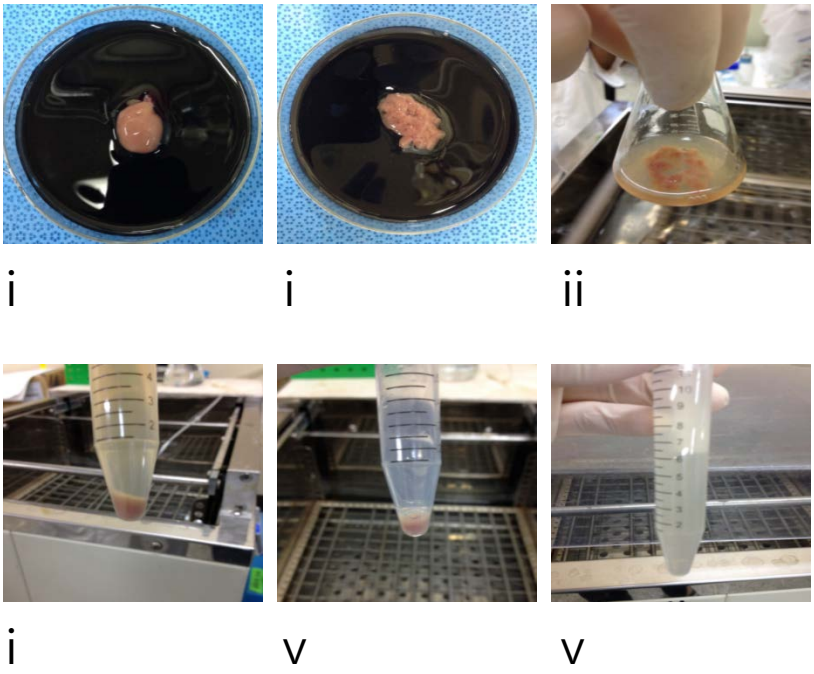

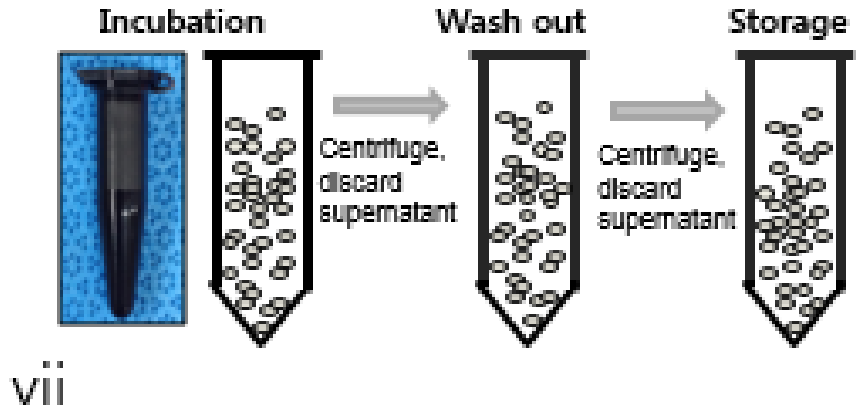

Figure 2. Procedures for isolating LV myocytes from rat heart. i-iii: The heart after digestion with collagenase solution 1; dissected LV tissue in dish and in the flask. iv – vi: myocyte suspension after collagenase solution 2; myocyte pellet after centrifugation; re-suspended myocyte pellet in storage solution. B vii: incubation: incubate LV myocytes in Fura-2AM – containing isolation solution (Fura-2 AM, 2 μM, Ca^{2+} 250 μM with 2 μl poloxamer 407); washout: wash LV myocytes with Isolation solution with Ca^{2+} 500 μM; storage: keep the Fura-2 loaded LV myocytes in fresh Isolation solution with Ca^{2+} 500 μM.

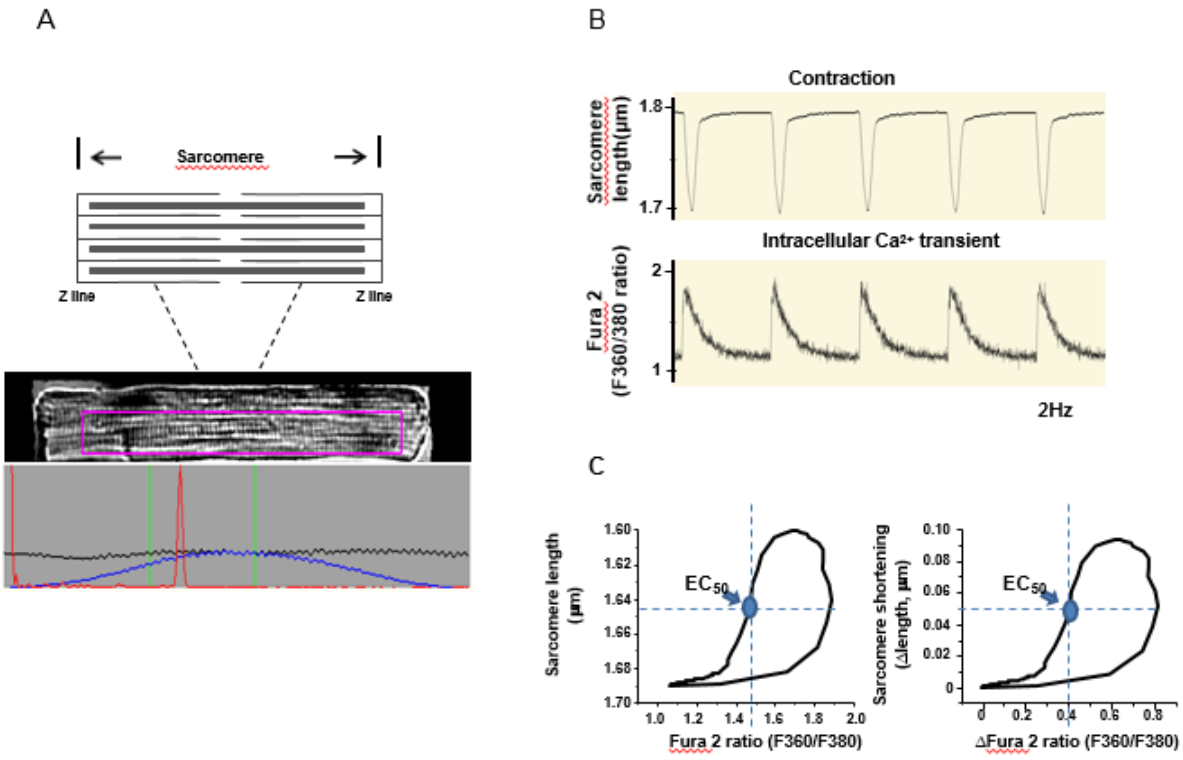

Figure 3. Measurement of sarcomere length and intracellular Fura-2 ratio (indicative of intracellular Ca^{2+} level)

A. Diagram of sarcomere, image of Fura-2 loaded LV myocyte and averaged sarcomere length (the red peak) are displayed on the computer. In the lower panel, the black line is the average of each horizontal pixel line within the purple region of interest. The blue line is the same data zeroed at each end. The red line is the fast Fourier transform (FFT) power spectrum, which represents the number of signals the FFT has calculated. One sharp peak means a clean sarcomere recording. B. Simultaneous recordings of sarcomere length and Fura-2 ratio in response to field stimulation (2Hz). C. Phase-plane plot of Fura-2 ratio *vs.* sarcomere length of the same LV myocyte (note that both actual length/Fura-2 ratio and delta changes of these parameters are analyzed). EC_{50} (Fura-2 ratio at 50% relaxation, circle indicated by arrow) is the qualitative comparison for myofilament Ca^{2+} sensitivity between the groups.

Results

Part I:

Assessment of Myofilament Ca^{2+} sensitivity underlying cardiac excitation-contraction coupling.

LV myocytes are isolated from normal and hypertensive rat hearts. Rod-shaped myocytes with clear striations (representing sarcomeres) and stable contractions in response to field stimulation are considered as the optimal myocytes and are selected for recordings (Fig. 2A). In the example shown in Fig. 3A, Fura-2-loaded LV myocyte is positioned horizontally and the aperture of the camera is adjusted so that the myocyte occupies most of the recording field and minimal background area is included. In the recording field, adjust the dimensions of the purple box by clicking and dragging the purple box on the computer screen (through the recording program). When the average sarcomere length shows one sharp red peak, start recording (Fig. 2A lower image).

Both sarcomere length and intracellular Ca^{2+} transients (Fura-2 ratios) are recorded simultaneously from the same myocytes (Fig. 4A) and the average traces of sarcomere length and Ca^{2+} transients are shown in Fig. 4B. Individually, diastolic/systolic sarcomere lengths, time to peak (PT) and sarcomere shortening are measured to investigate the amplitude and dynamic of myocyte contractility; time to 50% relaxation (TR_{50}) is analyzed to assess the relaxation of the myocyte. Similarly, diastolic and systolic Fura-2 ratios (Ca^{2+} transients), time to peak (TP) of Ca^{2+} transients and time constant of Ca^{2+} transient decay (tau) are analyzed for the assessment of myocyte contraction and relaxation (Table 1). In this example, the amplitudes of Ca^{2+} transients are moderately increased in LV myocytes from hypertensive rat and the contraction is moderately reduced (Fig. 4 & Table 1).

Furthermore, relationships between Fura-2 ratio and sarcomere length (indicating myofilament Ca^{2+} sensitivity of LV myocyte) are plotted in both sham and hypertensive rats (Fig. 4C). Since Fura-2-sarcomere length trajectory during relaxation phase of the myocyte defines a quasi-equilibrium of cytosol Ca^{2+}, myofilament Ca^{2+} binding and sarcomere length (Spurgeon, H.A., et al., 1992), the relaxation phase are analyzed between the two groups. The rightward shift of the trajectory in myocytes from the hypertensive group indicates reduced myofilament response to Ca^{2+} (Fig. 3C). Accordingly, intracellular Ca^{2+} required for half relaxation (EC_{50}) was increased (Fig. 3C), referring to myofilament Ca^{2+}-desensitization in hypertension.

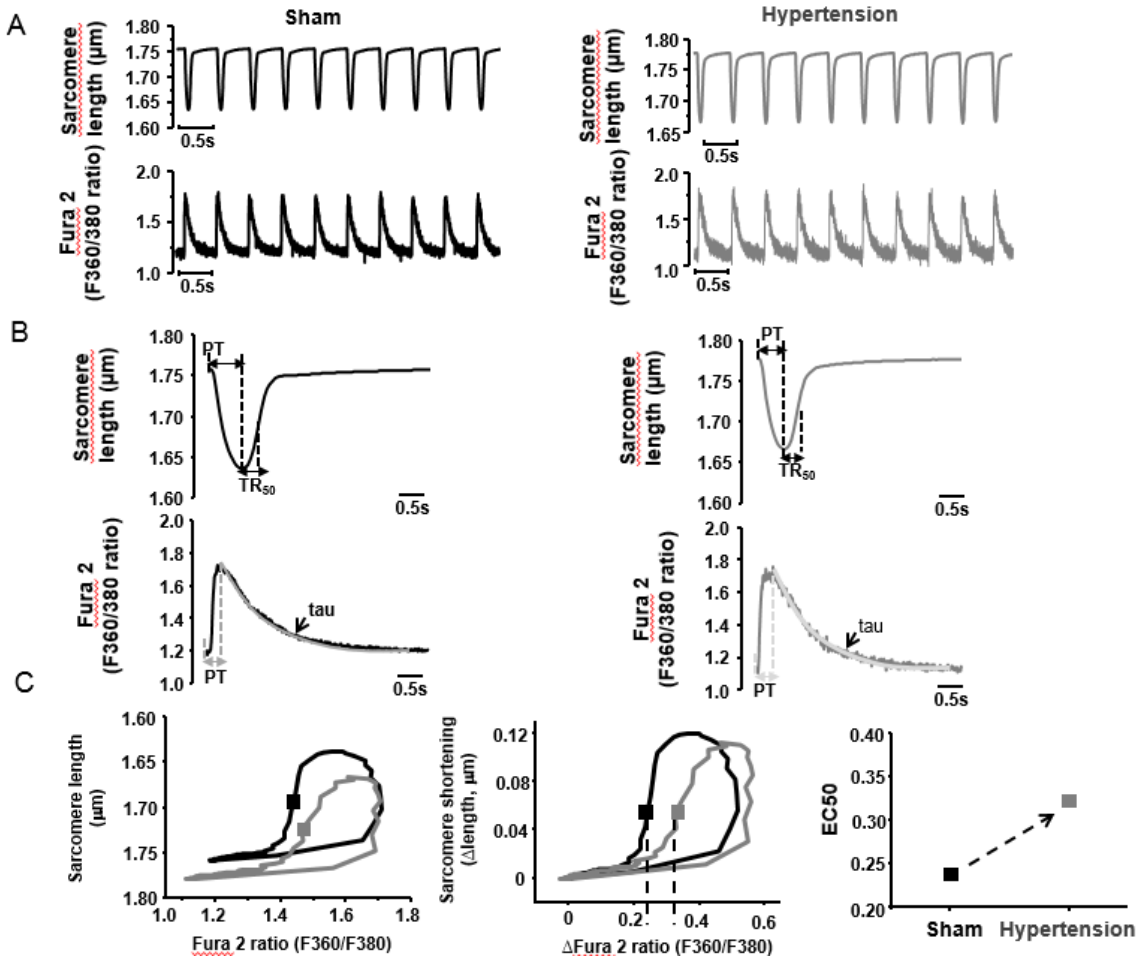

Figure 4. Representative results analyzing LV myocyte contraction in sham and hypertensive rats

A. Raw traces of sarcomere shortening and Fura-2 ratio measurement in LV myocytes from sham and hypertensive rats. B. Average traces of sarcomere length and Fura-2 signals. Parameters analyzed in the averaged traces are shown in Table 1. C. Phase-plane plots of Fura-2 ratio *vs.* sarcomere length (both actual length/Fura-2 ratio and delta changes of these parameters) in two groups. Trajectory loop shifted to the right and EC_{50} tends to be higher in hypertension, suggesting myofilament Ca^{2+} desensitization. PT: time to peak (s); Tau: time constant of Ca^{2+} transient decay (s) (obtained by fitting the decline phase of Fura-2 ratio with exponential function.

$$\int(t) = \sum_{i=1}^{n} A_i \, e^{-t/\tau_i} + C$$

TR_{50}: time to 50% relaxation (s).

	Parameters	Sham	Hypertension
Intracellular Ca^{2+}	Diastolic Ca^{2+}	1.189	1.124
	Systolic Ca^{2+}	1.71	1.691
	Amplitude (Δ ratio)	0.521	0.567
	Time to peak (PT, s)	0.021	0.031
	Tau (s)	0.079	0.076
Sarcomere	Diastolic	1.758	1.78
	sarcomere length (μm)		
	Sarcomere	0.122	0.115
	Shortening (Δ length,mm)		
	Time to peak (PT, s)	0.064	0.055
	Time to 50%	0.032	0.03
	Relaxation (TR_{50},s)		
EC50	$[Ca^{2+}]_i$ (Fura-2 ratio) for 50% sarcomere relengthening	0.2382	0.3224

Table 1. Analysis of the Fura-2 ratio (intracellular Ca^{2+}) and sarcomere length measurements.

Part II:

Cardiac inotropy, lusitropy, and Ca^{2+} handling with major metabolic substrate in rat heart

Left ventricular contraction and relaxation with metabolic substrates' supplementation (NF)

As shown in Fig. 5A, B, NF increased LV myocyte contraction ($P < 0.001$ between NT and NF, n = 29 & 29) and facilitated relaxation (time to 50 % relaxation, $P < 0.02$) without changing diastolic sarcomere length ($P = 0.5$). Supplementation of three types of FAs (linoleic acid, oleic acid and palmitic acid) increased sarcomere shortening ($P < 0.01$ between NT and 3FA, n = 15 and n = 15, Fig. 5C), similar to that observed with NF. These results suggest that metabolic substrates and FAs increase myocyte contraction in healthy rat heart. Since FAs are shown to increase intracellular ROS in cardiac myocytes (Shipp JC et al., 1961; Zhang YH et al., 2009) possibly due to increased beta-oxidation in mitochondria and ROS potentiates myocyte contraction in murine heart (YH et al., 2009), I tested whether ROS is responsible for the inotropic effect of metabolic substrates. Incubation of LV myocytes with a potent antioxidant, N-acetyl-cysteine (NAC, 100 μM), did not prevent NF augmentation of myocyte contraction ($P < 0.001$ between NT + NAC and NF + NAC, n = 16, Fig. 5D).

These results exclude the role of ROS in mediating NF-induced myocyte contraction in rat hearts.

Intracellular Ca^{2+} transient ($[Ca^{2+}]_i$) with NF

Next, I tested the effect of NF on $[Ca^{2+}]_i$. As shown in Fig. 6A, B, NF significantly increased

the diastolic and systolic $[Ca^{2+}]_i$ (F360/380: $P < 0.001$ and $P < 0.001$, $n = 18$, $n = 18$). Analysis of $[Ca^{2+}]_i$ profile showed that the time constant of $[Ca^{2+}]_i$ decay (tau, ms) was abbreviated in NF ($P < 0.001$, Fig. 6B). Nevertheless, the peak $[Ca^{2+}]_i$ duration (90 % peak time + 10 % time to relaxation, PT90 + TR10) and TR50 of $[Ca^{2+}]_i$ were prolonged ($P = 0.009$ and $P = 0.002$, $n = 18$ and $n = 18$, respectively).

These results suggest that NF increased $[Ca^{2+}]_i$ transients and decay kinetics of $[Ca^{2+}]_i$ but prolonged peak time of $[Ca^{2+}]_i$ during systole.

L-type Ca^{2+} current (I_{Ca}) and action potential profile

I aimed to test the key elements of excitation-contraction coupling responsible for increased myocyte $[Ca^{2+}]_i$ and contraction in NF. Figure 7A, B showed raw traces and averaged current–voltage (I–V) relationships of I_{Ca} in LV myocytes before and after NF. And the inset in Fig. 7A showed raw traces of I_{Ca} at 0 mV for Ca^{2+} influx analysis. NF reduced the amplitude of I_{Ca} at 0 mV (current density of I_{Ca} at 0 mV, pA/pF: $P = 0.03$ between NT and NF, $n = 34$, $n = 11$) but slowed the inactivation of I_{Ca} at 0 mV (in ms, tau-slow: $P = 0.005$; tau-fast: $P = 0.3$, Fig. 7C). As a result, total Ca^{2+} influx via LTCC (integral of I_{Ca}) was greater in NF ($P = 0.05$ between NT and NF at 0 mV, Fig. 7D). Similarly, integral of I_{Ca} was bigger at −20 mV ($P = 0.05$) but not at +20 mV. Greater I_{Ca} influx in NF may be responsible for the prolongations of action potential (AP) plateau (and therefore APD) and $[Ca^{2+}]_i$ duration. Accordingly, I examined the APD duration in NF. As shown in Fig. 8A, B, APD_{20}, APD_{50}, and APD_{90} were significantly prolonged in NF ($P < 0.05$, $P < 0.05$, and $P < 0.05$, $n = 12$).

These results suggest that Ca^{2+} influx via LTCC is greater and APD is prolonged, which may be responsible for increased $[Ca^{2+}]_i$ amplitudes and prolonged peak time of $[Ca^{2+}]_i$ in NF.

Myofilament Ca^{2+} sensitivity and desensitization (BDM) regulates $[Ca^{2+}]_i$ in NF

To test whether myofilament Ca^{2+} sensitivity is regulated by NF and contributes to greater contraction and faster relaxation, I recorded sarcomere shortening and $[Ca^{2+}]_i$ simultaneously in Fura-2-loaded LV myocytes and plotted a phase-plane loop of the changes in sarcomere length vs. $[Ca^{2+}]_i$ transient with and without NF. As shown in Fig. 9A, B, relaxation phase of the sarcomere length-$[Ca^{2+}]_i$ transient relationship shifted to the right in NF; $[Ca^{2+}]_i$ at 50 % sarcomere relengthening (EC50) was significantly increased ($P < 0.001$, n = 18).

Myofilament buffers Ca^{2+} and changing myofilament Ca^{2+} sensitivity affects $[Ca^{2+}]_i$ homeostasis (Briston, S.J. et al., 2014; Huke S et al., 2010). Accordingly, Itested whether myofilament Ca^{2+} desensitization with a potent myosin ATPase inhibitor, BDM, prevents increased $[Ca^{2+}]_i$ and facilitated tau of $[Ca^{2+}]_i$ in NF. As shown in Fig. 10A, B, incubation of LV myocytes with BDM (5 mM) abolished NF-induced increase in diastolic and systolic $[Ca^{2+}]_i$ and faster tau (P = 0.8 in diastole; P = 0.22 in systole; P = 0.96 for tau between NT and NF with BDM; n = 12).

These results suggest that myofilament Ca^{2+} sensitivity was significantly reduced by NF. And suggest that reduced myofilament Ca^{2+}sensitivity in NF may, at least in part, increase $[Ca^{2+}]_i$ and facilitate $[Ca^{2+}]_i$ decline in rat LV myocytes. The duration of $[Ca^{2+}]_i$ peak (90 % time to peak +10 % $[Ca^{2+}]_i$ decline, PT90 + TR10), however, remain prolonged in NF in the presence of BDM (P < 0.001, between NT + BDM and NF +BDM, n = 12, Fig. 10B).

Calculation of SR content with NF

Next, Iexamined the SR content total intracellular Ca^{2+} in Fluo-5F-loaded LV myocytes. Measurements were made of both the amplitude of the cytoplasmic Ca^{2+} transient with caffeine and the integral of the accompanying Na-Ca exchange (NCX) current (Varro, A. et al., 1993). As shown in Fig 11 A, NF increased both the caffeine-evoked increase of $[Ca^{2+}]_i$ and

accompanying intergrated NCX current in LV myocytes. On average (Fig. 11B), the SR Ca content was increased by 88% (from 118.27 ± 21.2 to 224.3 ± 34.3 μmol/L, n=5, $P<0.05$); the amplitude of caffeine-evoked of $[Ca^{2+}]_i$ was increased (n=5, $P<0.05$); and the rate constant of caffeine-evoked Ca transient decay was greater (n=5, $P<0.05$). These results suggest that the total amount of Ca in the SR is increased by NF, the increase of free cytosolic Ca when SR Ca is released is greater.

Regulation of intracellular pH by NF

To investigate whether intracellular pH ($[pH]_i$) is reduced by NF and contributes to reduced myofilament Ca^{2+} sensitivity, Idetected changes of pH_i in SNARF-1/AM loaded LV myocytes. As shown in Fig. 12A, the pH_i was gradually decreased with NF (3–5 min). Averaged results showed that NF significantly reduced pH_i ($P=0.03$, n =10, Fig. 12B). Increasing pH buffer capacity in NF using $NaHCO_3 + CO_2$ (5 %) weaken the changes in pH_i by NF (Fig. 12 C, D). Importantly, such a modification in pH_i abolished NF-induced myofilament Ca^{2+} desensitization, increase in the amplitude of $[Ca^{2+}]_i$ and the prolongation of the peak time of $[Ca^{2+}]_i$ (Fig. 13A, B, C, D).

These results suggest that reduced pH_i may play an important role in mediating the effects of NF on the myofilament Ca^{2+} sensitivity and its regulation of $[Ca^{2+}]_i$ handling.

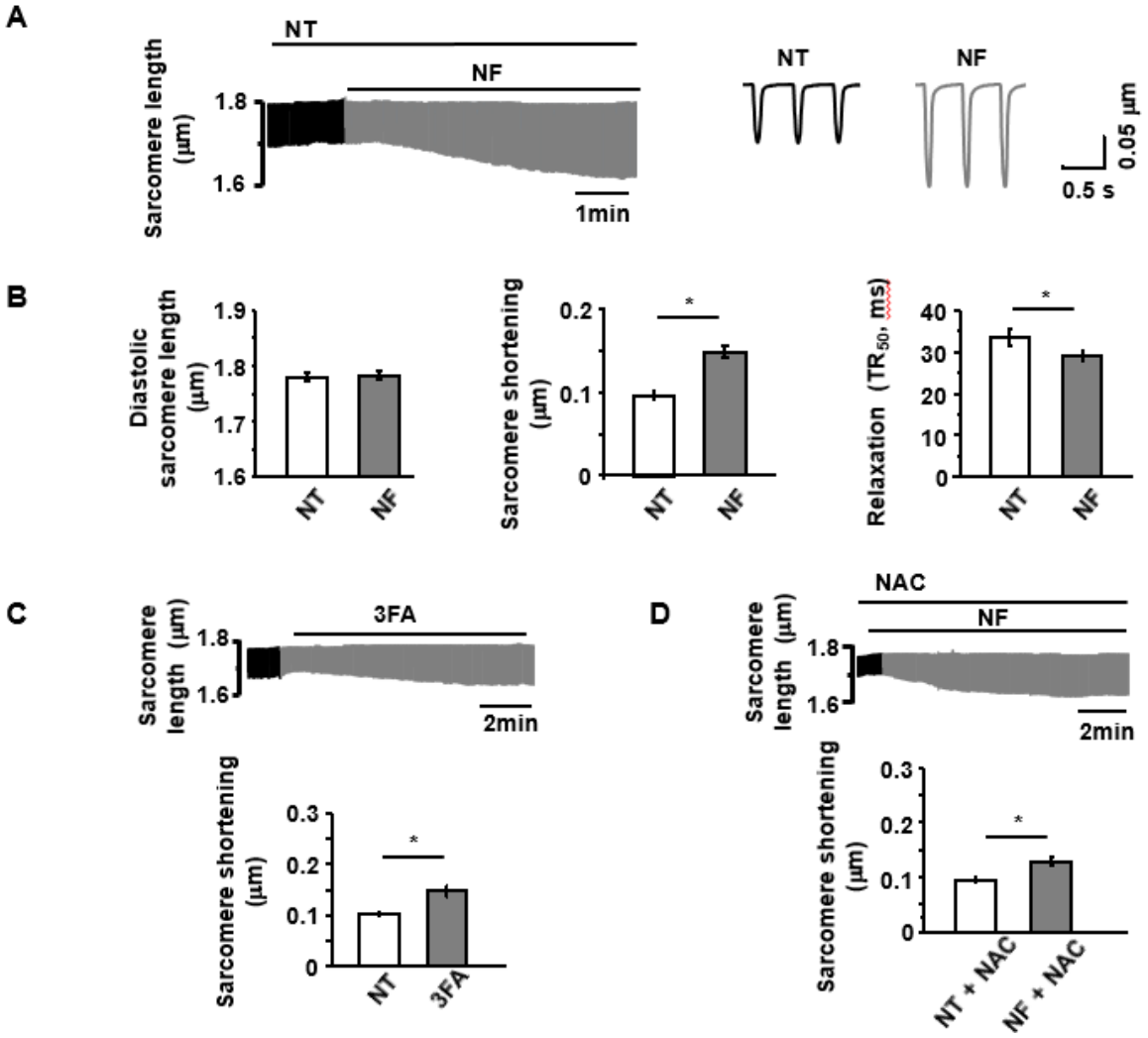

Figure 5. Effect of NF on LV myocyte contraction

A. Representative raw traces of sarcomere shortening and relengthening in the presence of NF. B. Mean values of the diastolic sarcomere length and the amplitude of sarcomere shortening (peak height) and 50 % relaxation time (TR_{50}). Diastolic sarcomere length was not different between NT and NF. Sarcomere shortening was significantly increased in NF and TR_{50} was shorter by NF. C. Representatives raw traces and mean values of three fatty acids (3FAs) only on myocyte contraction. 3FAs increased myocyte contraction. D. Representative raw traces and mean values of a potent antioxidant NAC on myocyte contraction in NF. NAC did not affect the increment of myocyte contraction by NF

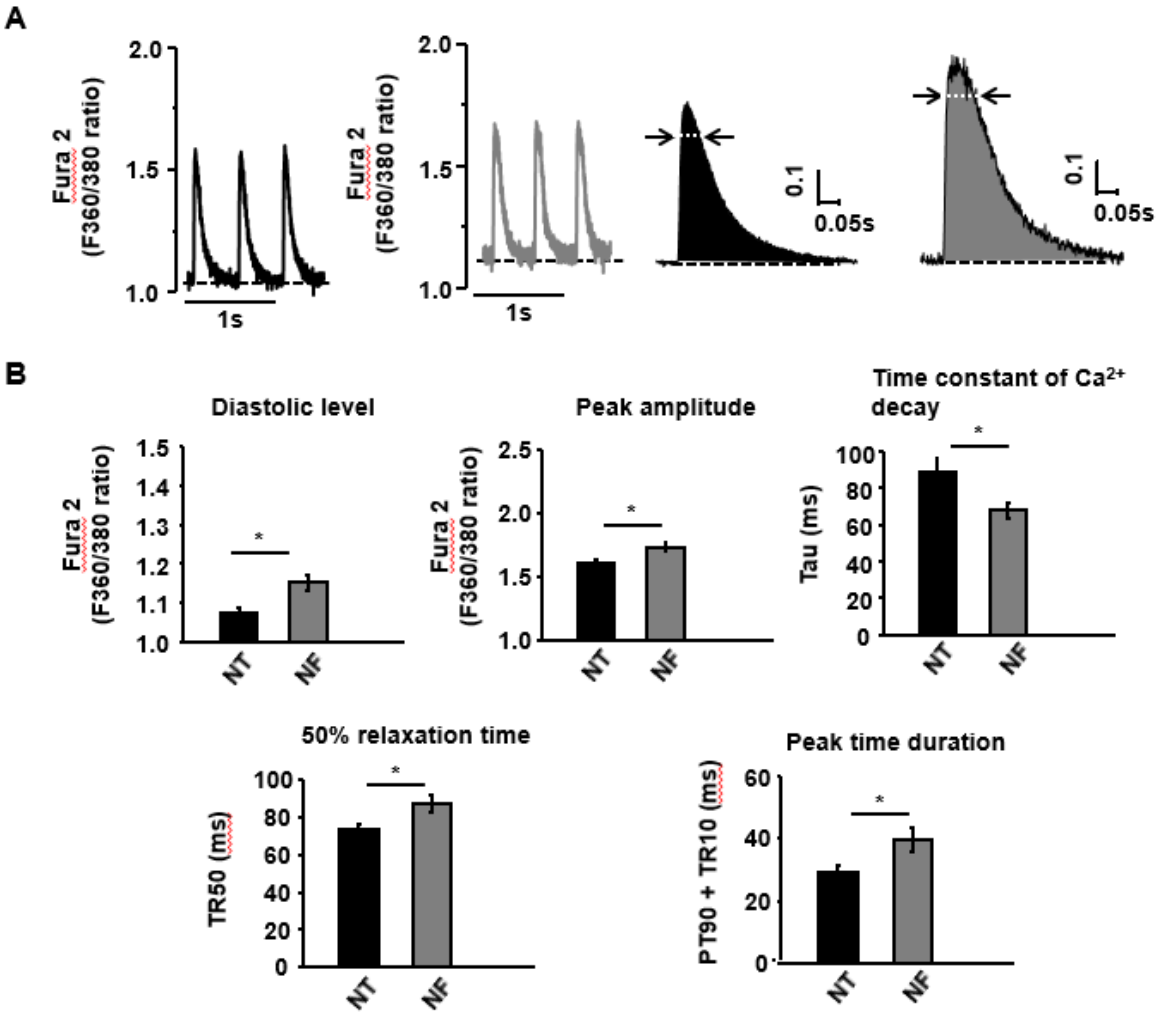

Figure 6. NF regulation of intracellular Ca^{2+} transients

A. Representative $[Ca^{2+}]_i$ transients in NT and NF. B. Mean values of $[Ca^{2+}]_i$ transient parameters. NF significantly increased diastolic $[Ca^{2+}]_i$ and peak amplitude of $[Ca^{2+}]_i$. Time to 50 % relaxation and peak time duration (PT_{90} + TR_{10}) were prolonged; however, time constant of $[Ca^{2+}]_i$ decay (tau) was facilitated in NF.

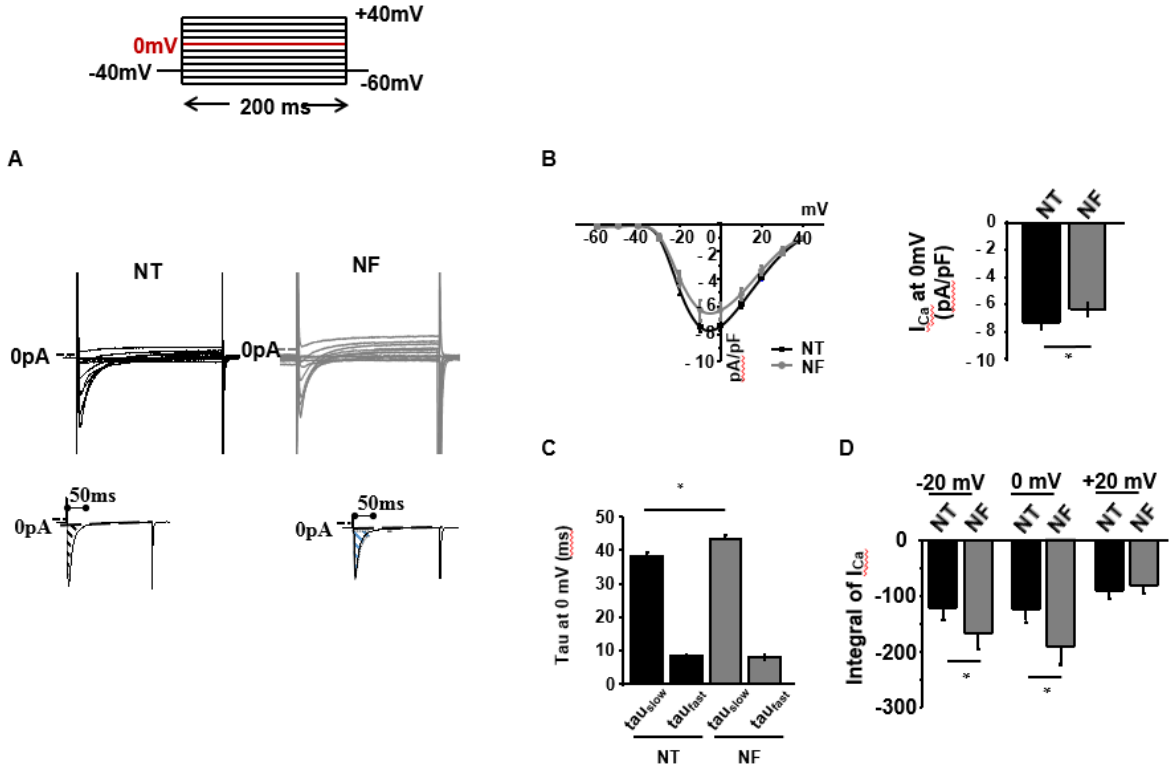

Figure 7. Patch-clamp recordings of LTCC activities in NF

A. Pulse protocol, representative I_{Ca} and the corresponding I-V relationship, peak I_{Ca} at 0 mV, inactivation parameters, and the integral of Ca^{2+} influx in NF. B, C, D. NF reduced peak I_{Ca} density, prolonged slow inactivation of I_{Ca}, and increased integral of I_{Ca} at 0 mVand −20 mV.

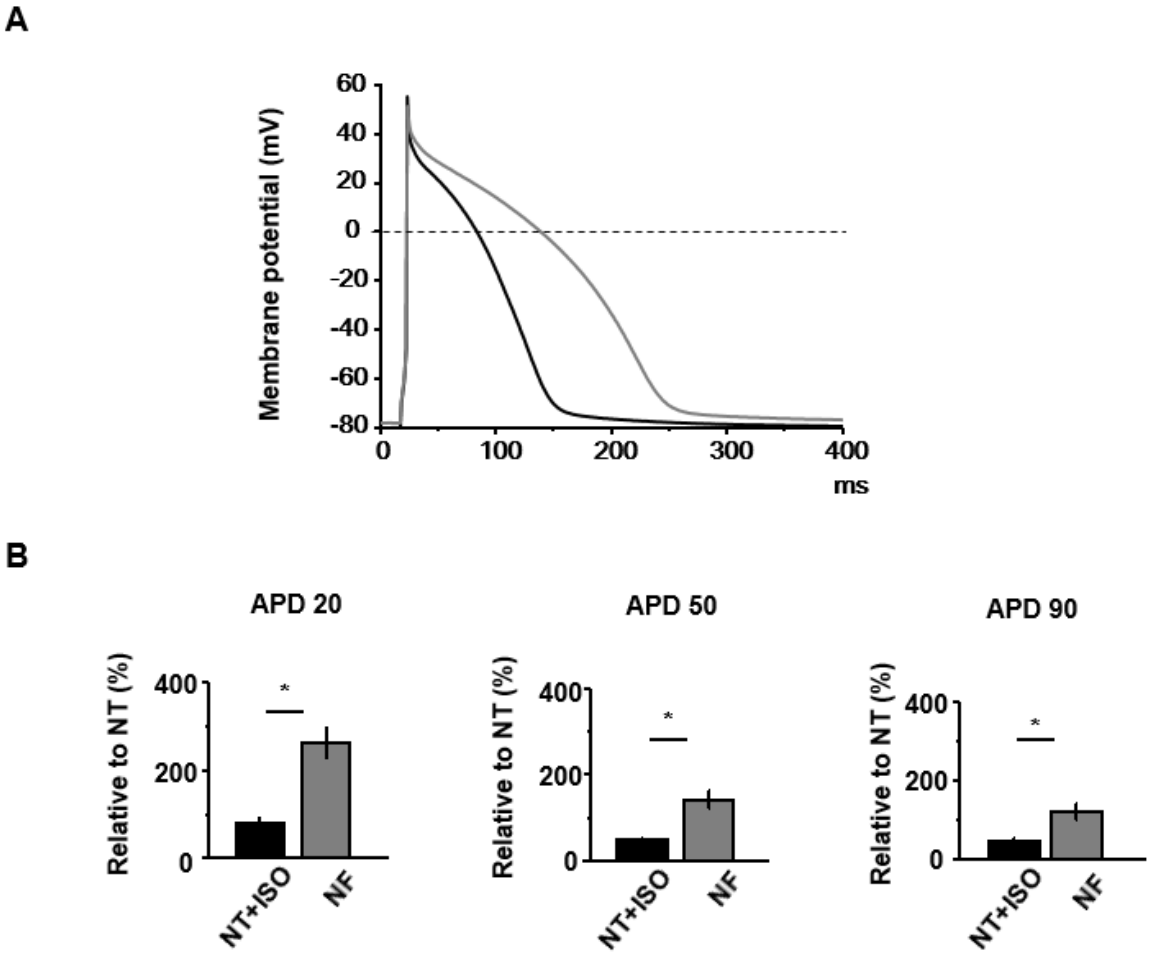

Figure 8. Effect of NF on action potential profile in sham rat

A. Representative action potential profile in NT and NF. B. Mean value of action potential duration parameters. NF significantly prolonged the repolarization duration of APD (APD_{20}, APD_{50}, APD_{90}).

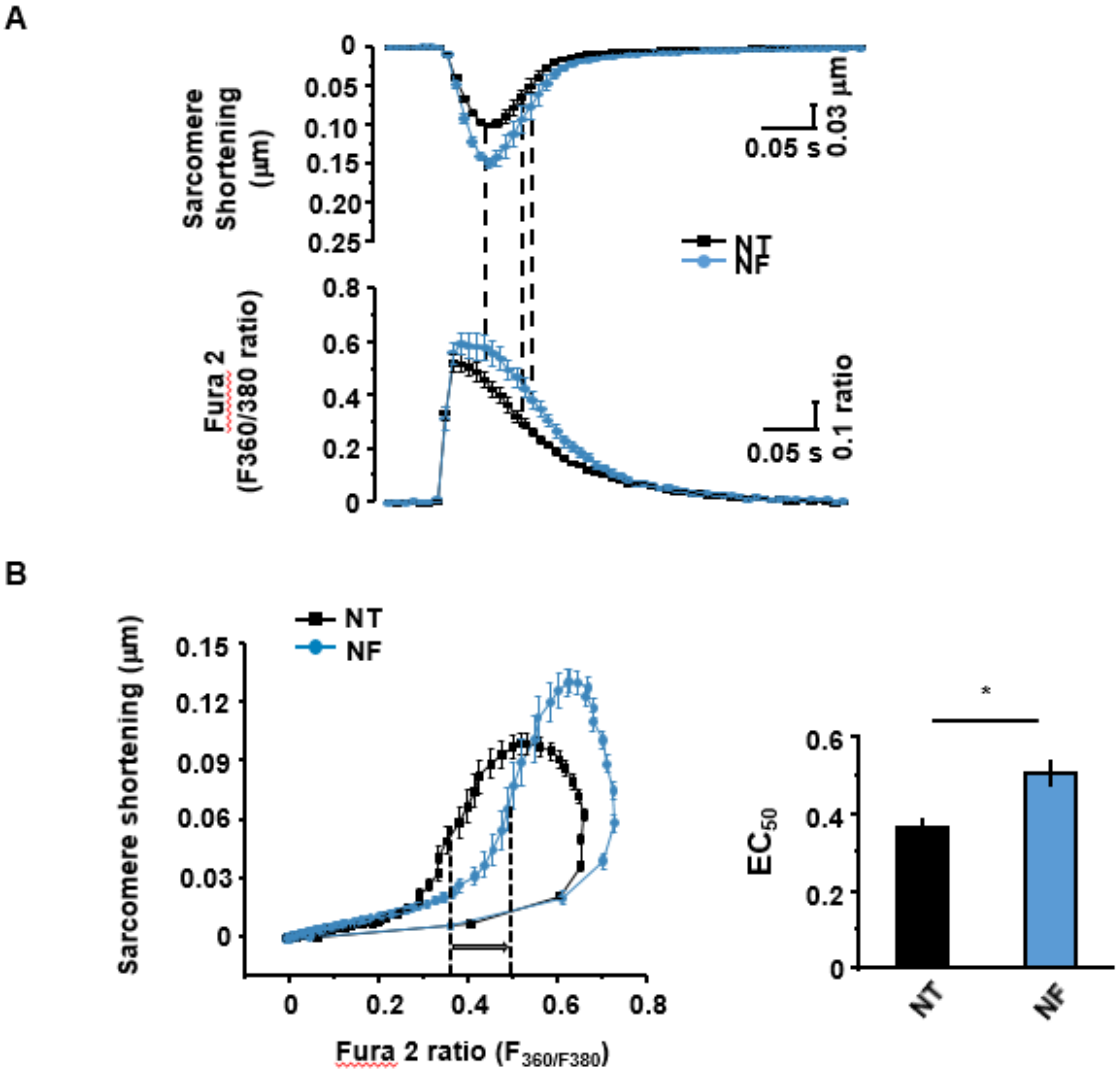

Figure 9. NF regulation of myofilament Ca^{2+} sensitivity in normal rats

A. Simultaneous recordings of LV myocyte sarcomere shortening/ relengthening and intracellular Ca^{2+} transients in NT and in NF. B. Phase-plane loop of sarcomere shortening/relengthening vs. $[Ca^{2+}]_i$ transient. The relaxation phase of the loop shifted to the right in NF compared to that in NT. Ca^{2+} concentration at 50 % sarcomere relengthening (EC_{50}) was significantly larger in NF.

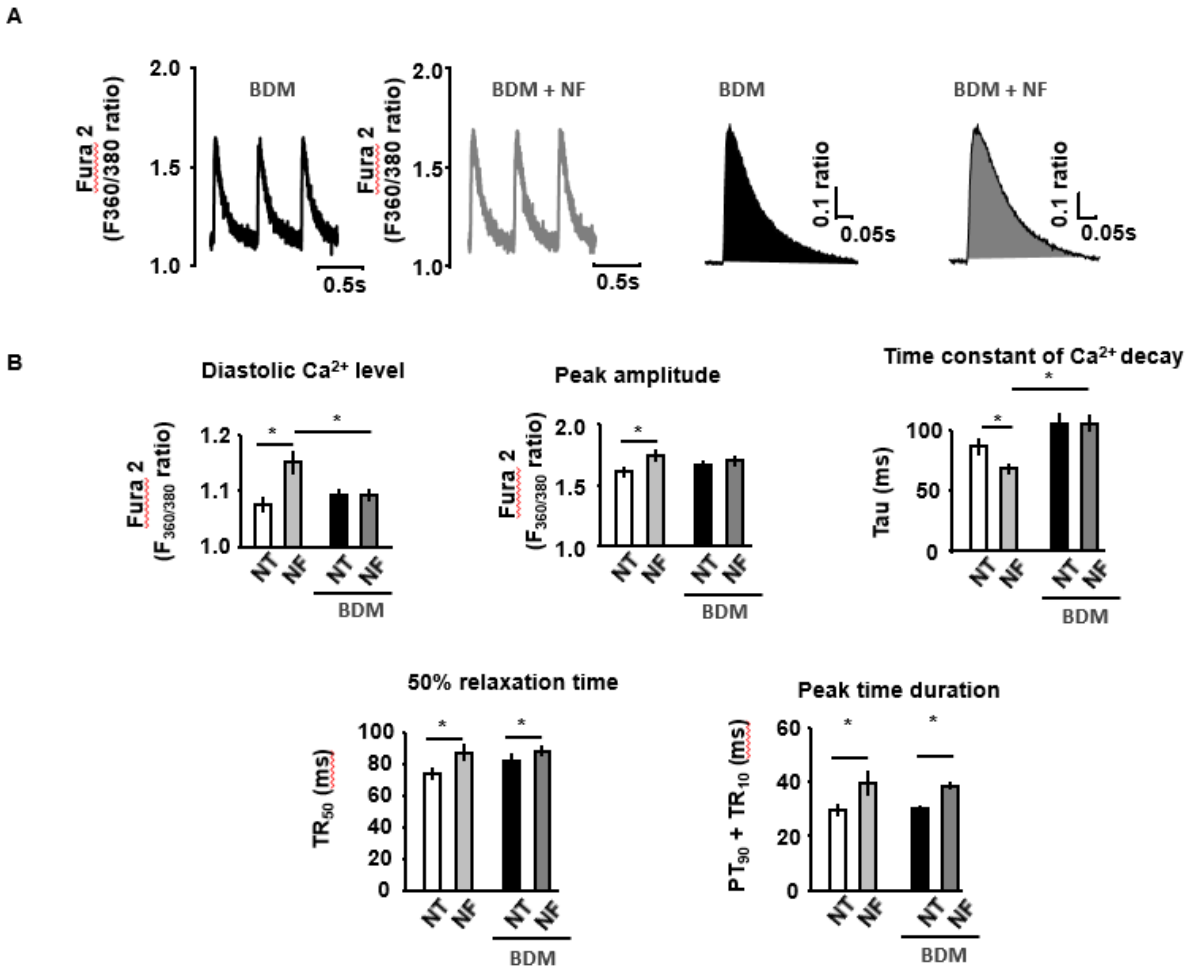

Figure 10. Effect of NF on $[Ca^{2+}]_i$ in BDM-pretreated LV myocytes

Representative $[Ca^{2+}]_i$ A. and mean vales of $[Ca^{2+}]_i$ transient parameters B. NF-induced increase in diastolic and systolic $[Ca^{2+}]_i$ were abolished by BDM (5 mM). Time constant of Ca^{2+} decay (tau) was not facilitated in NF in the presence of BDM. Peak time duration remained unaltered by BDM pretreatment.

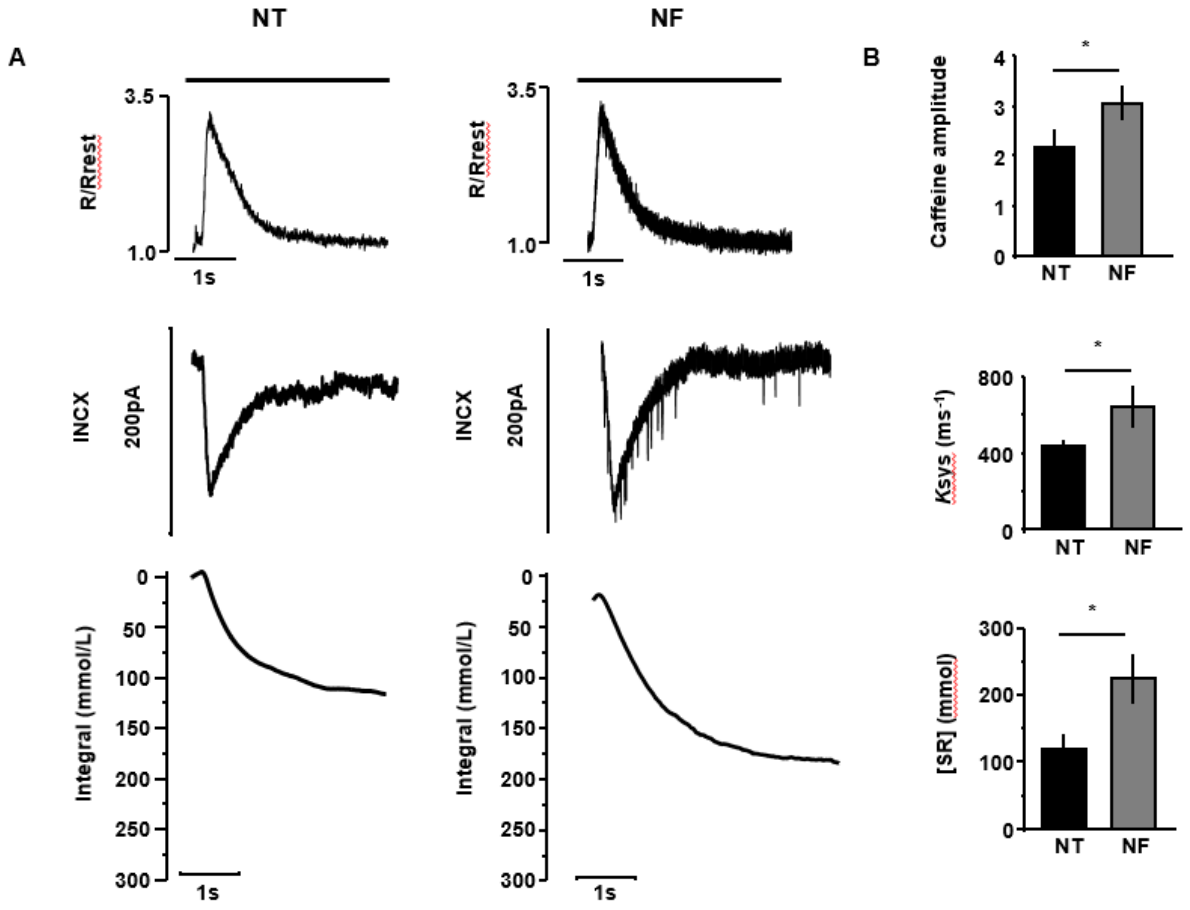

Figure 11. The effects of NF on Ca^{2+} signaling in ventricular myocytes from normal rat heart

A. Expended records of the effects of applying caffeine (5mM, for the period shown by the horizontal bars) to measure SR Ca content. Traces show (from top to botton): Ca, membrane current, and integrated current. B. From top to botton: Rate constant of decay of the systolic Ca transient (Caffeine); Amplitude of the caffeine-evoked increased of Ca; Calculated SR Ca content.

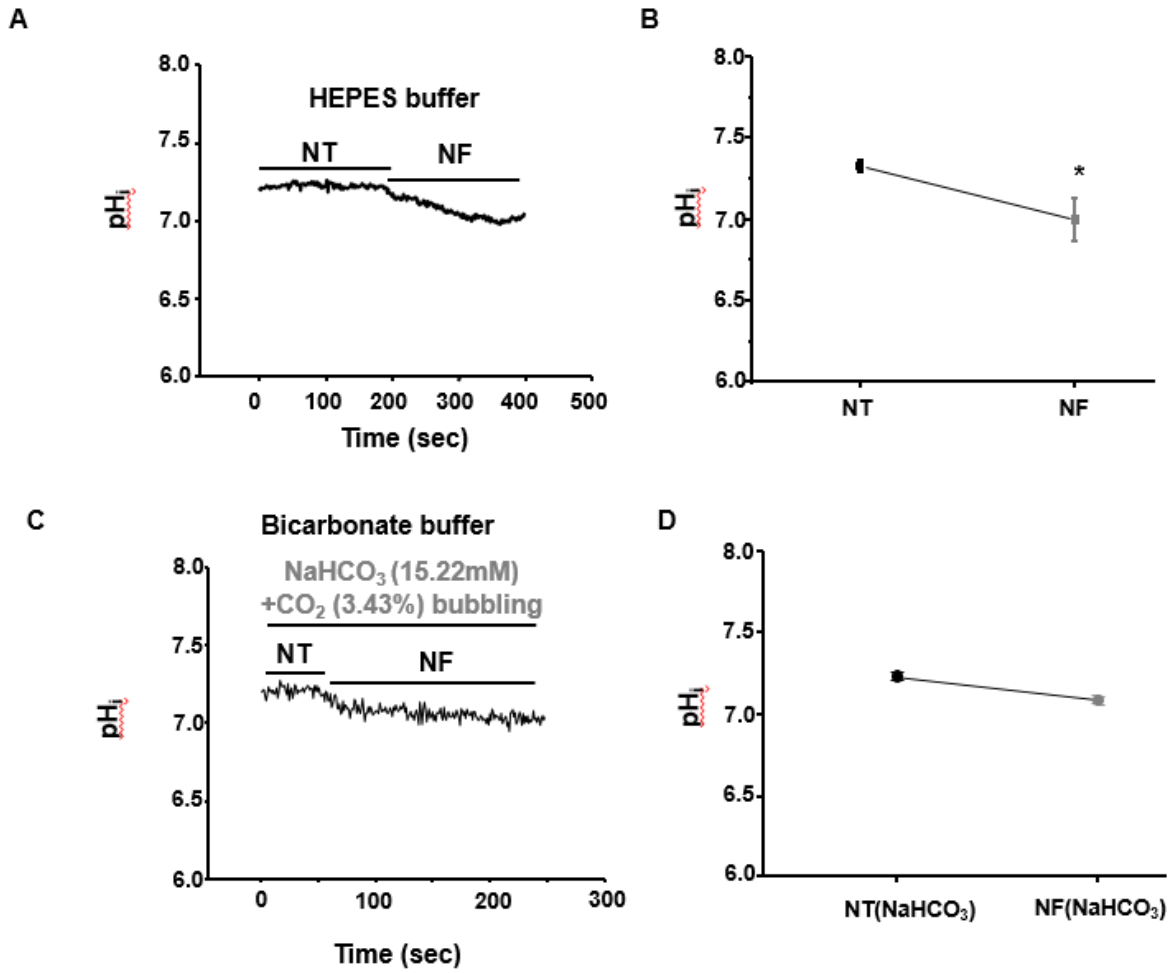

Figure 12. NF regulation of intracellular pH

A. Representative recording of pH_i in NT and NF using HEPES buffer. B. Mean values of pH_i in NT and NF, pH_i was significantly reduced by NF. C. Representative recording of pHi in NT and NF using HCO_3^- buffer. D. Mean values of pH_i in NT and NF, pH_i changes was weaken in NF with HCO_3^- buffering.

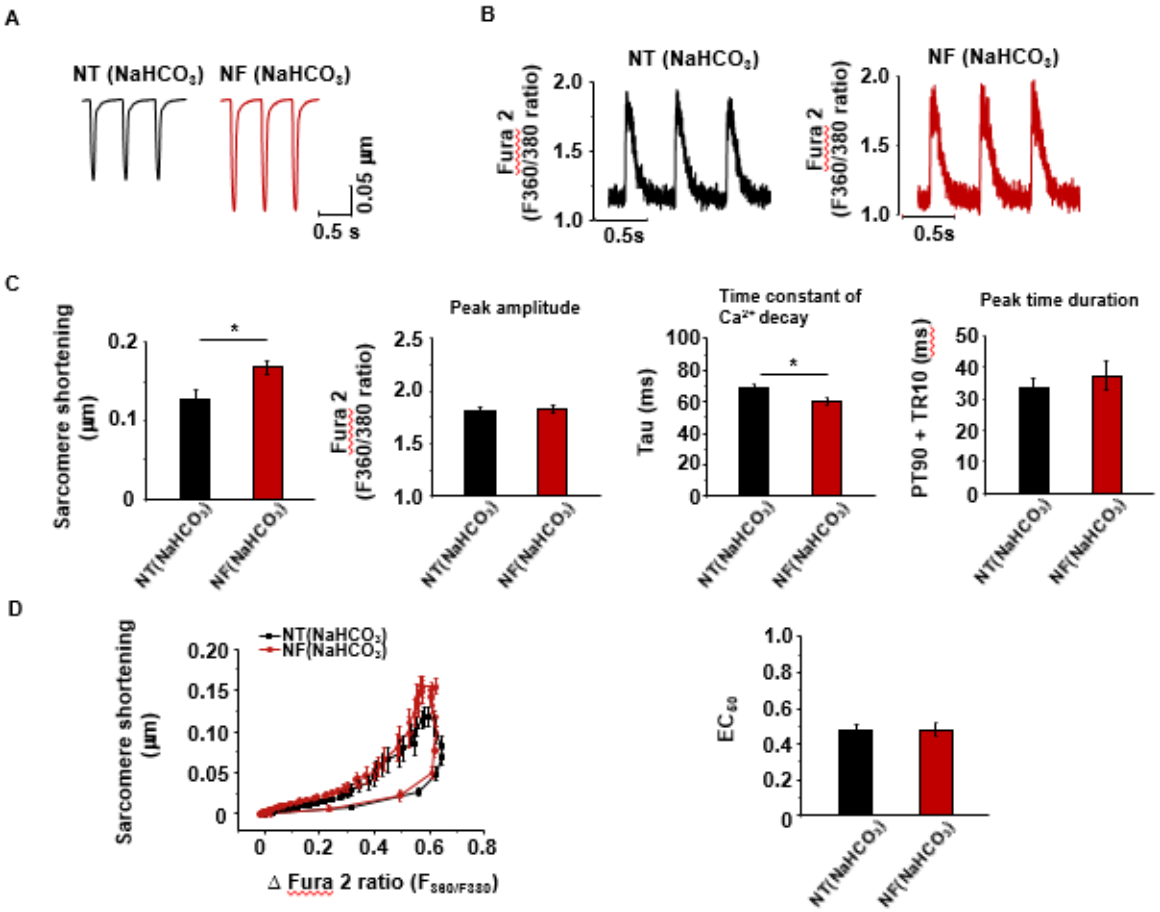

Figure 13. NF regulation of sarcomere shortening and intracellular Ca^{2+} transients in HCO_3^--pretreated LV myocytes

A. Representative sarcomere shortening in NT and NF with $NaHCO_3$ buffering. B. Representative $[Ca^{2+}]_i$ transient in NT and NF with $NaHCO_3$ buffering. C. Mean values of $[Ca^{2+}]_i$ transient parameters. NF significantly increase sarcomere shortening, however NF did not increase peak amplitude $[Ca^{2+}]_i$. Peak time duration (PT90 + TR10) was not change in NF; however, time constant of $[Ca^{2+}]_i$ decay (tau) was facilitated in NF. D. Phase-plane loop of sarcomere shortening/relengthening vs. $[Ca^{2+}]_i$ transient. The relaxation phase of the loop shifted to the right in NF compared to that in NT in the presence of HCO_3^-. Ca^{2+} concentration at 50 % sarcomere relengthening (EC_{50}) was not change in NF with HCO_3^- buffering.

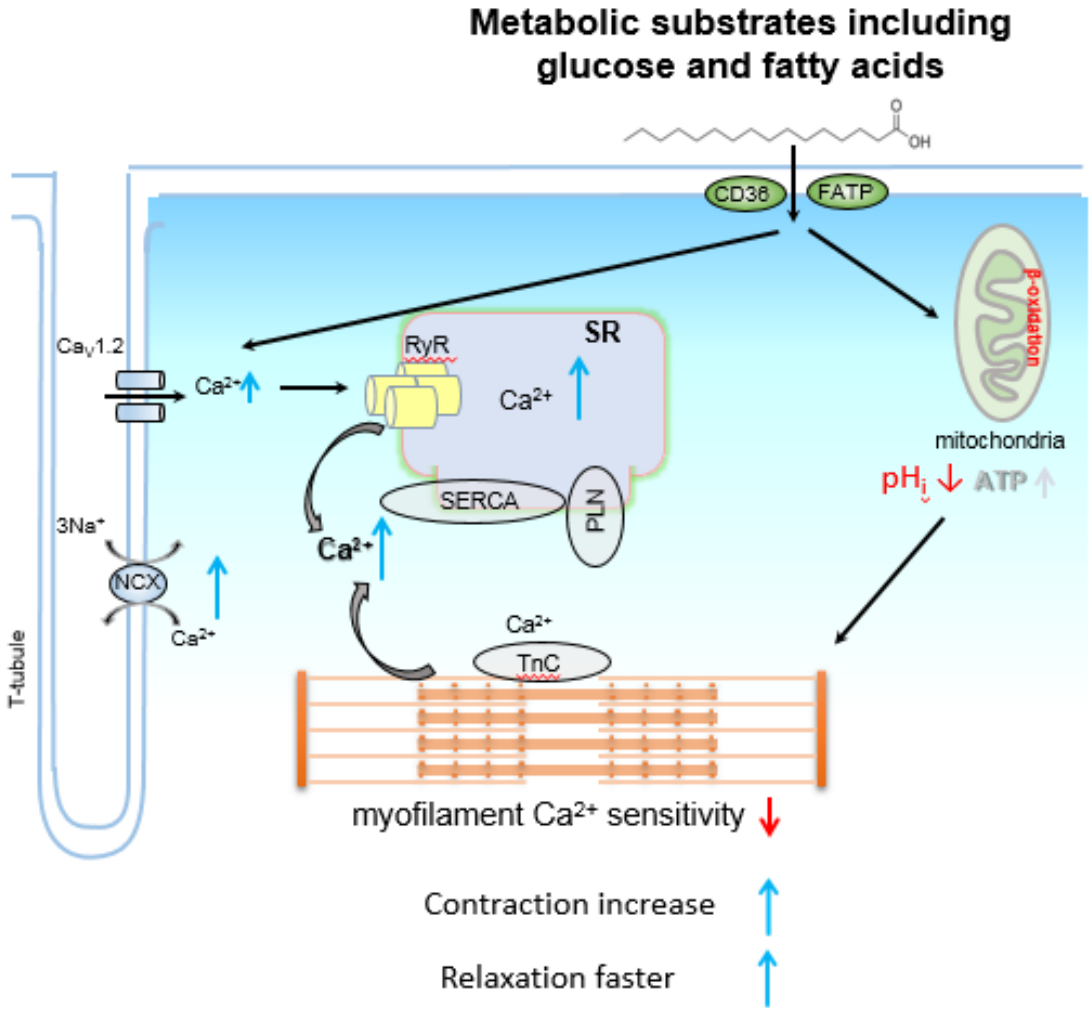

Figure 14. Summary

Schematic diagram of cardiac excitation–contraction coupling in the presence of major metabolic substrates including FAs and glucose at physiological concentration. Contraction is enhanced with metabolic substrates' supplementation. Mechanistically, Ca^{2+} influx through LTCC is increased, leads to greater Ca^{2+} release from the SR, and increases intracellular free Ca^{2+}. Reuptake of Ca^{2+} via SERCA is facilitated. Myofilament Ca^{2+} sensitivity is reduced, possibly via reduced pH_i, which in part is responsible for greater intracellular Ca^{2+} level and decline in rat LV myocytes.

Part III:

Metabolic substrate is affecting the LV myocyte contraction and $[Ca^{2+}]_i$ by regulating myofilament Ca^{2+} sensitivity in Ang II-induced hypertensive rat heart.

Systemic blood pressure is increased and fatty acid concentration is not changed in Ang II-treated rat hearts

Both systolic and diastolic blood pressures were increased 1 wk after Ang II infusion (125 ng/min/kg) and continuously increased up to the period studied (Figure 15A). At 4 wks., systolic blood pressure was 131.4±1.9 mmHg in shams *vs.* 156.9±2.8 mmHg with Ang II 4w (P<0.001, n=52, n=52); diastolic blood pressure was 97.2±1.4 mmHg in shams *vs.* 118.5±2.3 mmHg with Ang II 4w (P<0.001, n=52, n=52). Heart rate was significantly lower in Ang II 4w rats (heart rate, beats/min: 460.7±3.8 in shams and 448.3±5.0 with Ang II 4w, P=0.004). Autopsy weight of LV myocardium and dimensions of LV myocytes were measured to assess whether systemic hypertension in these rats was associated with myocardial hypertrophy. As shown in Table 2, heart weight or heart/body weight ratio of LV myocytes were not increased in Ang II-induced hypertensive rats (heart weight in g, 2.27±0.04 in sham *vs.* 2.33±0.04 with hypertensive rats, P=0.35, n=28 and 34; heart/body weight ratio×100%, 0.61±0.01% in shams *vs.* 0.64±0.01% with hypertensive rats, P=0.2, n=16 and n=18; the slack length of sarcomere was not changed (P=0.06, n=133 and n=97).

These results demonstrate that Ang II infusion induced hypertension in rats; at 4 weeks, systolic function was significantly impaired whereas diastolic function was not altered. And the fatty acid concentration in serum were not changed in hypertensive rat.

Intracellular myofilament Ca^{2+} sensitivity and change of intracellular Ca^{2+} ($[Ca^{2+}]_i$) in

basal condition in hypertensive rats.

NF increased myocyte contraction from hypertensive rats, similar to those shown in sham. First, I examined whether myofilament Ca^{2+} sensitivity is modulated in LV myocyte from hypertensive rat heart, I simultaneously recorded sarcomere shortening and $[Ca^{2+}]_i$ in Fura-2-loaded LV myocytes and plotted a phase-plane loop of the changes in sarcomere length vs. $[Ca^{2+}]_i$ transient in basal condition in sham and hypertensive rat. As shown in Fig. 17A, B, relaxation phase of the sarcomere length-$[Ca^{2+}]_i$ transient relationship shifted to the right in NT; $[Ca^{2+}]_i$ at 50 % sarcomere relengthening (EC_{50}) was significantly increased (P=0.006, n=12, n=17), indicative of myofilament Ca^{2+} desensitization in hypertensive rat heart.

Next, I tested whether intracellular Ca^{2+} transient ($[Ca^{2+}]_i$) was increased in LV myocytes from HTN rat heart. As shown in Fig. 18A, B, the diastolic and systolic $[Ca^{2+}]_i$ (F360/380: P <0.001 and P<0.001, n=26, n=18). Analysis of $[Ca^{2+}]_i$ profile showed that the time constant of $[Ca^{2+}]_i$ decay (tau, ms) was abbreviated in HTN (P =0.015).

These results suggest the changes of intracellular Ca^{2+} transient ($[Ca^{2+}]_i$) in basal condition in HTN, it's maybe caused by modulating myofilament Ca^{2+} desensitization.

Myofilament Ca^{2+} sensitivity and desensitization (BDM) regulates $[Ca^{2+}]_i$ in NT in HTN

To test whether myofilament Ca^{2+} sensitivity as a Ca^{2+} buffer regulated the intracellular Ca^{2+} transient, I tested whether myofilament Ca^{2+} desensitization with a potent myosin ATPase inhibitor, BDM, prevents increased $[Ca^{2+}]_i$ and facilitated tau of $[Ca^{2+}]_i$ in NT in HTN. As shown in Fig. 19A, B, incubation of LV myocytes with BDM (5 mM) abolished the increased diastolic and systolic $[Ca^{2+}]_i$ and faster tau (P=0.81 in diastole; P=0.41 in systole; P=0.53 for tau in NT between sham and HTN; n=25, n=12).

These results suggest that $[Ca^{2+}]_i$ was authentically changed in basal condition in HTN. And suggest that reduced myofilament Ca^{2+} sensitivity in NT in HTN, at least in part, increase $[Ca^{2+}]_i$ and facilitate $[Ca^{2+}]_i$ decline in rat LV myocytes.

Intracellular myofilament Ca^{2+} sensitivity and change of intracellular Ca^{2+} ($[Ca^{2+}]_i$) in NF condition in hypertensive rat

To test whether myofilament Ca^{2+} sensitivity is modulated in LV myocyte from hypertensive rat heart, I simultaneously recorded sarcomere shortening and $[Ca^{2+}]_i$ in Fura-2-loaded LV myocytes and plotted a phase-plane loop of the changes in sarcomere length vs. $[Ca^{2+}]_i$ transient in NF in hypertensive rat. As shown in Fig. 20A, B, relaxation phase of the sarcomere length-$[Ca^{2+}]_i$ transient relationship shifted to the right in NF; $[Ca^{2+}]_i$ at 50 % sarcomere relengthening (EC_{50}) was significantly increased (P<0.001, n=17), indicative of NF decreased myofilament Ca^{2+} sensitization in hypertensive rat heart.

Next, I tested whether NF increased $[Ca^{2+}]_i$ in HTN. As shown in Fig. 21A, B, NF significantly increased the diastolic and systolic $[Ca^{2+}]_i$ (F360/380: P < 0.001 and P < 0.001, n = 18, n = 18). Analysis of $[Ca^{2+}]_i$ profile showed that the time constant of $[Ca^{2+}]_i$ decay (tau, ms) was abbreviated in NF (P < 0.001, Fig. 6B).

These results suggest that metabolic substrate changed of intracellular Ca^{2+} transient ($[Ca^{2+}]_i$) in HTN, and it's maybe caused by modulating myofilament Ca^{2+} desensitization.

L-type Ca^{2+} current (I_{Ca}) and action potential profile

I aimed to test the key elements of excitation-contraction coupling responsible for increased myocyte $[Ca^{2+}]_i$ and contraction in NF in HTN. Fig. 22A, B showed raw traces and averaged current–voltage (I–V) relationships of I_{Ca} in LV myocytes before and after NF. And the inset

in Fig.22A showed raw traces of I_{Ca} at 0 mV for Ca^{2+} influx analysis. NF reduced the amplitude of I_{Ca} at 0 mV (current density of I_{Ca} at 0 mV, pA/pF: $P<0.05$ between NT and NF, n =4, n =4) and the inactivation of I_{Ca} at 0 mV was not changed (in ms, Tau_{slow}: P =0.201; Tau_{fast}: P = 0.12, Fig. 22B). As a result, total Ca^{2+} influx via LTCC (integral of I_{Ca}) was reduced in NF in HTN (P = 0.05 between NT and NF at 0 mV). However, integral of I_{Ca} was not changed at 0 mV (P = 0.989). Furthermore, NF did not affect the repolarization duration of APD (Fig. 22C).

These results suggest that Ca^{2+} influx via LTCC is not the major source of increased intracellular Ca^{2+} $[Ca^{2+}]_i$ in NF in HTN.

Myofilament Ca^{2+} sensitivity and desensitization (BDM) regulates $[Ca^{2+}]_i$ in NF in HTN

To test whether NF increased the intracellular Ca^{2+} by regulating myofilament Ca^{2+} sensitivity as a Ca^{2+} buffer, I tested whether myofilament Ca^{2+} desensitization with a potent myosin ATPase inhibitor, BDM, prevents increased $[Ca^{2+}]_i$ and facilitated tau of $[Ca^{2+}]_i$ in NF in HTN. As shown in Fig. 23A, B, incubation of LV myocytes with BDM (5mM) abolished the increased the diastolic and systolic $[Ca^{2+}]_i$ and faster tau (P=0.10 in diastole; P=0.26 in systole; P=0.65 for tau in NT between sham and HTN; n=12, n=12).

These results suggest that $[Ca^{2+}]_i$ was authentically changed by myofilament Ca^{2+} buffer in NF in HTN. And suggest that reduced myofilament Ca^{2+} sensitivity in NF in HTN, at least in part, increase $[Ca^{2+}]_i$ and facilitate $[Ca^{2+}]_i$ decline in rat LV myocytes.

Table 2. Body weight, heart weight and LV myocyte dimensions in sham and hypertensive rat.

	sham (n)	Hypertension (n)	P value
Body weight (g)	363.7±1.69 (196)	359±1.73 (197)	0.1
Heart weight (g)	2.27±0.04 (28)	2.33±0.04 (34)	0.35
Heart weight/ body weight x 100%	0.61±0.01 (28)	0.64±0.01 (34)	0.01
Sarcomere length (mM)	1.77±0.004 (133)	1.76±0.004 (97)	0.06

Values are expressed as means ± SEM. *P< 0.05 .

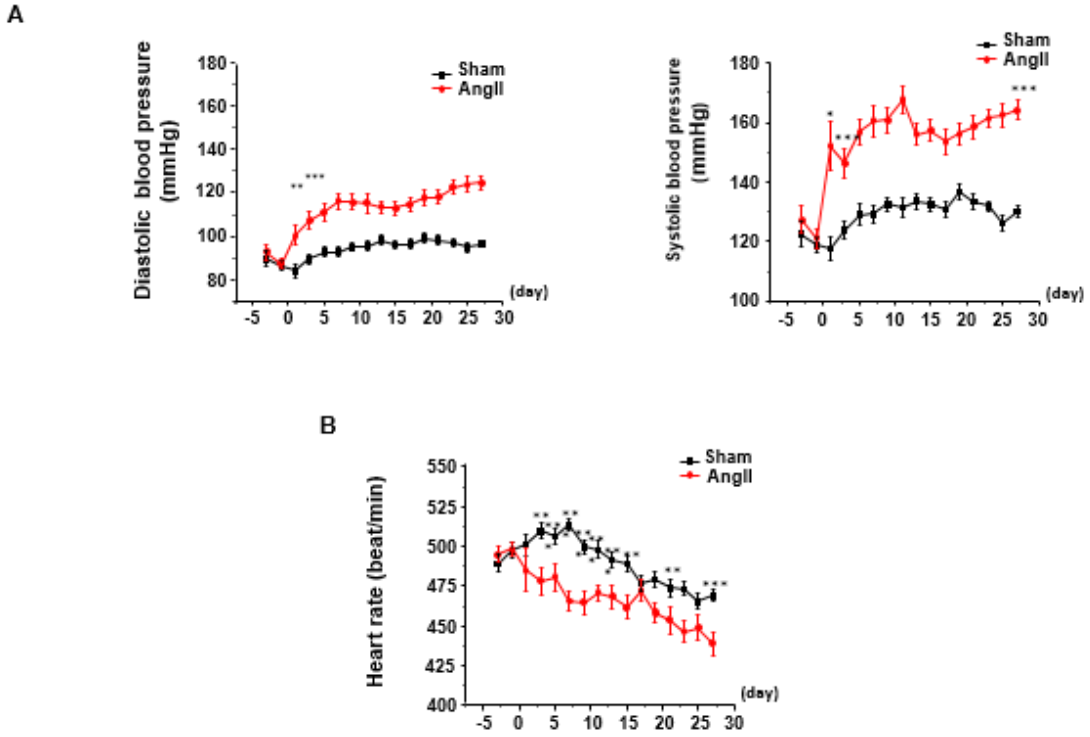

Figure 15. Systolic and diastolic blood pressure measurements in normal and hypertensive rats

A. Time course of the mean systolic (left) and diastolic (right) blood pressures in Ang II-rats vs. sham. High blood pressure develops from 1 wk infusion with Ang II and continuously increases until 4 wks (systolic blood pressure, $P<0.001$, n=52, n=52; diastolic blood pressure, $P<0.001$. n=52, n=52). B. Heart rate was significantly lower in Ang II 4w rats ($P=0.004$, n=52, n=52).

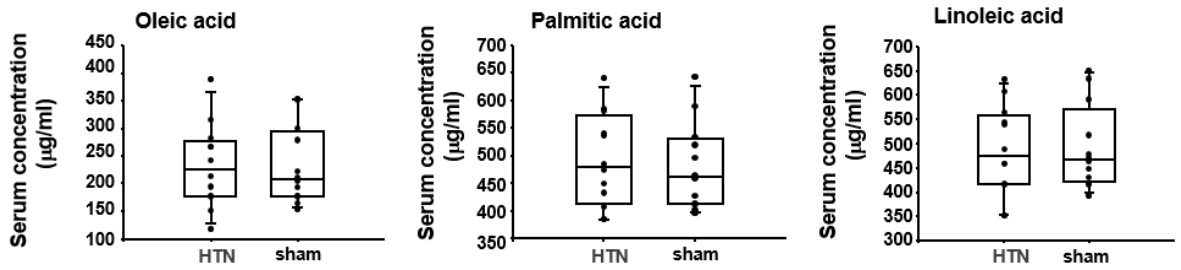

Figure 16. Fatty acid concentration in the plasma from sham and hypertension rats.

Oleic, Palmitic acid and Linoleic acid concentration were not changed in sham and hypertensive rat.

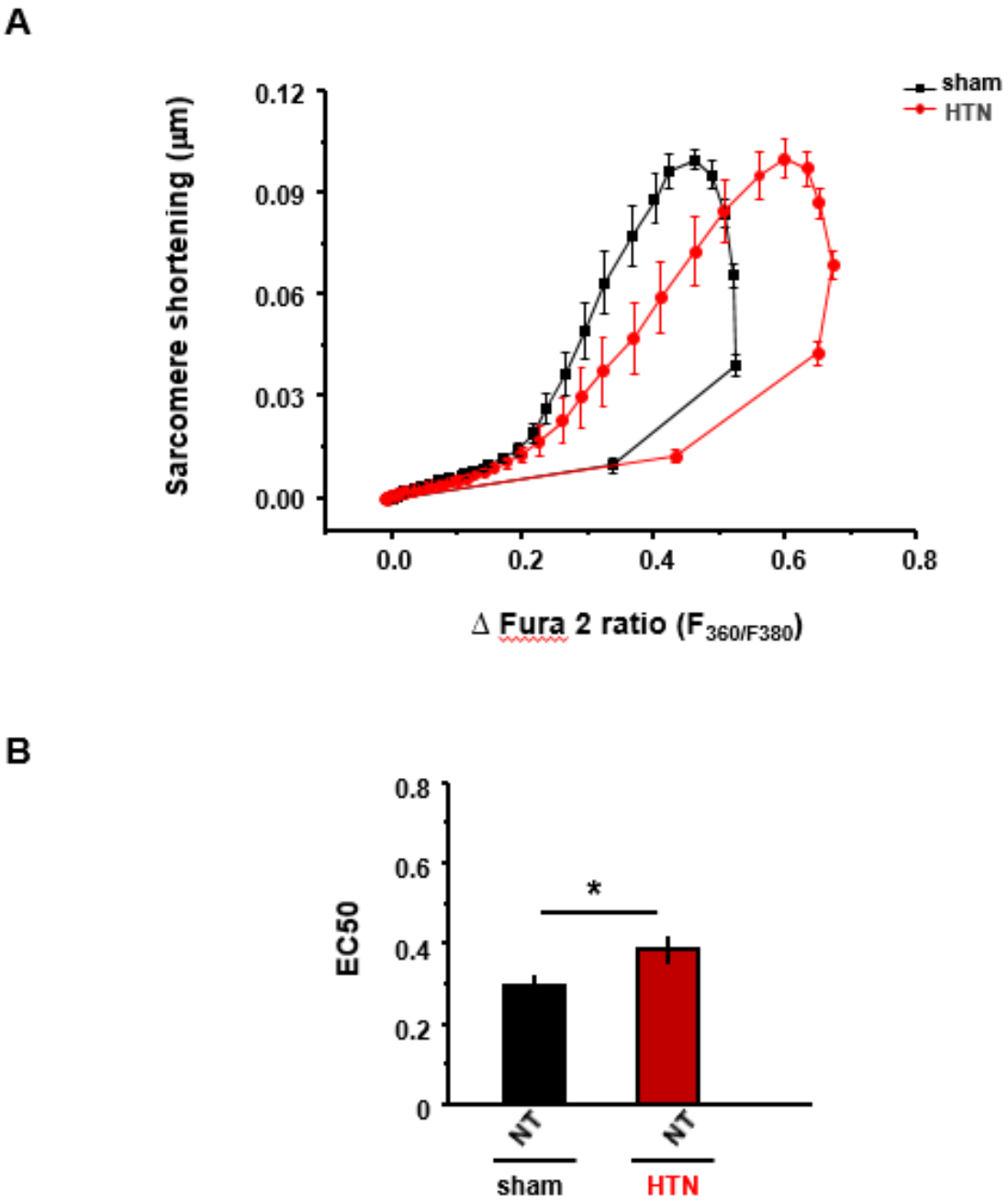

Figure 17. Difference of myofilament Ca^{2+} sensitivity in sham and hypertensive rats.

A. Phase-plane loop of sarcomere shortening/relengthening vs. $[Ca^{2+}]_i$ transient. The relaxation phase of the loop shifted to the right in hypertensive compared to in sham. B. Ca^{2+} concentration at 50 % sarcomere relengthening (EC_{50}) was significantly larger in hypertensive rats.

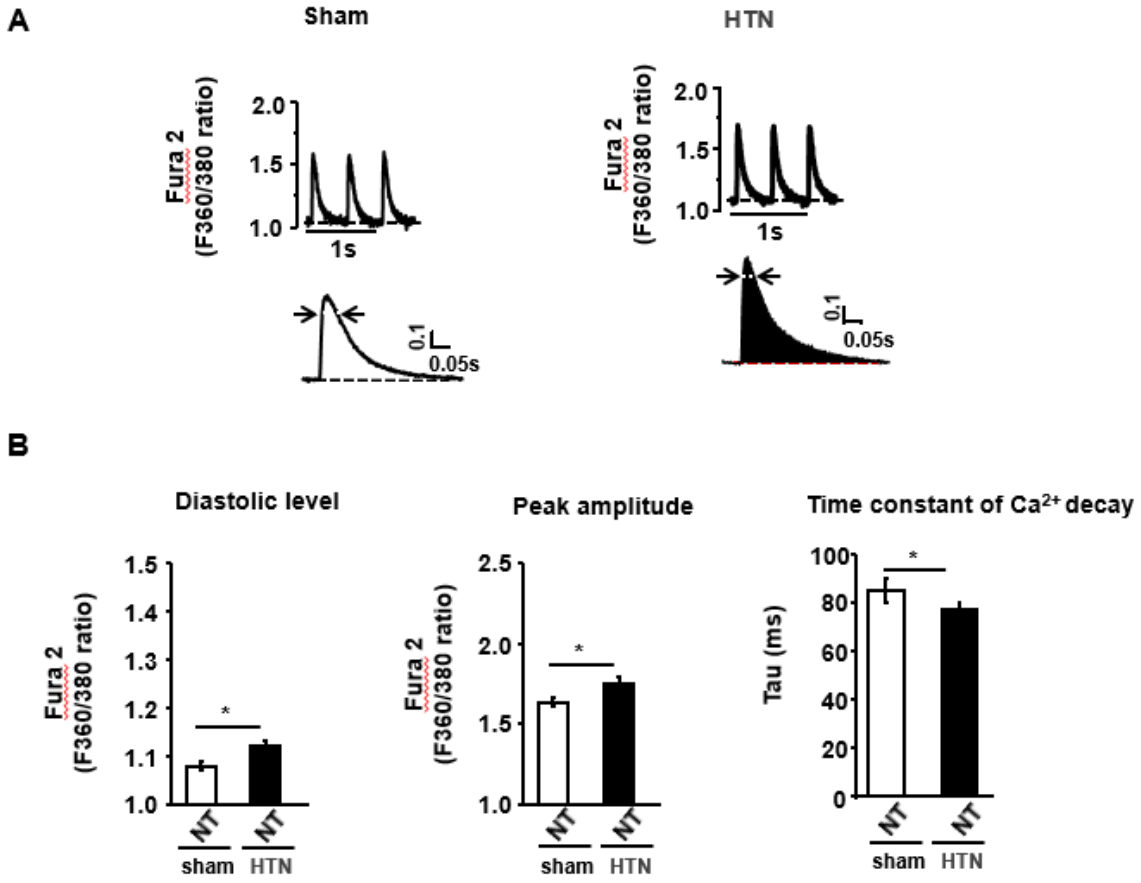

Figure 18. Difference of intracellular Ca^{2+} transient from sham and hypertensive rat heart

A. Representative $[Ca^{2+}]_i$ transients in LV myocyte from sham and hypertensive rats. B. Mean values of $[Ca^{2+}]_i$ transient parameters. Diastolic and peak amplitude of $[Ca^{2+}]_i$ were significantly increased and time constant of $[Ca^{2+}]_i$ decay (tau) was facilitated in hypertensive rats.

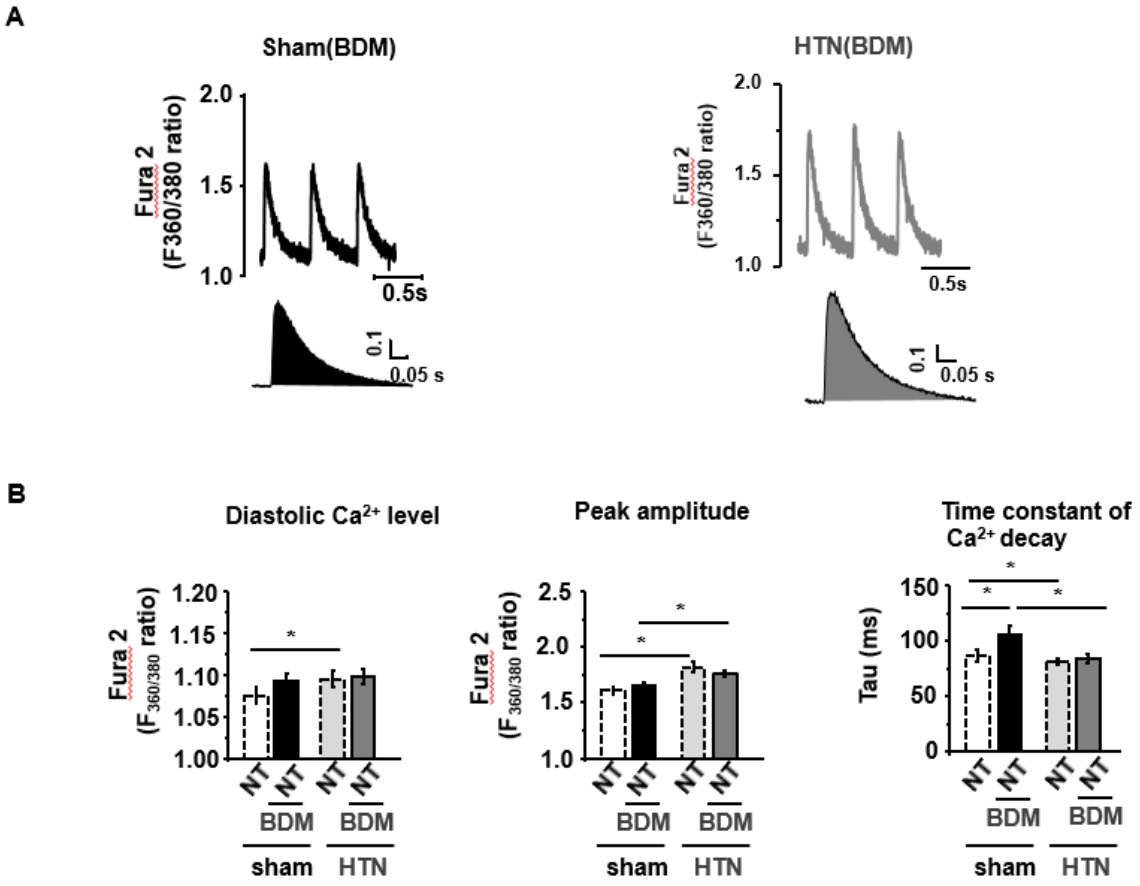

Figure 19. Effect of BDM on $[Ca^{2+}]_i$ in LV myocytes from sham and hypertensive rat hearts

Representative $[Ca^{2+}]_i$ (A) and mean vales of $[Ca^{2+}]_i$ transient parameters (B). The increased diastolic and systolic $[Ca^{2+}]_i$ in hypertensive were abolished by BDM (5 mM). Time constant of Ca^{2+} decay (tau) was facilitated in hypertensive rat heart that compared to sham in the presence of BDM.

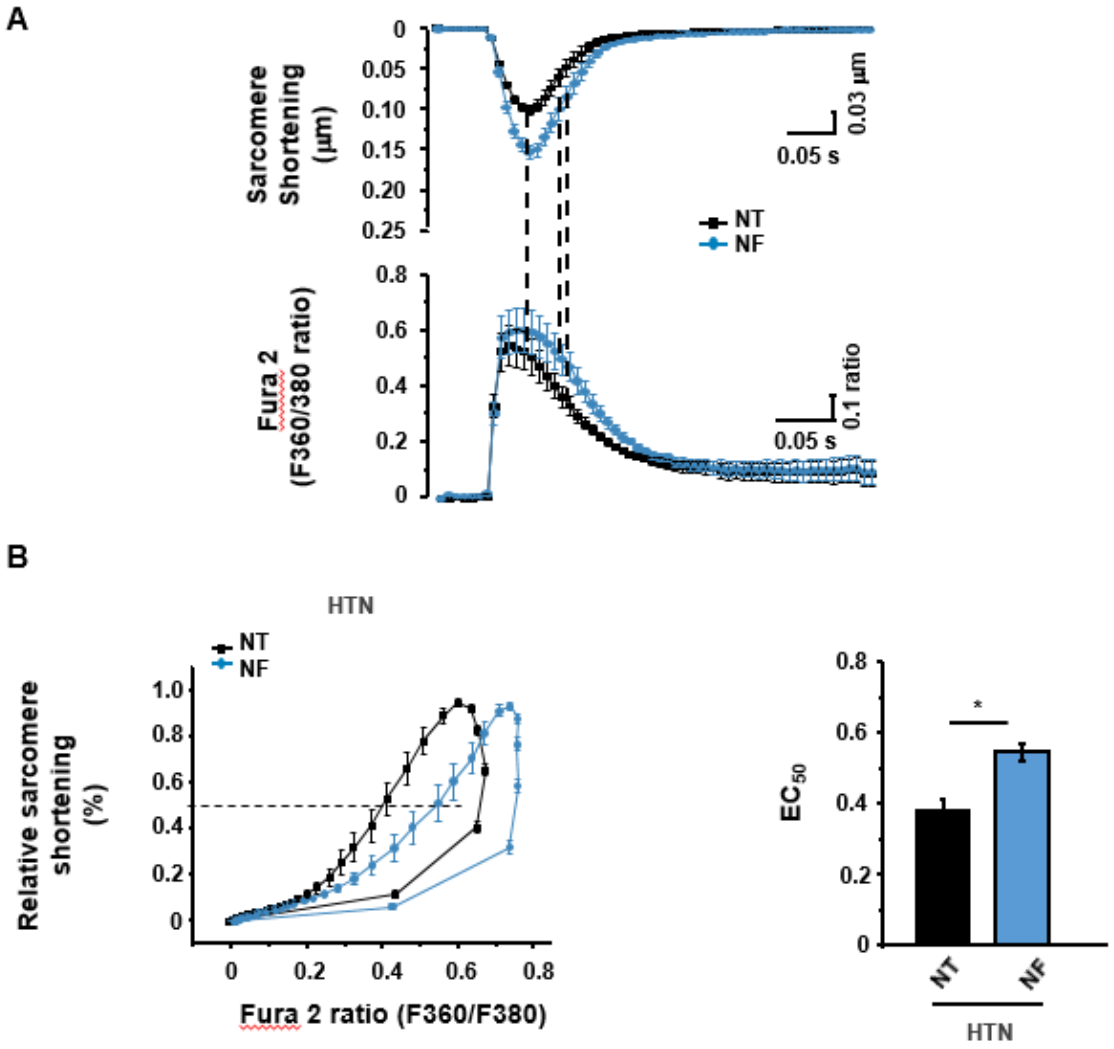

Figure 20. NF regulation of myofilament Ca^{2+} sensitivity in hypertensive rats

A. Simultaneous recordings of LV myocyte sarcomere shortening/ relengthening and intracellular Ca^{2+} transients in NT and NF. B. Phase-plane loop of sarcomere shortening/relengthening vs. $[Ca^{2+}]_i$ transient. The relaxation phase of the loop shifted to the right in NF compared to that in NT. Ca^{2+} concentration at 50 % sarcomere relengthening (EC_{50}) was significantly larger in NF in hypertensive rat heart.

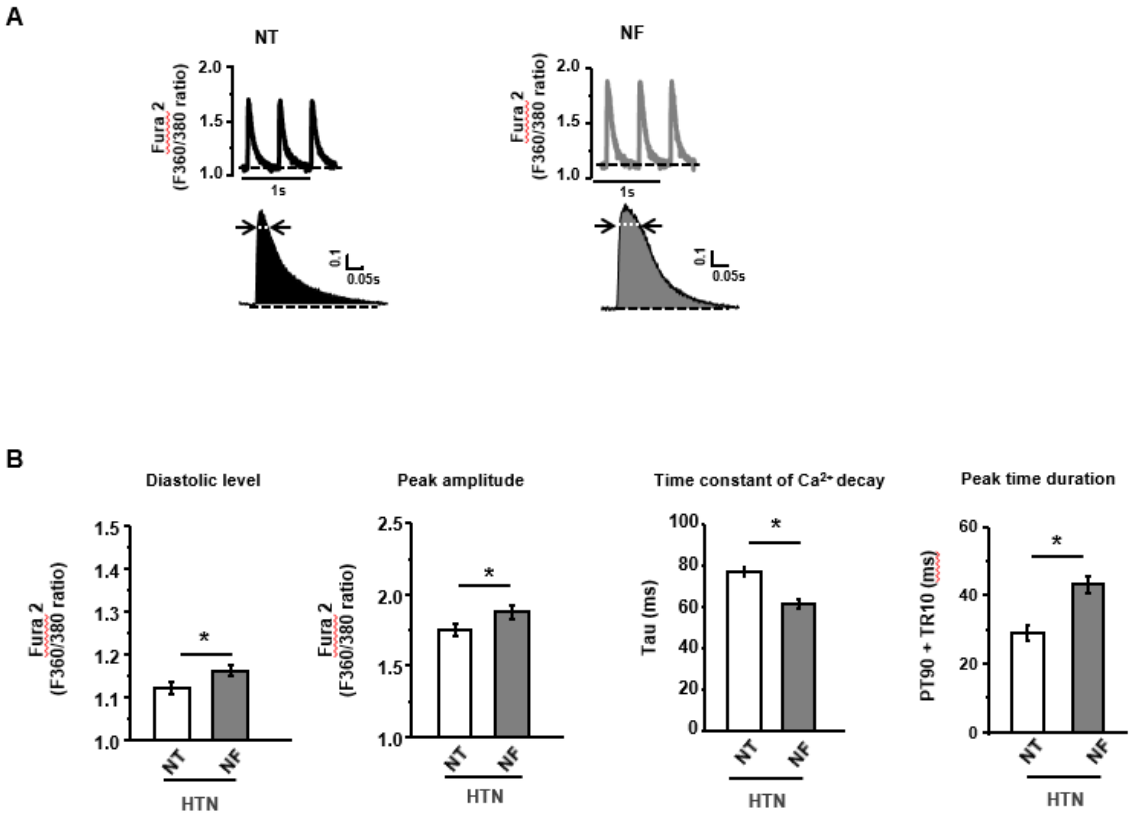

Figure 21. NF regulation of intracellular Ca^{2+} transients in hypertensive rat hearts

A. Representative $[Ca^{2+}]_i$ transients in NT and NF. B. Mean values of $[Ca^{2+}]_i$ transient parameters. NF significantly increased diastolic $[Ca^{2+}]_i$ and peak amplitude of $[Ca^{2+}]_i$. Time constant of $[Ca^{2+}]_i$ decay (tau) was facilitated in NF. Peak $[Ca^{2+}]_i$ duration (90% peak time+10% time to relaxation, PT90+TR10) was prolonged.

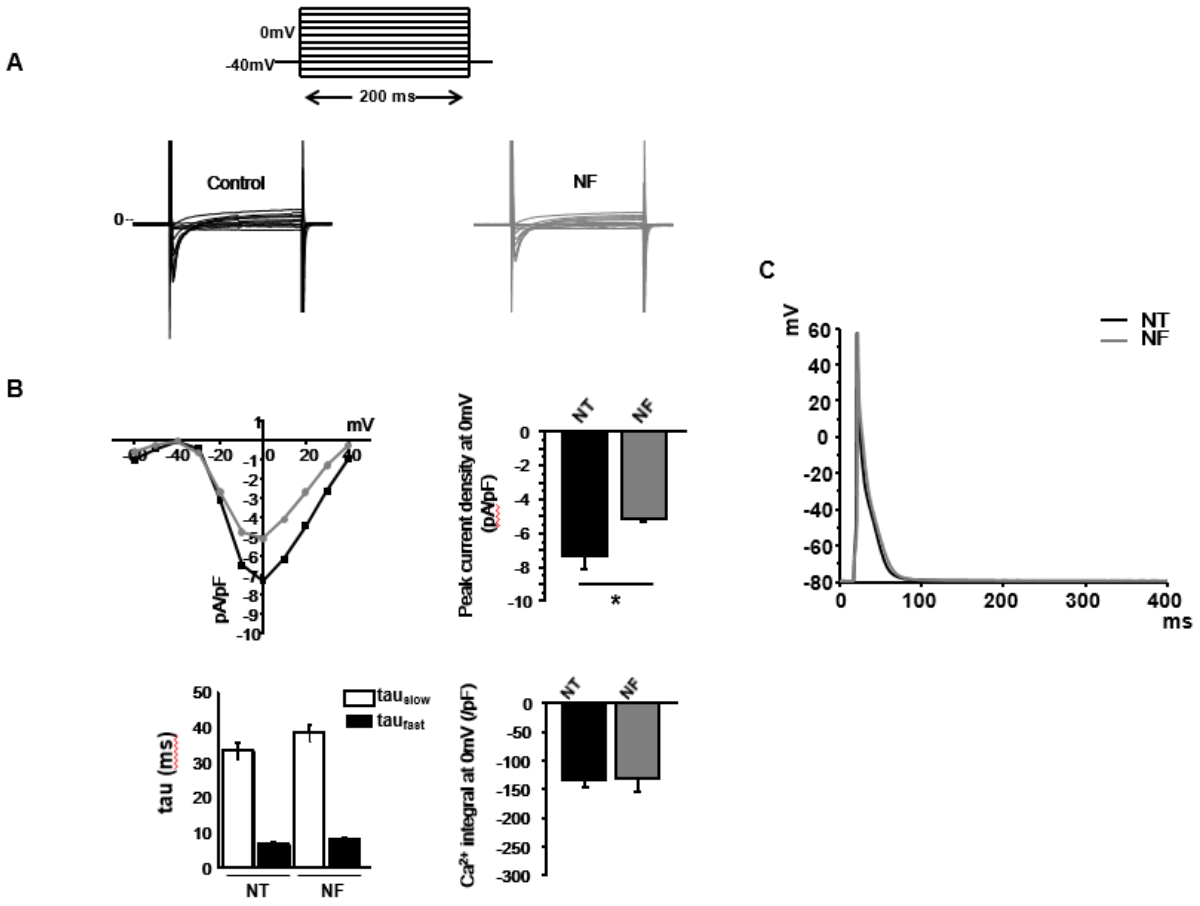

Figure 22. Patch-clamp recordings of LTCC activities with NF in hypertensive rat

A, B. Pulse protocol, representative I_{Ca} and the corresponding I-V relationship, peak I_{Ca} at 0 mV, Tau of I_{Ca} inactivation parameters, and the integral of Ca^{2+} influx in NF. NF reduced peak I_{Ca} density, and the integral of I_{Ca} at 0 mV was not changed. C. Representative action potential recordings in NT and NF in HTN. NF did not affect the action potential profile.

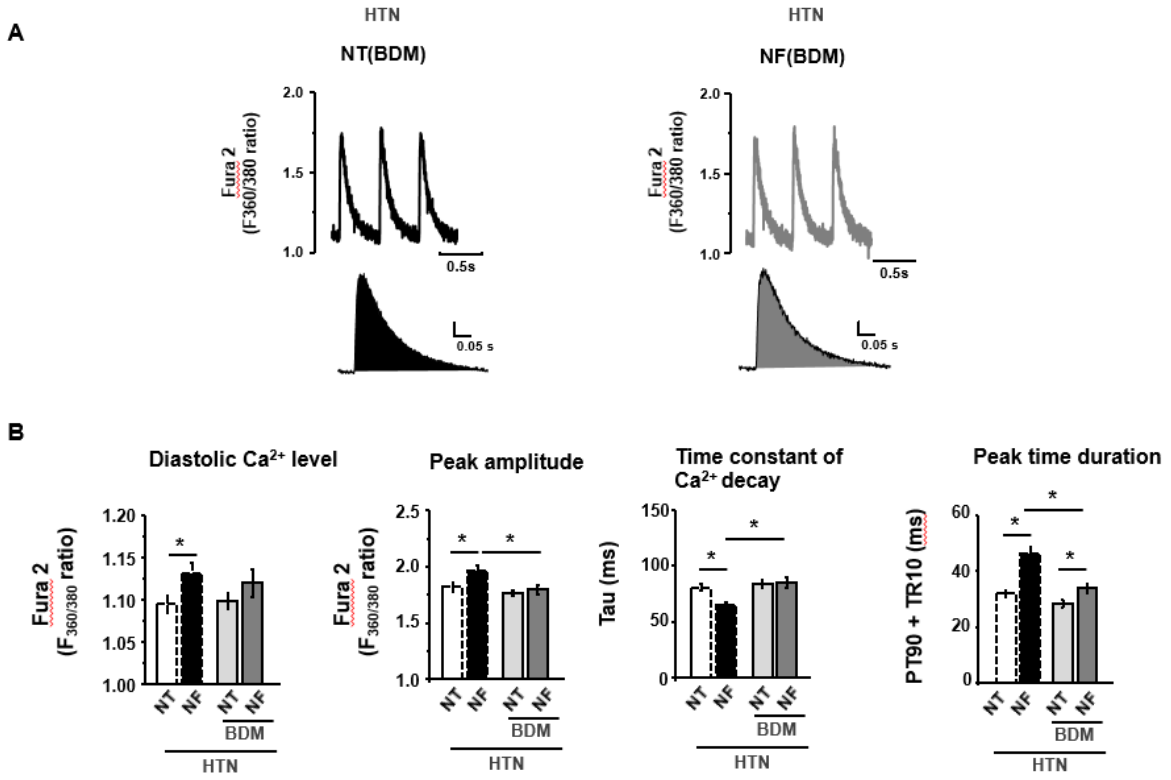

Figure 23. Effect of NF on $[Ca^{2+}]_i$ in BDM-pretreated LV myocytes in hypertensive rat

Representative $[Ca^{2+}]_i$ (A) and mean vales of $[Ca^{2+}]_i$ transient parameters (B). NF-induced increase in diastolic and systolic $[Ca^{2+}]_i$ were abolished by BDM (5 mM). Time constant of Ca^{2+} decay (tau) was not facilitated in NF in the presence of BDM. Peak time duration remained unaltered by BDM pretreatment.

Part IV:

1. Metabolic substrate' regulation of cardiac myocyte contraction and the roles of eNOS and nNOS in LV myocytes from sham rat heart.

Metabolic substrates' regulation of LV myocyte contraction in normal rats

As shown in Fig. 24A, B, supplementation of metabolic substrates (NF) increased LV myocyte contraction (delta amplitude of sarcomere shortening in NF at steady-state: $P<0.001$ compared to that in NT, n=29 & 29) and facilitated relaxation (time to 50% relaxation, $P<0.02$) without changing peak time (time to peak, $P=0.1$). Beta-adrenergic stimulation with isoprenaline (ISO, 50 nM) increased myocyte shortening in NF ($P<0.001$ between NF+ISO and NF), so that the sarcomere shortening in NF+ISO was significantly greater than NT+ISO ($P<0.001$, n=29 & n=29). The delta increment by ISO was comparable before and after NF (P<0.05, between NF and NF+ISO, data not shown).

Notably, NF induced delayed after contraction (DAC) (Fig. 24A, B, C) during diastole following ISO application in almost all the myocytes tested. The frequency of DAC (2 min after ISO treatment for 50s) was ~ 10% (Fig. 24D). In contrast, no DAC was induced in NT+ISO (Fig. 24D).

These results demonstrate that supplementation of cardiac favorable metabolic substrates (e.g. fatty acids) increased myocyte contraction in rat hearts. However, LV myocytes were vulnerable to arrhythmic contractions in the presence of the metabolic substrates after beta-adrenergic stimulation.

Insulin and NO signaling in NF and NF+ISO

Insulin-dependent signaling pathway is an important mechanism to support glucose and fatty acid uptake into the myocytes and is an essential element in cardiac metabolism (Randle PJ et al., 1963; Sowers JR et al., 1997). On the other hand, impaired insulin signaling has been associated with metabolic syndrome and predisposes cardiac arrhythmias. Therefore, I tested whether insulin signaling is affected by NF and NF+ISO.

As shown in Fig. 25A, tyrosine phosphorylation of insulin receptor β-subunit (IRβ-Tyr) and insulin receptor substrate-1 (IRS-1-Tyr) were significantly increased by insulin in NT in normal rat (IRβ-Tyr/IRβ ratio, P=0.016, n=5; IRS-1-Tyr/IRS-1 ratio, P=0.03, n=4). ISO did not affect tyrosine phosphorylation of IRβ or IRS-1 with insulin either in NT or in NF (P=0.39 and P=0.9 before and after ISO, Fig. 25A). However, IRβ-Tyr and IRS-1-Tyr were blunted in NF (IRβ-Tyr/IRβ ratio, P=0.6, n=5; IRS-1-Tyr/IRS-1 ratio, P=0.9, n=4).

eNOS is an important downstream target of insulin signaling (Montagnani M et al., 2002; Yu QJ et al., 2008), which has been shown to mediate anti-adrenergic effect of insulin on cardiac myocytes (Yu QJ et al., 2008). It is possible that impaired insulin signaling in NF is associated with eNOS down-regulation. Indeed, eNOS phosphorylation at an active phosphorylation site (eNOS-Ser^{1177}) was significantly reduced by NF (between NT and NF: eNOS-Ser^{1177}/eNOS, P=0.01, without insulin; P=0.05 with insulin, n=3, Fig. 25B).

Subsequently, I examined the functional relevance of insulin- and eNOS-regulation of myocyte contraction in NT and in NF. Fig. 25C & E showed that insulin abolished the positive inotropic effect of ISO (sarcomere shortening between NT+INS and NT+INS+ISO: P=0.54, n=29) without changing the basal sarcomere shortening (between NT and NT+INS: P=0.18). However, inhibition of eNOS with L-NAME (1 mM, >30 min) restored ISO-stimulation of

myocyte contraction in NT (*P*=0.003, between INS+L-NAME and INS+L-NAME+ISO, n=7, Fig. 25C & E). In contrast, insulin did not affect NF-enhancement of sarcomere shortening in basal (NT+INS and NF+INS, P<0.001, n=29, n=20) or with ISO (between NF+INS and NF+INS+ISO: P< 0.001, n=20, Fig. 25D & E). Furthermore, L-NAME pretreatment did not affect myocyte contraction in NF and NF+ISO with insulin (*P*<0.001 between L-NAME+INS and L-NAME+NF+INS, n=7, n=8; *P*<0.001 between L-NAME+NF+INS and L-NAME+ISO+NF+INS, n=8, Fig. 25D & E).

Since L-NAME is a non-specific inhibitor of NOS which blocks both eNOS and nNOS, I tested whether nNOS inhibitor, SMTC, mimics the effect of L-NAME. Fig. 25C & E showed that unlike L-NAME, SMTC pretreatment (100 μM, >30 min) did not restore the positive inotropic effect of ISO in NT (P=0.08, INS+SMTC & INS+ISO+SMTC, n=19). Furthermore, SMTC pretreatment did not affect myocyte contraction in NF and NF+ISO with insulin (*P*=0.007, between SMTC+INS and SMTC+NF+INS, n=19, n=10; *P*<0.001, between SMTC+NF+INS and SMTC+NF+INS+ISO, n=10)

These results suggest that eNOS is the effective downstream NOS of insulin signaling that mediates anti-adrenergic effect in cardiac myocytes. With metabolic supplementation, insulin and eNOS-dependent signaling are impaired.

Regulation of intracellular Ca^{2+} transient ($[Ca^{2+}]_i$) and myofilament Ca^{2+} sensitivity by NF and NF+ISO in normal rat heart.

Intracellular Ca^{2+} profiles were examined with NF in the presence of ISO. NF+ISO significantly increased the diastolic and systolic $[Ca^{2+}]_i$ ($F_{360/F380}$, *P*=0.001 & *P*=0.001, n=13, n=13, Fig. 26A). Analysis of $[Ca^{2+}]_i$ profile showed that time constant of $[Ca^{2+}]_i$ decay (tau, ms) was significantly facilitated in NF+ISO compared to that in NF (P<0.001, n=13, Fig. 26A).

Sarcomere shortening and $[Ca^{2+}]_i$ transient relationship between NF and NF+ISO were changed in Fura-2-loaded LV myocytes (Fig. 26B), phase-plane loop of sarcomere length vs. $[Ca^{2+}]_i$ transient was not changed with NF+ISO. The $[Ca^{2+}]_i$ (Fura-2 ratio) at 50% sarcomere relengthening (EC_{50}) was similar between NF and NF+ISO (EC_{50}: P>0.05, NF=13, NF+ISO=13).

Action potential profile and delay after contraction (DAC)

As described above (in Part II), to test whether induced DAC was responsible for the prolongations of action potential (AP) plateau (and therefore APD), I recorded the APD in NF+ISO. As shown raw APD trace in Fig. 27A, the depolarization of AP was significantly prolonged than compared to in NF. And as shown in Fig 27B, Fig 28A,B, increasing stimulation frequency to 4Hz and 8Hz or inhibition of NCX activity by KB-R7943 (100 μM), however, abolished DAC and spontaneous Ca^{2+} release.

These results suggest that NF with ISO increased possibilities of spontaneous Ca^{2+} release and DAC in the presence of ISO, and APD and NCX activity underlie mechanism.

Role of nNOS in myocyte intracellular $[Ca^{2+}]_i$ and myofilament Ca^{2+} sensitivity in NF+ISO

As eNOS-dependent signaling was impaired by NF, and nNOS-derived NO is associated with controlling cardiac arrhythmogenesis in diseased heart, I studied the effect of nNOS on $[Ca^{2+}]_i$ regulation in NF and NF+ISO. As shown in Fig.29A, C, nNOS inhibition with SMTC (100 nM) increased diastolic and systolic $[Ca^{2+}]_i$ in NF (P=0.02 in diastolic; P<0.001 in systolic, n=26, n=25), however these parameter were not changed in NF+ISO (P=0.73 in diastolic; P=0.35 in systolic, n=26, n=25). Tau of $[Ca^{2+}]_i$ decline was facilitated in NF affect by SMTC, but was not changed in NF+ISO (in NF P=0.02; in NF+ISO P=0.94 , n=25, n=26). And the

phase-plane loop of sarcomere length *vs.* $[Ca^{2+}]_i$ shifted to the right in the present of SMTC in NF and in NF+ISO. Identically EC_{50} were increased (*P*=0.006 in NF *vs.* NF+SMTC; *P*=0.006 in NF+ISO vs. NF+ISO+SMTC, n=12, n=9). Suggesting that Myo-Ca-Sen was significantly reduced by SMTC in NF and in NF+ISO.

These results suggest that nNOS-derived NO prevents DAC by maintaining Myo-Ca-Sen and controlling $[Ca^{2+}]_i$ in the presence of metabolic substrates in LV myocytes.

Nebivolol and cordycepin regulation myocyte contraction and intracellular Ca^{2+} handling

β-adrenoceptor activation is linked to NO formation in endothelial cells through increased levels of cAMP, release of calcium and concomitant eNOS activation (Conti, V. et al., 2013). Nebivolol, a third generation β-adrenoceptor blocker, β1-receptor antagonist, but it also activates β_3-adrenoceptors, which increases NO formation (Dessy, C. et al., 2005). Here, I detected the effect of NF in the presence of nebivolol. As shown in Fig. 30A, B, nebivolol (100nM~1μM) significantly decreased the diastolic and systolic $[Ca^{2+}]_i$ in NF+ISO (F360/F380, nebivolol: 100nM P=0.02 & P=0.005; nebivolol: 1μM *P*=0.04 & *P*=0.001 n=10). Analysis of $[Ca^{2+}]_i$ profile showed that time constant of Ca^{2+} transient decay (tau, ms) was significantly increased in NF+ISO (nebivolol: 100nM *P*=0.004; nebivolol: 1μM *P*<0.001, n=10). Then, I examine whether nebivolol effect the myofilament Ca^{2+} sensitivity. As shown in Fig. 30C, D, relaxation phase of the sarcomere length-$[Ca^{2+}]_i$ transient relationship shifted to the left in NF+ISO in the presented of nebivolol, Ca^{2+} level at 50% sarcomere relengthening (EC_{50}) was significantly decreased in these groups. (Nebivolol: 100nM *P*=0.008; nebivolol: 1μM *P*=0.01, n=10). As shown figure 31 A,B, cordycepin (50 μM-100 μM), which was an adenosine mimetic and exerts anti-adrenergic effect, reduced DAC in NF+ISO without changing myocyte contraction.

These results suggest that impaired insulin and eNOS-signaling in beta-adrenergic stimulation is important in improved myocyte contraction and intracellular Ca^{2+} homeostasis. Interestingly, the percentage of arrhythmias was significantly reduced by nebivolol and cordycepin.

2. Metabolic substrate' regulation of cardiac myocyte contraction and the roles of eNOS and nNOS in LV myocytes from hypertensive rat heart.

NF regulation of myocyte contraction in hypertension

First, I examined the effect of NF and NF+ISO on LV myocyte contraction in hypertension. As shown in Fig. 32A and B, myocyte shortening was significantly increased by NF (P=0.007, n=8). β-adrenergic stimulation with ISO (50 nM) further increased myocyte contraction (P<0.001, n=8 between NF and NF+ISO) and induced DAC without changing time to 50% relaxation (P=0.71, n=8). In hypertension, the occurrence rate of DAC was ~40%, significantly higher than that in sham rats (P<0.001, n=20, n=8, Figure 32C).

Next, we examined whether NF affects insulin signaling (ratios for IRβ-Tyr/IRβ and IRS-1-Tyr/IRS-1) and eNOS-Ser^{1177} in LV myocytes from hypertensive rat hearts. As shown in Fig. 33A, IRβ-Tyr/IRβ was not affected by insulin in hypertension in NT (P=0.9 with insulin & P=0.9 with INS+ISO, n=4) or in NF (P=0.9 with insulin & P=0.9 with INS+ISO, n=4, Fig. 33A). Similarly, IRS-1-Tyr/IRS-1 was not affected by insulin in NT (P=0.9 with insulin and P=0.9 with INS+ISO, n=4) or in NF (P=0.9 with insulin and P=0.9 with INS+ISO, n=4, Fig. 33A). eNOS phosphorylation at Ser^{1177} was significantly reduced in NF in hypertension (P=0.05 and P<0.001 before and after insulin with NF, n=4 and n=5, Fig. 33B).

These results suggest that insulin signaling is impaired in LV myocytes with or without

metabolic substrates' supplementation. NF increased myocyte contraction and DAC in the presence of ISO.

Regulation of intracellular Ca^{2+} transient ($[Ca^{2+}]_i$) and myofilament Ca^{2+} sensitivity by NF and NF+ISO in hypertensive rat heart.

As described above NF increased diastolic and peak $[Ca^{2+}]_i$ in LV myocytes from hypertension. ISO significantly increased both Ca^{2+} parameters and induced ectopic Ca^{2+} transients in NF (Fig. 34A, $P<0.001$ for diastolic $[Ca^{2+}]_i$ and $P<0.001$ for peak $[Ca^{2+}]_i$). It should be noted that the diastolic and peak $[Ca^{2+}]_i$ were significantly higher than those in sham. Analysis of $[Ca^{2+}]_i$ profile showed time constant of $[Ca^{2+}]_i$ decay (tau, ms) was significantly facilitated in NF+ISO compared to in NF ($P<0.001$, n=28, Fig. 34A). The sarcomere shortening and $[Ca^{2+}]_i$ transient simultaneously in Fura-2-loaded LV myocytes and plotted a phase-plane loop of sarcomere length vs. $[Ca^{2+}]_i$ transient. As shown in Figure 34**B**, relaxation phase of the sarcomere length-$[Ca^{2+}]_i$ transient relationship was not changed in NF+ISO, and the $[Ca^{2+}]_i$ (Fura 2 ratio) at 50% sarcomere relengthening (EC_{50}) was not changed similar to in NF (EC_{50}: $P=0.72$, n=17).

These results suggest that further increased intracellular Ca^{2+} in NF+ISO was not caused by myofilament Ca^{2+} buffer in NF+ISO.

L-type Ca^{2+} current (I_{Ca}) and action potential profile

I aimed to test the key elements of excitation-contraction coupling responsible for increased myocyte $[Ca^{2+}]_i$ and contraction in NF+ISO. Fig. 35A, B showed raw traces and averaged current–voltage (I–V) relationships of I_{Ca} in LV myocytes before and after NF in the presence of ISO. And the inset in Fig. 7A showed raw traces of I_{Ca} at 0 mV for Ca^{2+} influx analysis. NF increased the amplitude of I_{Ca} at 0 mV in the presence of ISO (current density of I_{Ca} at 0 mV,

pA/pF: $P < 0.05$ between NT and NF+ISO, n = 5, n = 5) but the inactivation of I_{Ca} at 0 mV was not changed. As a result, total Ca^{2+} influx via LTCC (integral of I_{Ca}) was greater in NF+ISO ($P < 0.05$ between NT and NF+ISO at 0 mV). Next, I analyzed the AP in NF+ISO. APD was slightly prolonged with NF+ISO as shown in Fig. 36A.

These results suggest that Ca^{2+} influx via LTCC which may be responsible for increased $[Ca^{2+}]_i$ amplitudes and prolonged peak time of $[Ca^{2+}]_i$ in NF+ISO.

Regulation of delay after contraction in NF after beta-adrenergic stimulation in HTN rat heart

It is possible that increased diastolic Ca^{2+} level and ectopic Ca^{2+} release after beta-adrenergic stimulation in NF activates plasmalemmal Na^+-Ca^{2+} exchanger which triggers DAC. Therefore, I tested whether the Na^+-Ca^{2+} exchanger is responsible for DAC. KB-R7943 (10 μM), an inhibitor of the Na^+-Ca^{2+} exchanger, abolished ISO-induced DAC in NF in hypertension ($P<0.001$, n=6, Fig. 37A & B). Like sham cordycepin also decreased the percentage of arrhythmias ($P<0.001$, n=5, Fig. 37 C,D).

Role of nNOS in myocyte intracellular $[Ca^{2+}]_i$ and myofilament Ca^{2+} sensitivity in NF+ISO in HTN.

Next, I studied the effect of nNOS on $[Ca^{2+}]_i$ regulation in NF and NF+ISO. As shown in Fig. 38A, C, nNOS inhibition with SMTC (100 nM) decreased diastolic and systolic $[Ca^{2+}]_i$ in NF ($P=0.03$, n=18, n=20), however these parameter were not changed in NF+ISO ($P=0.82$, n=18, n=20). Tau of $[Ca^{2+}]_i$ decline was slowed in NF affect by SMTC, but was not changed in NF+ISO ($P=0.25$ in NF; $P=0.22$ in NF+ISO, n=18, n=20). And the phase-plane loop of sarcomere length *vs.* $[Ca^{2+}]_i$ shifted to the left in the present of SMTC in NF and in NF+ISO. Identically EC_{50} were decreased ($P=0.001$ NF *vs.* NF+SMTC, n=17, n=14; $P=0.02$, NF+ISO

vs. NF+ISO+SMTC, n=17, n=14). Suggesting that Myo-Ca-Sen was significantly increased by SMTC in NF and in NF+ISO.

These results suggest that essentially nNOS-derived NO prevents DAC by maintaining Myo-Ca-Sen and controlling $[Ca^{2+}]_i$ in the presence of metabolic substrates in LV myocytes.

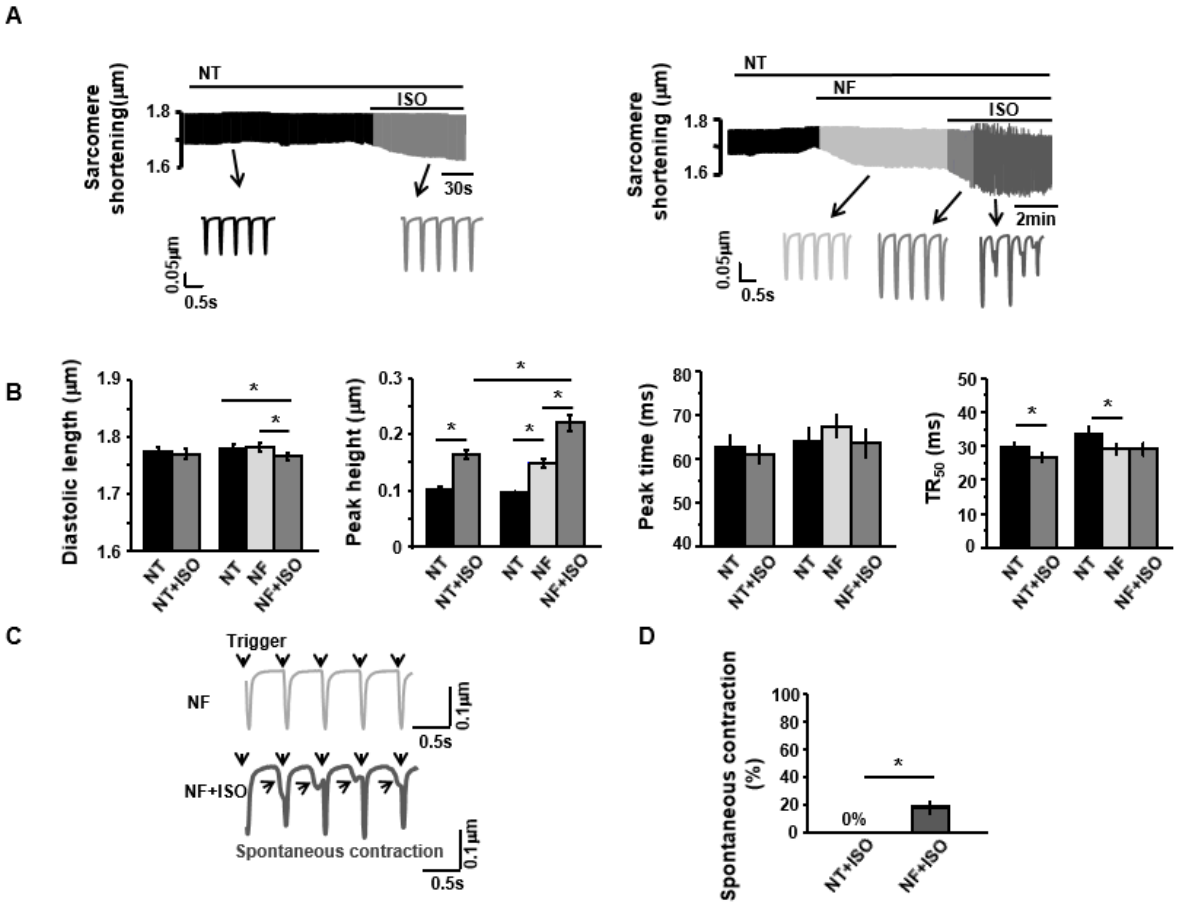

Figure 24. Sarcomere length in NF with and without ISO

A. Representative raw traces of sarcomere shortening and re-lengthening in the presence of ISO in NT and NF. B. Mean values of the diastolic sarcomere length and the amplitude of sarcomere shortening (peak height) and time to peak and 50% relaxation time (TR_{50}). The amplitude of sarcomere shortening was greater with NF under basal conditions (between NF and NT) and after ISO pre-treatment (between NT+ISO and NF+ISO). C. ISO induced delayed after-contractions (DAC) in NF. D. Mean values of the percentage of DAC in NT+ISO and NF+ISO.

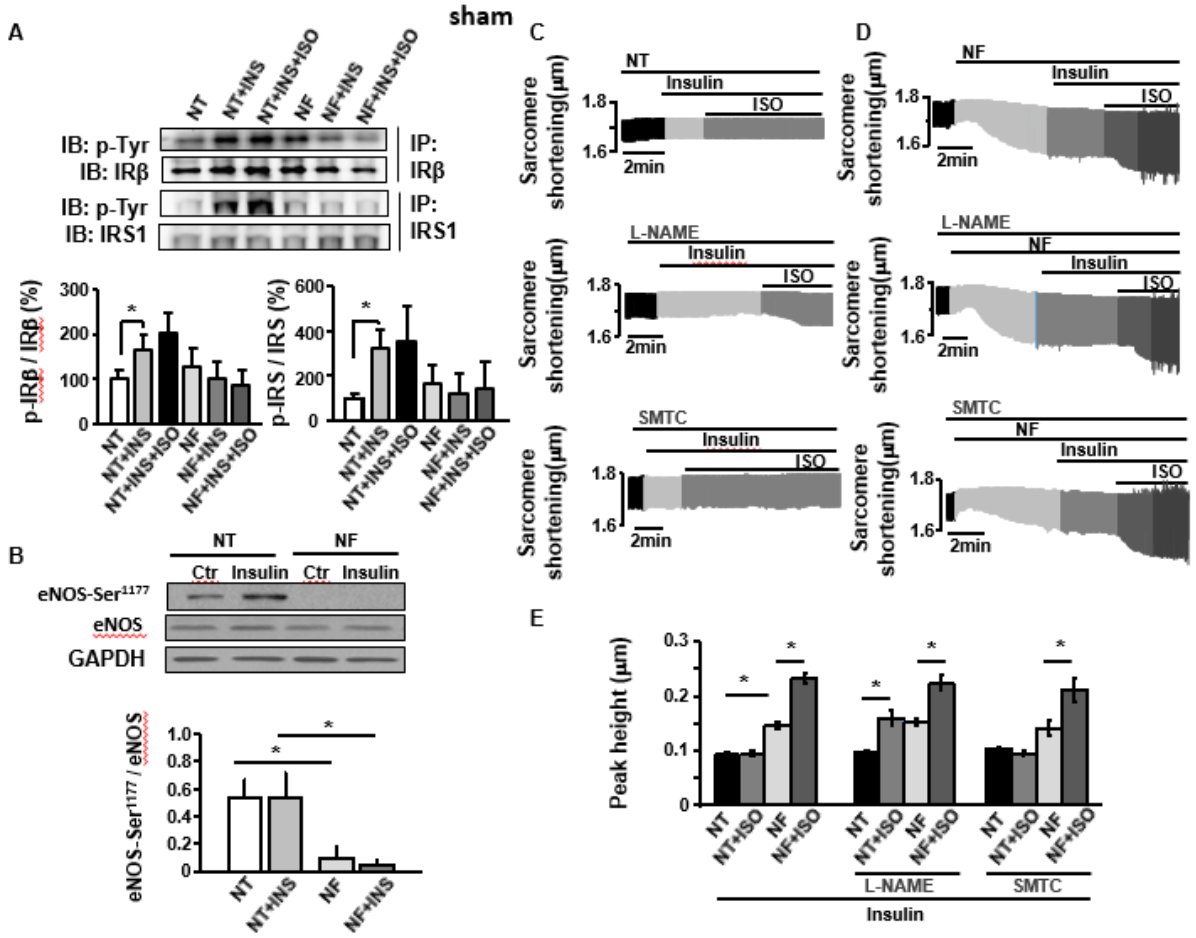

Figure 25. Effect of NF on insulin signaling and change of LV myocyte contraction after the pretreatment of eNOS and nNOS inhibition.

A. Representative immunoprecipitation data of IR, IR-Tyr and IRS-1-Tyr with insulin before and after NF, NF+ISO application. IR– Tyr/IR and IRS-1-Tyr/IRS-1 were increased by insulin and insulin+ISO in NT but was not affected in NF or in NF+ISO. B. Representative immunoblotting of eNOS and eNOS Ser^{1177} and the mean $eNOS^{1177}$/eNOS. $eNOS^{1177}$/eNOS was significantly increased by insulin in NT but the response was abolished with NF. C, D. Representative raw traces of sarcomere shortening and re-lengthening with insulin before and after SMTC and L-NAME treatment in NT and NF. E. Mean values of the amplitude of sarcomere shortening with these intervent. Insulin did not affect basal myocyte shortening abolished ISO-induced positive inotropic effect in NT, but L-NAME restored ISO-

enhancement of LV myocyte contraction in NT. However, Insulin did not affect NF-enhancement of sarcomere shortening in basal or with ISO. SMTC, myocyte contraction with insulin was not different in NF after SMTC and L-NAME pre-treatment.

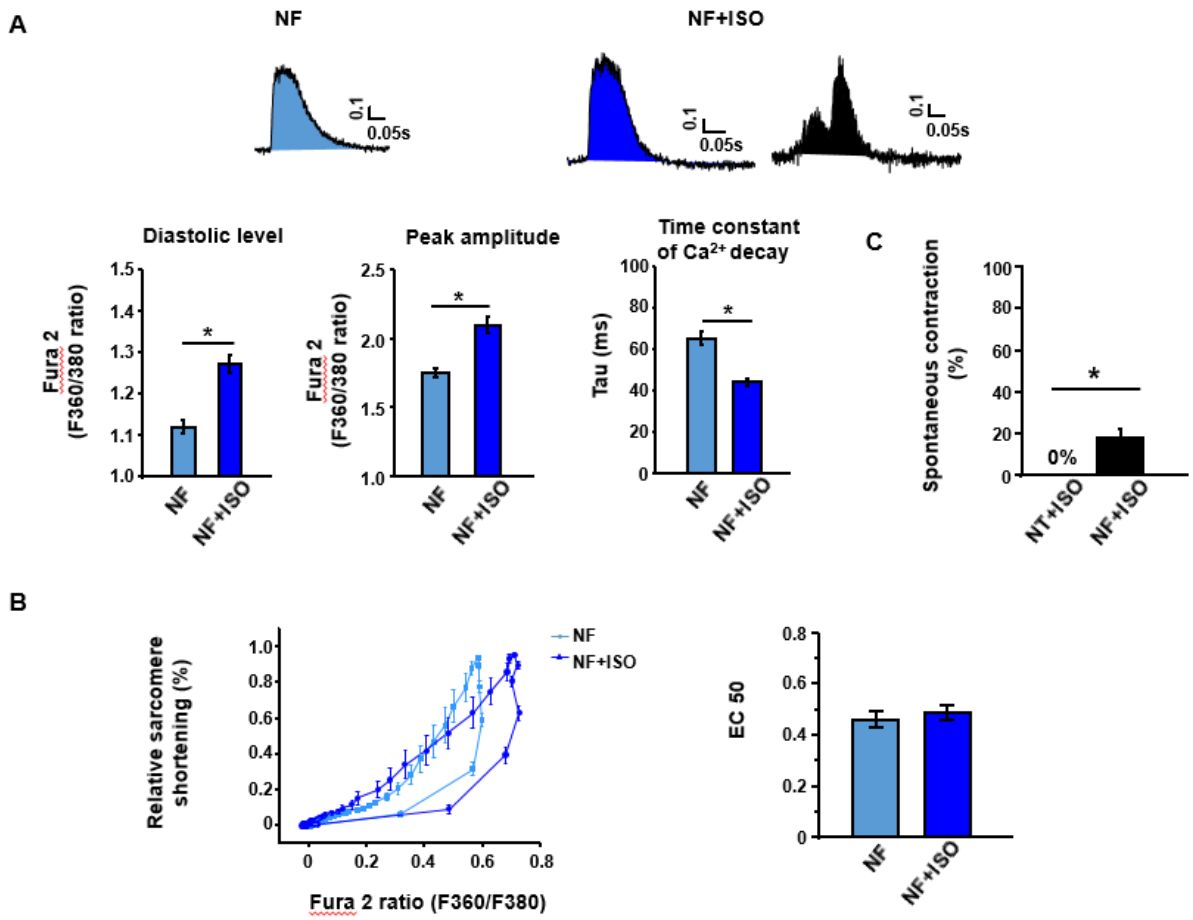

Figure 26. Effect of ISO on $[Ca^{2+}]_i$ and myofilament Ca^{2+} sensitivity in the presence of NF

A. Phase-plane loop of sarcomere shortening/relengthening *vs.* $[Ca^{2+}]_i$ transient in NF and NF+ISO. Ca^{2+} concentration at 50 % sarcomere relengthening (EC_{50}) was not different between two groups. B. Representative $[Ca^{2+}]_i$ transients in NF and NF+ISO. ISO significantly increased diastolic $[Ca^{2+}]_i$ and peak amplitude of $[Ca^{2+}]_i$ in NF. Time constant of $[Ca^{2+}]_i$ decay (tau) was facilitated by NF+ISO. C. The percentage of spontaneous Ca transient was increased by ISO in NF.

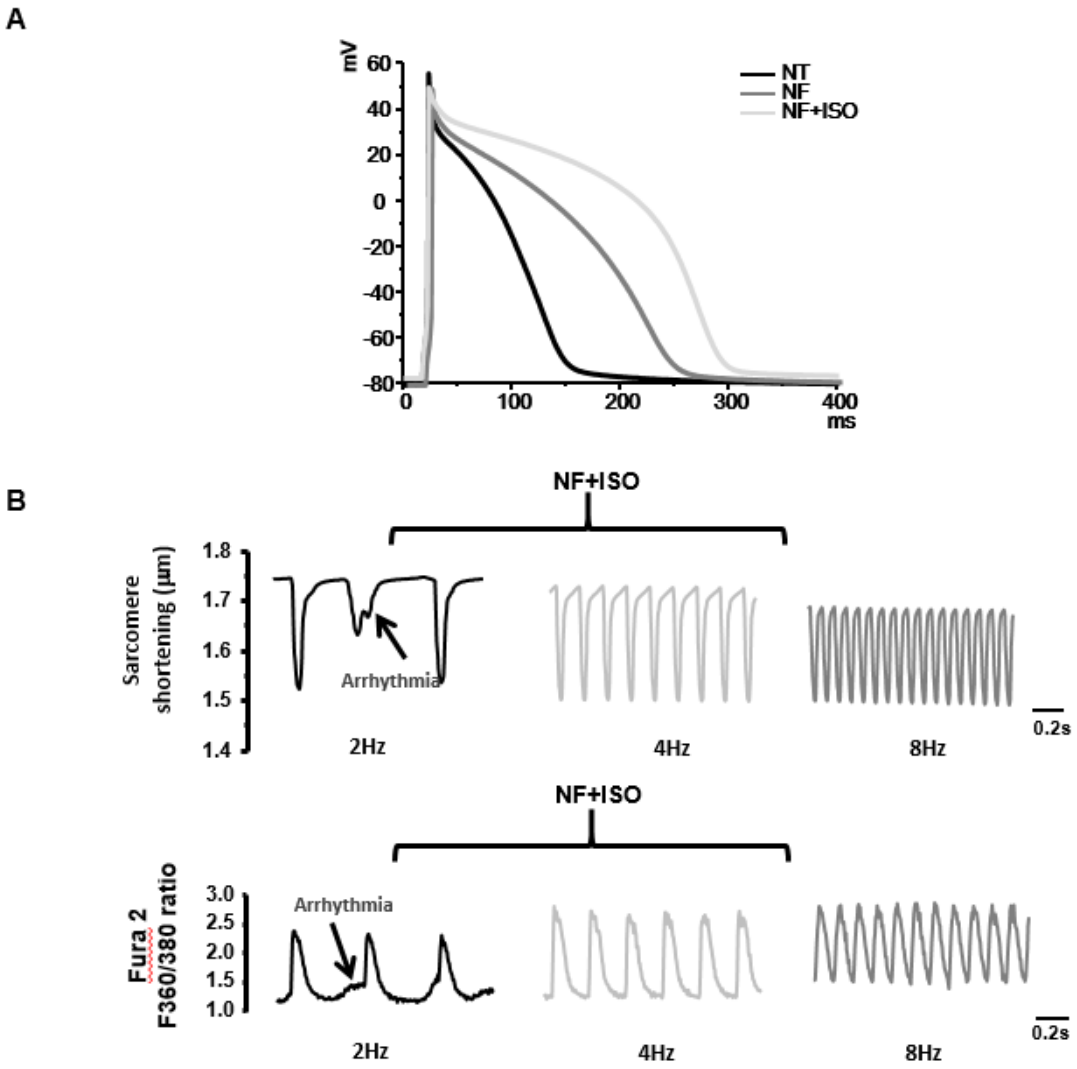

Figure 27. Effect of ISO on action potential profile and the change of DAC at different stimulation frequency

A. Representative action potential profile in NT, NF and NF+ISO. NF and NF+ISO significantly prolonged the AP duration. B. Representative raw traces of sarcomere shortening showed that increasing stimulation frequencies from 2Hz to 4 - 8Hz prevented DAC and ectopic Ca^{2+} release in NF+ISO.

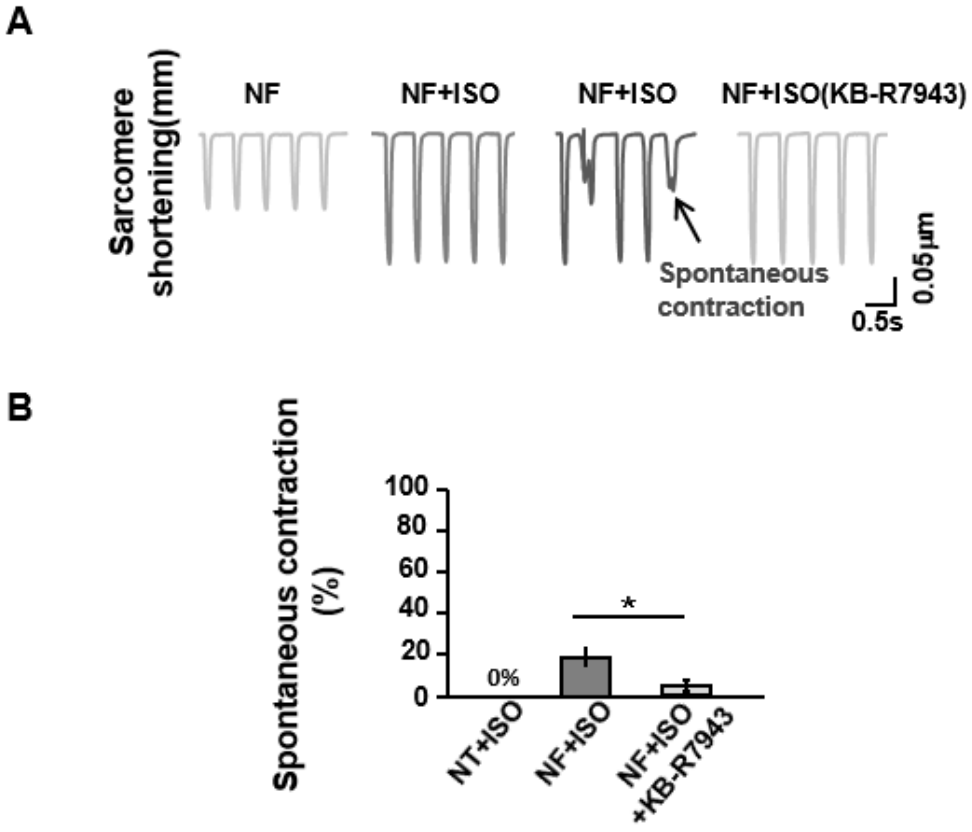

Figure 28. Na^+-Ca^{2+} exchanger is pivotal in mediating beta-adrenergic stimulation of DAC in NF

A. Representative sarcomere shortenings in NF and NF+ISO in sham before and after Na^+-Ca^{2+} exchanger inhibitor KB-R7943. B, Averaged results showed that KB-R7943 significantly reduced the occurrence rate of DAC in sham.

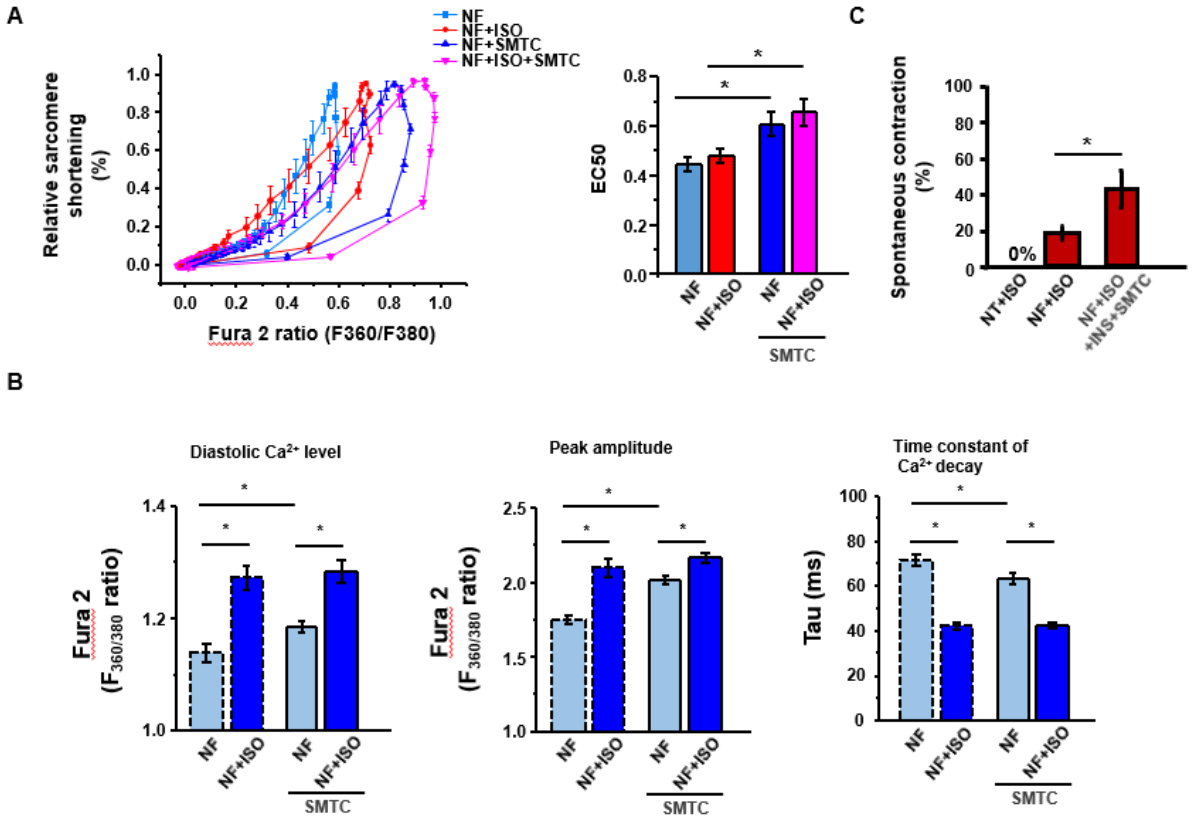

Figure 29. Effect of nNOS on myofilament Ca^{2+} sensitivity in NF and NF+ISO

A. Phase-phase loop of sarcomere shortening/relengthening vs. $[Ca^{2+}]_i$ transient. The relaxation phase of the loop shifted to the right in NF and NF+ISO with SMTC. Ca^{2+} concentration at 50% sarcomere relengtheing (EC50) was significantly larger in NF and NF+ISO with SMTC. B. Mean values of $[Ca^{2+}]_i$ transient parameters. SMTC significantly increased the diastolic $[Ca^{2+}]_i$ and peak amplitude $[Ca^{2+}]_i$ in NF. The time constant of $[Ca^{2+}]_i$ decay (tau) was facilitated in NF with SMTC, however these parameters were not different in NF+ISO with and without SMTC.

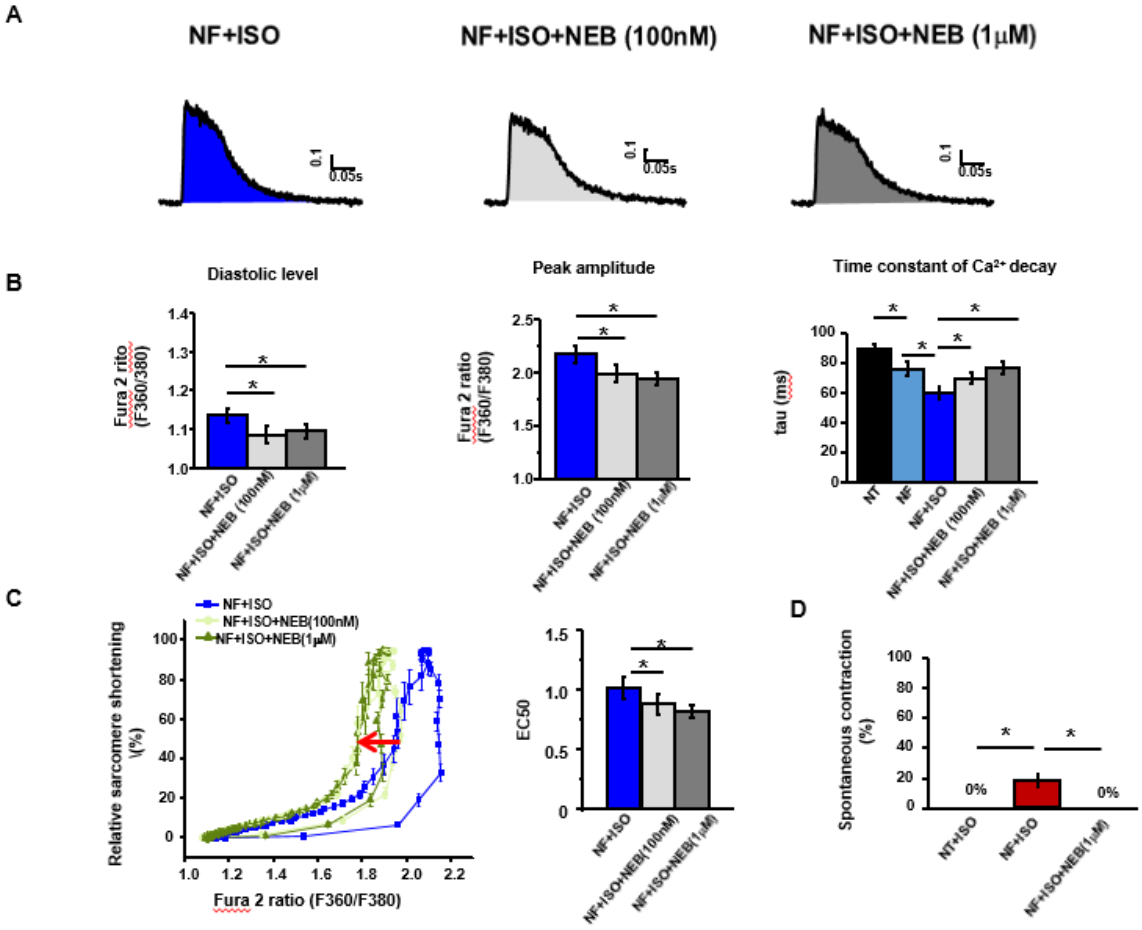

Figure 30. Effect of β-adrenoreceptor blocker (Nebivolol) on $[Ca^{2+}]_i$ and myofilament Ca^{2+} sensitivity after NF treatment

A. Representative trace of $[Ca^{2+}]_i$ transients in NF+ISO with and without nebivolol. B. Mean values of $[Ca^{2+}]_i$ transient parameters. Nebivolol significantly decreased diastolic $[Ca^{2+}]_i$ and peak amplitude of $[Ca^{2+}]_i$. Time constant of $[Ca^{2+}]_i$ decay (tau) was prolonged in NF+ISO in the presence of nebivolol. C. Phase-plane loop of sarcomere shortening/relengthening *vs.* $[Ca^{2+}]_i$ transient. The relaxation phase of the loop shifted to the left in NF+ISO in the presence of nebivolol compared to that in NF+ISO. Ca^{2+} concentration at 50 % sarcomere relengthening (EC_{50}) was significantly decreased in NF+ISO pre-treated nebivolol. D. Mean value of arrhythmias percentage was significantly decreased by nebivolol, even was 0%.

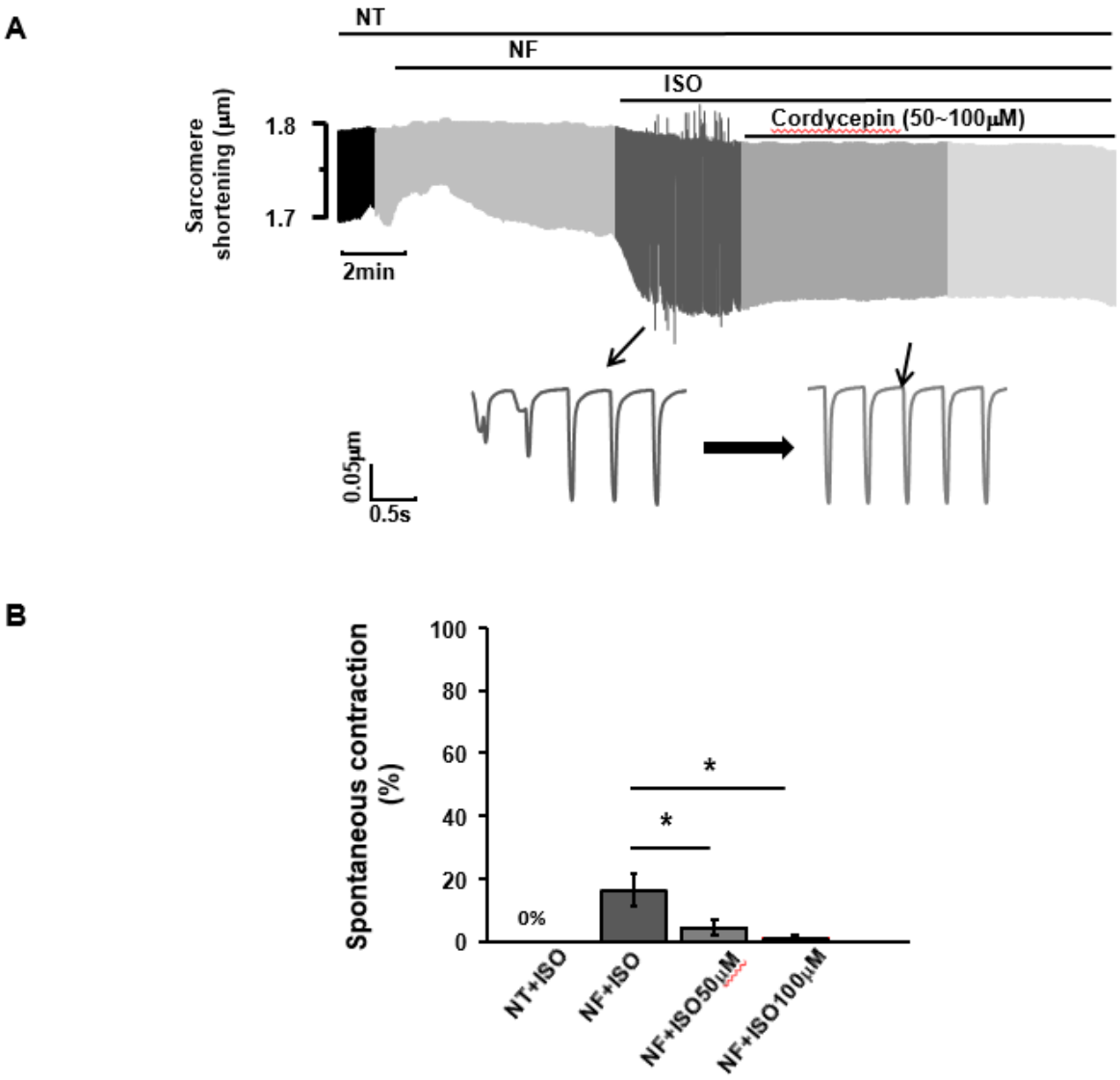

Figure 31. Cordycepin abolished the DAC induced by NF+ISO

A. Representative raw traces of sarcomere shortening and relengthening in the presence of cordycepin. B. Mean value of the percentage of DAC was significantly decreased in NF+ISO.

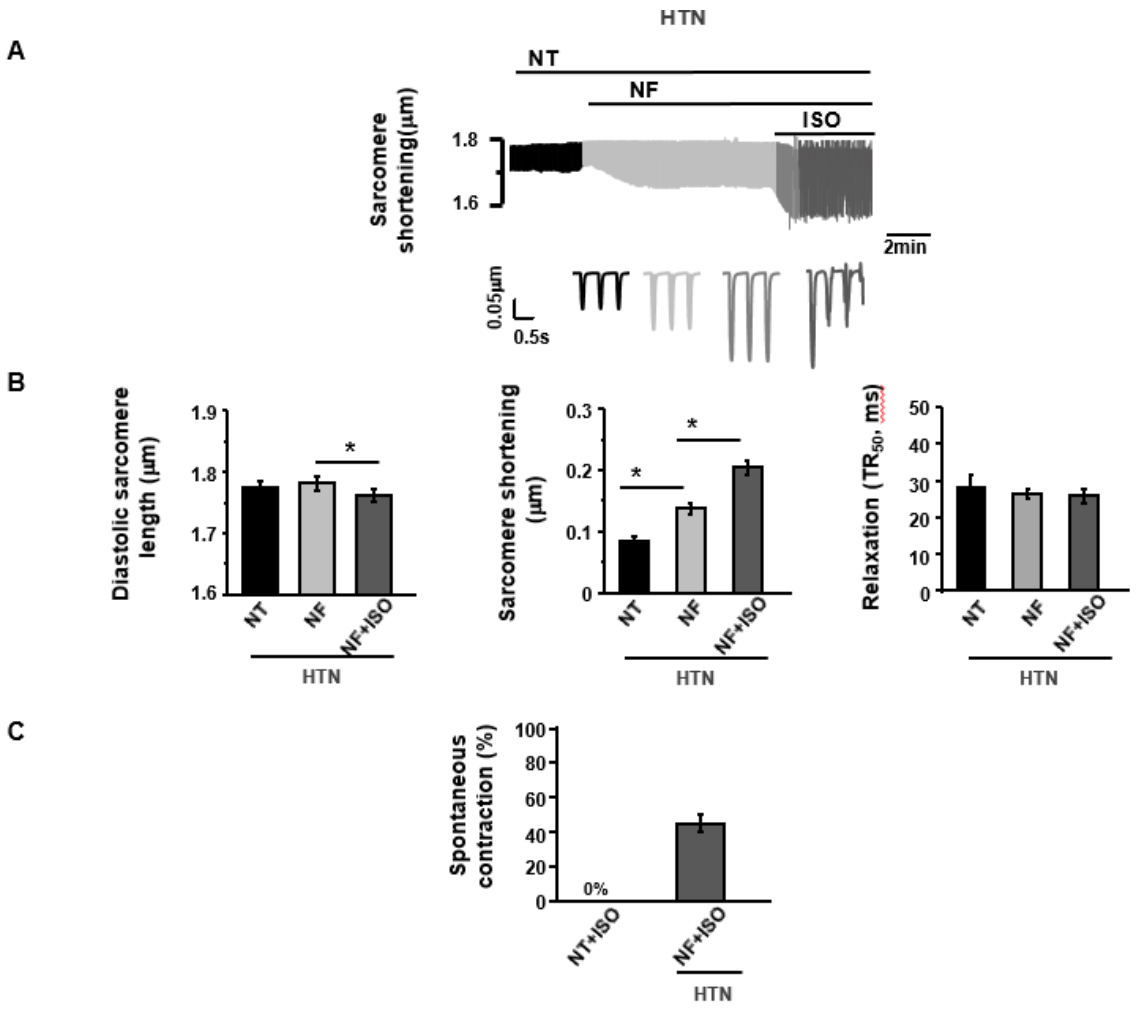

Figure 32. NF induced DAC in the presence of beta-adrenergic stimulation with ISO in hypertensive rat heart

A. Representative raw traces of sarcomere shortening and re-lengthening in the presence of ISO in NF. B. Mean values of the diastolic length and the amplitude of sarcomere shortening (peak height) and time to peak and 50% relaxation time (TR_{50}). The amplitude of sarcomere shortening was greater with NF under basal conditions and after ISO pre-treatment (NF+ISO). C. Mean values of the percentage of DAC induced in NF+ISO. The percentage of DAC was greater in hypertensive rat compared to sham.

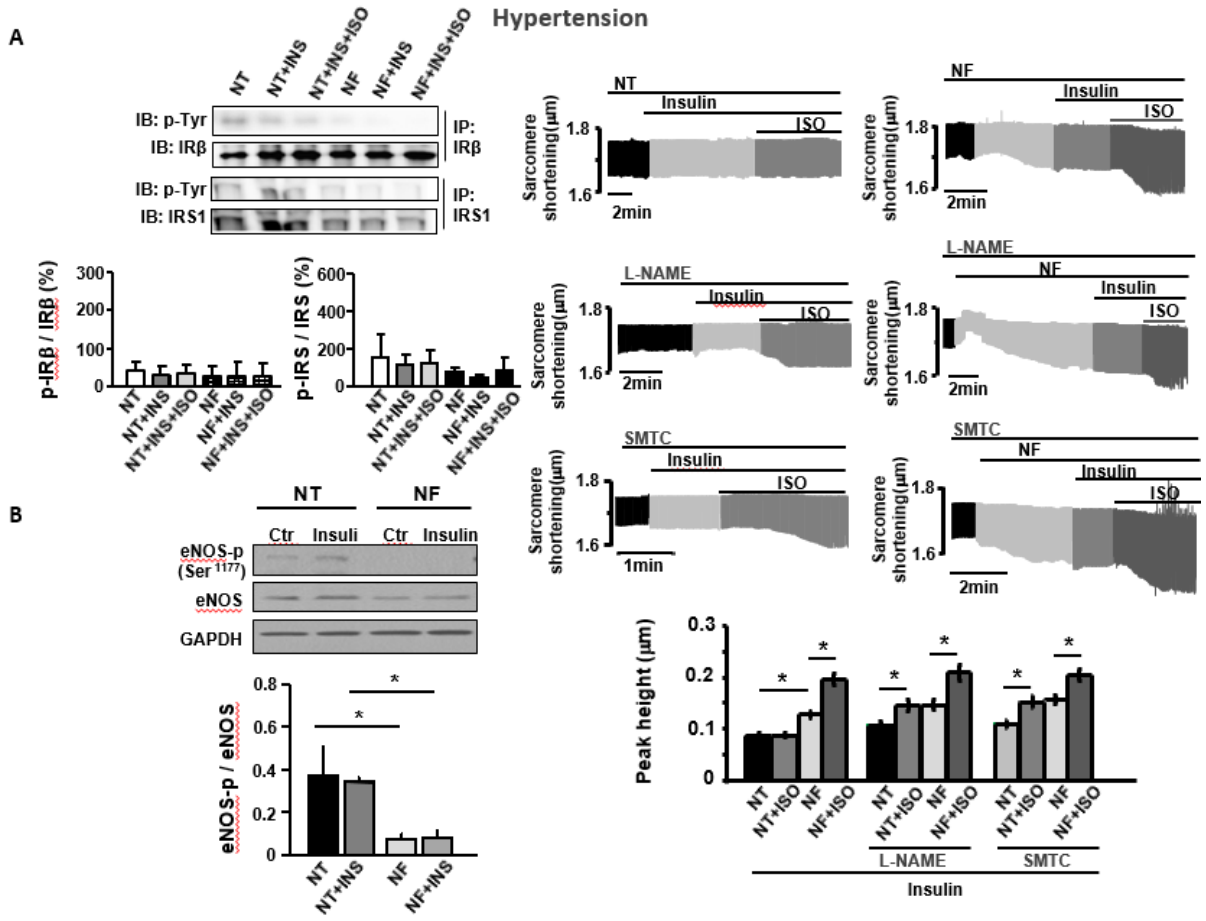

Figure 33. Effect of NF on regulation of insulin signaling and eNOS phosphorylation in hypertensive rat heart

A. Representative immunoprecipitation of IR-Tyr/IR and IRS-1-Tyr/IRS-1. IR– Tyr/IR and IRS-1-Tyr/IRS-1 were increased by insulin in NT but was not affected by insulin in NF. B. Representative immunoblotting of eNOS and eNOS Ser^{1177} and the mean eNOS^{1177}/eNOS. eNOS^{1177}/eNOS was significantly decreased by insulin in NT but the response was abolished with NF. C, D. Representative raw traces of sarcomere shortening and re-lengthening with insulin before and after SMTC and L-NAME treatment in NT and NF. E. Mean values of the amplitude of sarcomere shortening with these intervent. Insulin did not affect basal myocyte shortening abolished ISO-induced positive inotropic effect in NT, but L-NAME restored ISO-enhancement of LV myocyte contraction in NT. However, Insulin did not affect NF-

enhancement of sarcomere shortening in basal or with ISO. SMTC, myocyte contraction with insulin restored ISO enhancement of LV myocyte contraction in NT, however, was not different in NF after SMTC and L-NAME pre-treatment.

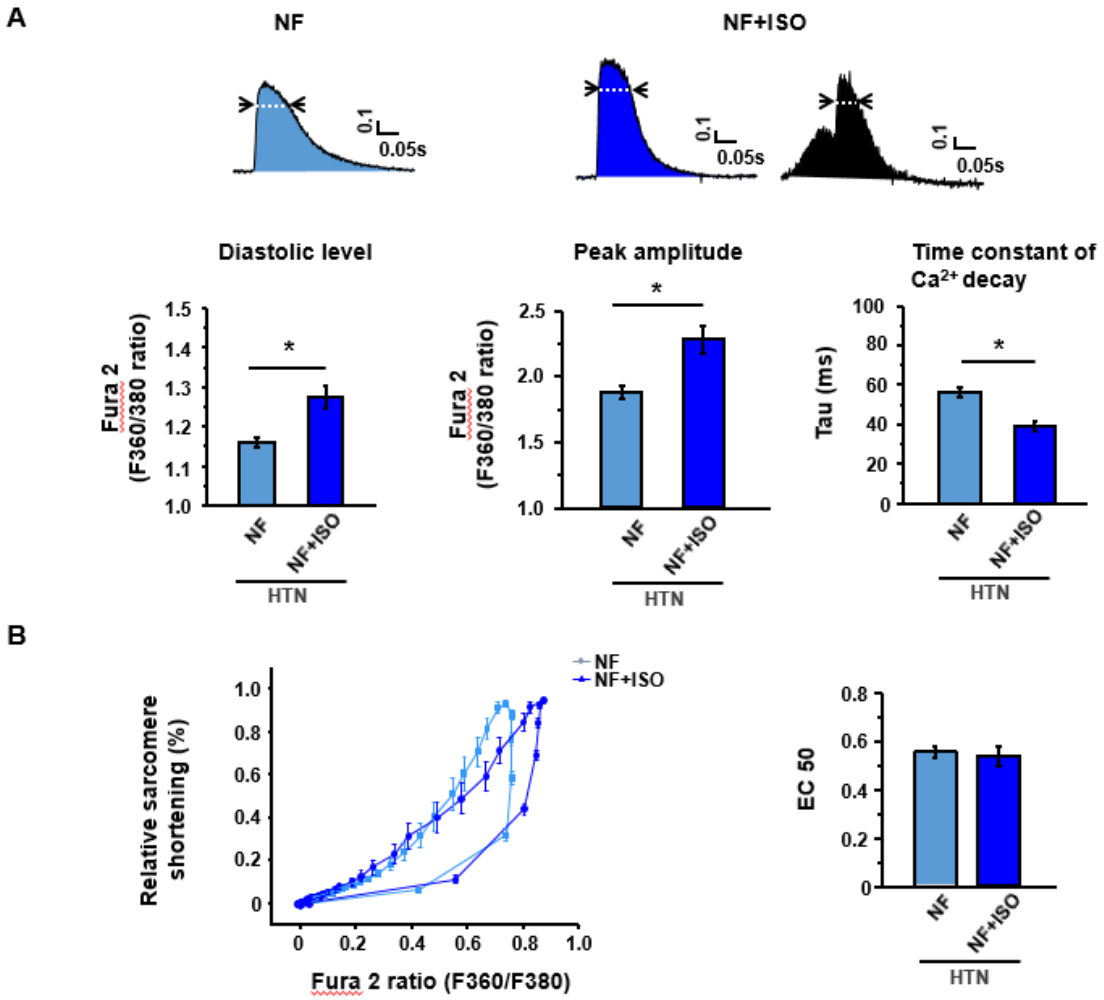

Figure 34. Effect of ISO on $[Ca^{2+}]_i$ and myofilament Ca^{2+} sensitivity in the presence of NF in hypertensive rat heart

A. Representative $[Ca^{2+}]_i$ transients in NF and NF+ISO. ISO significantly increased diastolic $[Ca^{2+}]_i$ and peak amplitude of $[Ca^{2+}]_i$. Time constant of $[Ca^{2+}]_i$ decay (tau) was facilitated in NF+ISO. B. Phase-plane loop of sarcomere shortening/relengthening *vs.* $[Ca^{2+}]_i$ transient in NF and NF+ISO. The relaxation phase of the loop was not change in NF+ISO compared to that in NF. Ca^{2+} concentration at 50 % sarcomere relengthening (EC_{50}) was not changed.

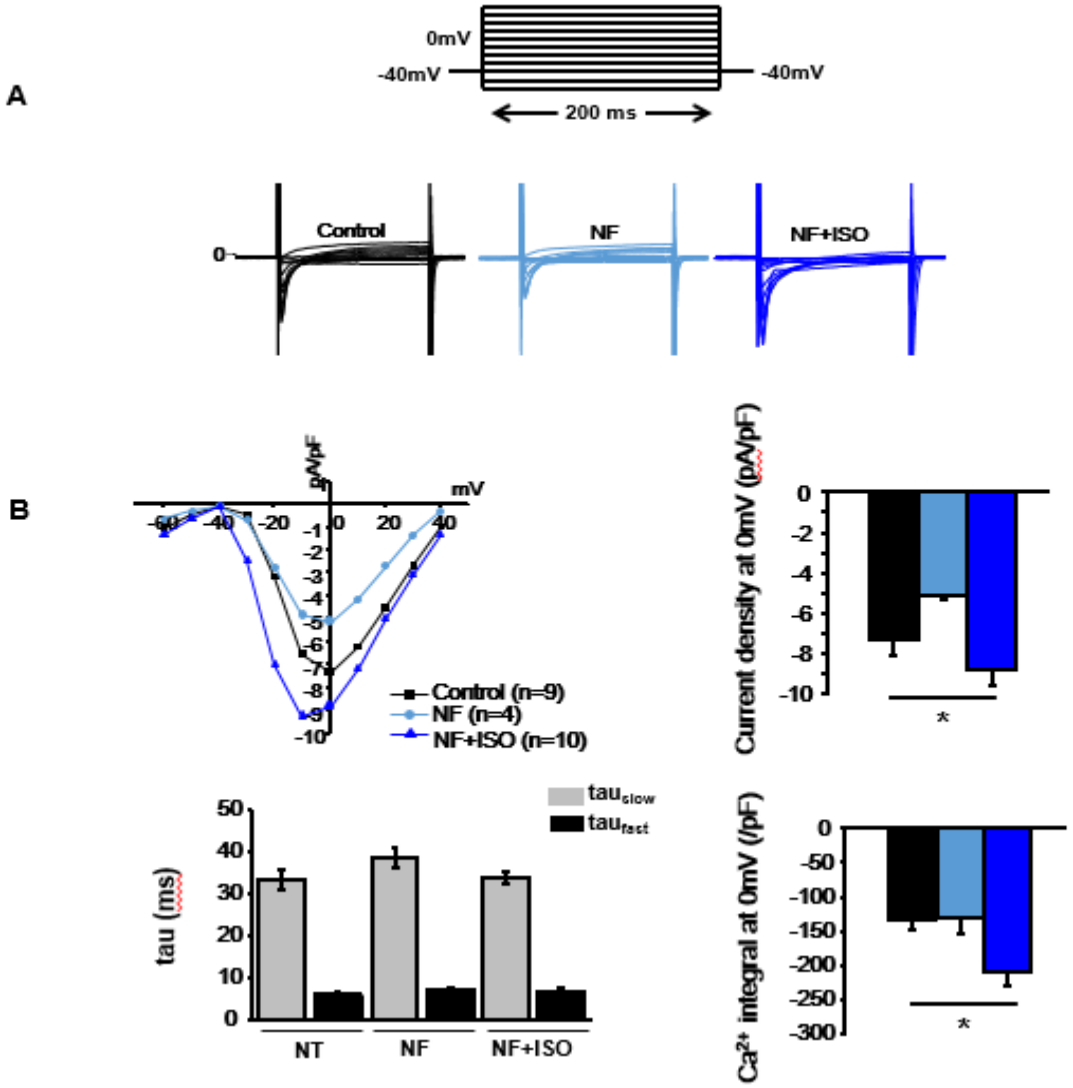

Figure 35. Patch-clamp recording of LTCC activities with NF in hypertensive rats

A. Pulse protocol, representative I_{Ca}. B. Corresponding I-V relationship, peak I_{Ca} at 0 mV, tau of I_{Ca} inactivation, and the integral of Ca^{2+} influx in NF and NF+ISO. ISO increased peak I_{Ca} density and integral of I_{Ca} at 0 mV in the present of NF. The tau of inactivation of I_{Ca} was not affected by NF+ISO.

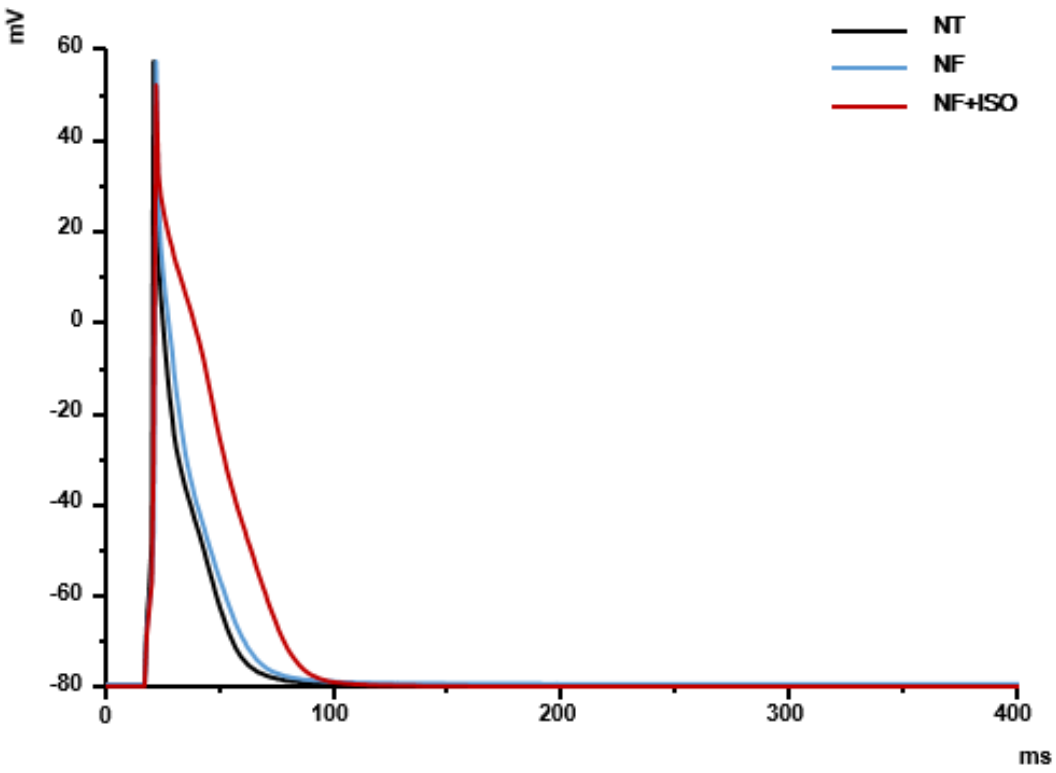

Figure 36. Action potential profile in NF and NF+ISO in hypertensive rat LV myocytes

Representative action potential profile in NT, NF and NF+ISO. NF did not change the AP, however the duration of AP in NF did not change. However, the duration of AP in NF+ISO was prolonged.

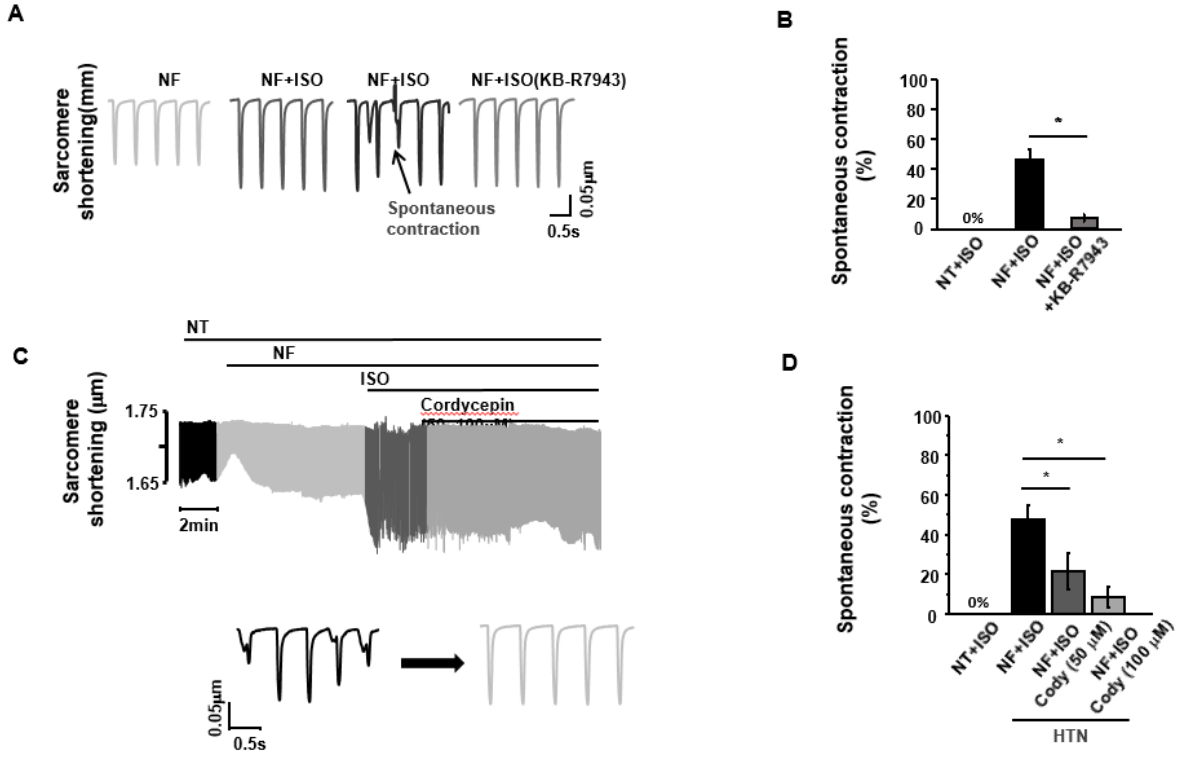

Figure 37. Effect of KB-R7943 and cordycepin on DAC with beta-adrenergic stimulation in hypertensive rats

A. Representative sarcomere shortening in NF+ISO in hypertension after treated Na^{+}-Ca^{2+} exchanger inhibitor KB-R7943. The percentage of arrhythmias was significantly decreased after treated KB-R7943. B. Representative raw trace of sarcomere shortening and relenghening in the presence of cordycepin. Mean value of arrhythmias percentage was significantly decreased by cordycepin.

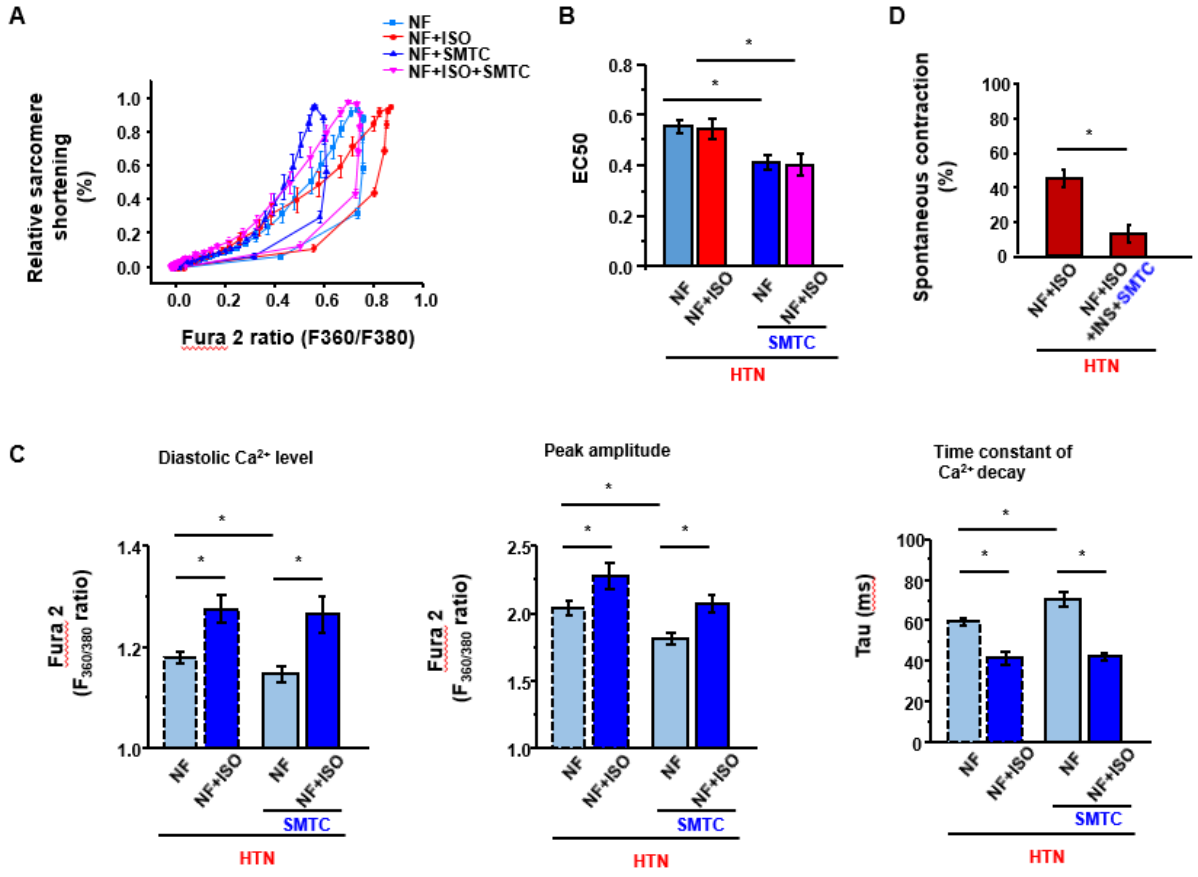

Figure 38. Effect of nNOS on regulation of myofilament Ca^{2+} sensitivity in the present of beta-adrenergic stimulation

A. Phase-phase loop of sarcomere shortening/relengthening vs. $[Ca^{2+}]_i$ transient. B. The relaxation phase of the loop shifted to the left in NF and NF+ISO after pre-treated nNOS inhibitor SMTC. Ca^{2+} concentration at 50% sarcomere relengtheing (EC50) was significantly smaller in NF and NF+ISO pre-incubation with SMTC. C. Mean values of $[Ca^{2+}]_i$ transient parameters. SMTC significantly decreased the diastolic $[Ca^{2+}]_i$ and peak amplitude $[Ca^{2+}]_i$ in NF, and time constant of $[Ca^{2+}]_i$ decay (tau) was prolonged in NF pre-incubation with SMTC, however these parameters were not change in NF+ISO.

Discussion

Part I:

Assessment of myofilament Ca^{2+} sensitivity underlying cardiac excitation-contraction coupling.

Here, I describe the protocols assessing the changes of myofilament Ca^{2+} sensitivity in single isolated cardiac myocyte and emphasize the importance of measuring this parameter alongside electrophysiological properties, intracellular Ca^{2+} transient and myofilament dynamics. This is because the recordings of one or two of the parameters may not explicate the mechanisms underlying cardiac contraction and relaxation. Unlike conventional methods that measure myocyte contraction and intracellular Ca^{2+} profile individually, the present method examines both parameters simultaneously from the same cardiac myocytes.

In fact, a number of methods are generally been used to assess myofilament Ca^{2+} sensitivity of muscles or myocytes (Preston, L.C. et al., 2007; Willott, R.H. et al., 2010; Yasuda, S.I. et al., 2001) e.g. examine interactions between exogenous Ca^{2+} and the sarcomere/cell length/tension in skinned myocytes (with detergents such as saponin or beta-sin to permeabilize the membrane. Lengths are measured with photo-diode and laser beam diffraction techniques and tension with force transducers or carbon fibers). These techniques are widely used in muscle studies because it merits quantitative assessments of myofilament Ca^{2+} sensitivity. However, it is diverged from E-C coupling conditions of cardiac myocytes where Ca^{2+} handlings and ion channel activities in the plasma membrane are required to initiate the mechanics of the myofilament. In addition, the muscle strips or myocytes under study are "pre-stretched" to certain diastolic length, under which conditions, the initial sarcomere length can

be different from the "actual" diastolic length of the myocytes (especially in disease conditions and with interventions). This highlights the advantage of the current measurement where cellular organelles remain relatively unperturbed and therefore, enables comprehensive evaluation of myocyte contractile function.

Understandably, the quality of the myocytes (Ca^{2+}-tolerating) and the optimal loading of the Fura-2AM are two key elements for successful assessment of myofilament Ca^{2+} sensitivity. Accordingly, several modifications are applied to the protocol to obtain viable rod-shaped myocytes (60-80% of total cells, as described previously (Sears, C.E., et al., 2003; Ashley, E.A., et al., 2002; Zhang, Y.H., et al., 2008). First, Ca^{2+} is added to the solutions at low dose during digestion processes (e.g. Ca^{2+} concentration is 50 μM in collagenase solutions and 200 μM in storage solution). Second, during digestion process, BSA is added to the collagenase solutions to enhance the membrane stability. Third, most of the solutions are oxygenated during isolation, which enhances the percentage of functional myocytes and the duration for the experiments (6-8 hours). Fourth, isolated myocytes are kept in the storage solution with 200 μM Ca^{2+}.

To obtain optimal loading with Fura-2AM, two different Ca^{2+} concentrations (250 μM and 500 μM) are used and poloxamer 407 (2 μl, 20% in DMSO) is added to assist the permeability of Fura-2AM through the membrane and its stability in the myocytes. It should be noted that all Ca^{2+} indicative dyes are Ca^{2+} buffers (Roe, M.W. et al., 1990). Therefore, one should avoid using high concentration or longer duration of incubation with Fura-2AM to avoid too much buffer and reduced myocyte contractility. It is recommended that, as a routine, one should check the myocyte contraction without Fura-2 loading, which is an essential step to estimate the quality of myocyte of the day and the status of the loading. Variability is inevitable in

loading.

Therefore, it is important to check the variability of myocyte contraction: whether the number of contracting myocytes in the chamber is similar before and after the loading. Avoid analyzing hyper- or hypo-contracting myocytes because they do not represent average status of the myocytes and may cause biased results and evaluations.

It should be noted that the measured changes in Fura-2 ratio are reflections of intracellular Ca^{2+} level rather than actual chemical concentration of Ca^{2+}. Therefore, the method described here evaluates "qualitative" changes of myofilament Ca^{2+} sensitivity rather than "actual" sensitivity of the myofilament to Ca^{2+}. Calibration of Fura-2 signal to intracellular Ca^{2+} concentration is the solution to acquire reliable Ca^{2+} concentrations in individual myocytes. The calibration procedure requires loading myocytes with various Ca^{2+}-conjugated Fura-2AMs (Ca^{2+} concentration ranges from 0 to 39 μM and the obtained Fura-2 ratios are calculated with the formula: $[Ca^{2+}]_i = Kd * (R - Rmin) / (Rmax - R) * F380max / F380min$ (Grynkiewicz, G. et al., 1985). It is possible to derive the "pooled" average values of Ca^{2+} concentration through such a calibration procedure. However, due to the fact that loading of Ca^{2+} indicators are variable among myocytes and the calibration is not performed in individual cell, one may not acquire Ca^{2+} concentrations accurately. Furthermore, if one measures F360/F380 rather than F340/F380 (as in the present study), the Fura-2 ratio is less accurate (because F360 is the isosbestic wavelength of Fura-2 fluorescence (Grynkiewicz, G. et al., 1985)). Nevertheless, it is still a valid method to assess the "qualitative" changes in myofilament Ca^{2+} sensitivity in physiological experiments, especially in diseased human heart, where myofilaments can be concomitantly altered subsequent to the changes in intracellular environment. It is recommended to combine with alternative methods (as described previously in the discussion) to precisely analyze the "true sensitivity" of myofilament to Ca^{2+}.

The other limitation of the method is to study myocyte contraction in unloaded condition. It may underestimate or overestimate the changes in the myofilament Ca^{2+} sensitivity. Therefore, to accurately evaluate myofilament Ca^{2+} sensitivity, one has to analyze with alternative measurements for both qualitative and quantitative assessment.

The technique is applicable for assessing myocardial function in healthy and diseased heart, including human cardiac samples, where cellular redox environment and post-transcriptional modifications are changed, result in concomitant alterations in myofilament functions. In particular, ion channels, intracellular ion homeostasis and regulatory proteins in myofilament are interactive so that all the components play in concert to determine heart function in vivo (e.g. measured in echocardiography).

In conclusion, in part I, I describe a method to evaluate the changes of myofilament Ca^{2+} sensitivity and emphasize the importance of analyzing this parameter in conjunction with cardiac electrophysiology, intracellular Ca^{2+} handling and myocyte contraction to obtain a full profile of myocyte function. Myofilament Ca^{2+} sensitivity should be measured routinely in mechanistic studies using diseased heart models, where changes in these parameters as well as various intracellular signaling pathways are interrelated.

Part II:

Cardiac inotropy, lusitropy, and Ca^{2+} handling with major metabolic substrates in normal rat hearts.

Here, I showed that supplementation of metabolic substrates (including fatty acids, physiological concentration of glucose) increased LV myocyte contraction and facilitated relaxation from rat heart by increasing Ca^{2+} influx via LTCC and increasing $[Ca^{2+}]_i$ transients,

despite that myofilament Ca^{2+} sensitivity was reduced. Importantly, experimental results suggested that myofilament $[Ca^{2+}]_i$ sensitivity was reduced but greater contraction, abbreviated tau, and faster relaxation are induced by NF. Intracellular pH, which is reduced by NF, is important in mediating the effects of NF on myocyte contraction, relaxation, and $[Ca^{2+}]_i$. These results suggest that supplementation of metabolic substrates (including fatty acids) potentiates myocyte inotropy and lusitropy by regulating key elements of Ca^{2+} handling processes and myofilament Ca^{2+} sensitivity, in addition to their effects on cardiac metabolism. The main theme of the study was that supplementation of metabolic substrates is essential for cardiac metabolism (e.g. FAs for beta-oxidation in addition to glucose, NF) influenced myocyte function from normal rat hearts. That is, NF enhanced LV myocyte contraction and promoted myocyte relaxation in almost all the myocytes studied. Furthermore, NF increased diastolic and systolic $[Ca^{2+}]_i$, facilitated Ca^{2+} reuptake into the SR via SERCA, and prolonged peak time duration of $[Ca^{2+}]_i$. Since LTCC and Ca^{2+} release from the SR are important in shaping AP and $[Ca^{2+}]_i$ profiles and myofilament. Ca^{2+} sensitivity and myofilament mechanics dominate myocyte contraction, I analyzed these parameters in the presence of NF. As shown results, peak I_{Ca} density was reduced by NF; however, the integral of I_{Ca} (total Ca^{2+} influx) was increased due to slower inactivation of LTCC (especially at the voltage range of AP plateau, −20 and 0 mV), suggesting more Ca^{2+} is fluxed into the myocyte under these conditions. Accordingly, APD was prolonged remarkably with NF. These results suggest that $[Ca^{2+}]_i$ elevation with NF may be due to increased Ca^{2+} influx via LTCC and the changes in LTCC are likely responsible for the prolongations of APD and the peak duration of $[Ca^{2+}]_i$. NF regulation of myofilament Ca^{2+} sensitivity was analyzed in contracting LV myocytes. My results showed a significant reduction in myofilament Ca^{2+} sensitivity with NF but myocyte contraction was increased. The seemingly counterintuitive results stress the importance of Ca^{2+} handling in greater myocyte contraction with NF. It should be noted that alterations in the myofilament Ca^{2+} sensitivity, in

general, is associated with changes in Ca^{2+} binding affinity to TnC and $[Ca^{2+}]_i$ buffering capacity (Huke S et al., 2010; Robinson P et al., 2007). For example, Robinson et al. showed that the Ca^{2+} binding affinity of the myofilament complex was reduced in dilated cardiomyopathy due to the mutations in thin filament, where myofilament Ca^{2+} sensitivity was reduced (Robinson P et al., 2007). Conversely, hypertrophic cardiomyopathy with myofilament Ca^{2+}-sensitizing mutant increased Ca^{2+}- binding affinity and Ca^{2+} buffering (Robinson P et al., 2007; Schober T et al., 2012). In fact, previous results from our laboratory have shown that myofilament Ca^{2+} desensitization in LV myocytes from angiotensin II-induced hypertensive rat hearts was associated with greater $[Ca^{2+}]_i$ (Jin CZ et al., 2013) and myofilament Ca^{2+} desensitization with BDM increased $[Ca^{2+}]_i$ in sham but not in hypertension (where myofilament Ca^{2+} sensitivity was reduced). Furthermore, myofilament Ca^{2+} desensitization in hypertension, with BDM or with high stimulation frequency, prompted greater I_{Ca} inhibition due to $[Ca^{2+}]_i$ increment (Wang Y et al., 2015). Here, the current findings that myofilament Ca^{2+} desensitization with BDM prevented NF-induced increase in the amplitude of $[Ca^{2+}]_i$ are consistent to our previous results.

It is possible that enhanced mitochondrial activity secondary to the supplementation of metabolic substrates may produce greater ROS via oxidative phosphorylation (Lopaschuk GD et al., 2010) and ROS can potentiate myocyte contraction via the activation of second messengers including protein kinase A (PKA) (de Hemptinne A et al., 1983; Zhang YH et al., 2009). As such, I tested whether intracellular ROS is involved in greater myocyte contraction with NF. Although I did not detect the ROS production from LV myocytes with NF, preincubation with a potent antioxidant, NAC failed to prevent the effect of NF on myocyte shortening. Furthermore, inhibition of PKA (with membrane permeable PKA inhibitor, PKA-amide 14-22) failed to affect NF regulation of myocyte contraction. These results excluded the

involvement of ROS in mediating the effect of NF. My results showed that intracellular pH was reduced by NF. Since low pH is a potent modulator of myofilament Ca^{2+} sensitivity in cardiac and skeletal muscle (Ashley CC et al., 1977; Fabiato A et al., 1978; Liou YM et al., 2008; Takahashi R et al., 2001), reduced pH may mediate the reduced myofilament Ca^{2+} sensitivity and the subsequent regulation of $[Ca^{2+}]_i$. To confirm, when intracellular pH buffering was increased with $NaHCO_3$+CO_2, the effects of NF on myofilament Ca^{2+} sensitivity and $[Ca^{2+}]_i$ were diminished. Alternatively, reduced pH may increase $[Ca^{2+}]_i$ via enhancing the activity of Na^+-H^+ exchanger and the reverse mode of cardiac Na^+-Ca^{2+} exchanger (Cingolani HE et al., 2011). It is possible that increased cellular metabolic status in NF reduced intracellular pH. Alternatively, it is well established that pyruvate or lactate enters the myocyte with one proton through the sarcolemmal monocarboxylate-proton symporter (Dong F et al., 2006) and consequently reduces intracellular pH (Poole RC et al., 1993). Mechanism leading to the changes in intracellular pH needs further investigation. Another possible mechanism for myofilament Ca^{2+} desensitization is intracellular ATP. This is because ATP desensitizes myofilament response to Ca^{2+} in muscle and myocardium (Best PM et al., 1977; Godt RE et al., 1974). Preliminary results showed that cellular ATP level tended be elevated in normal rat LV myocyte homogenates preincubated with palmitic acid (30 min) (data not shown). The level of ATP was not detected with NF due to the lack of possibility for real-time temporal measurement in the current experimental setting. The details of myofilament Ca^{2+} desensitization and myofilament buffering of Ca^{2+} with metabolic substrates need further investigation.

Part III:

Effects of metabolic substrates on LV myocyte contraction in Ang II-induced hypertensive rat heart.

In this part, I showed that metabolic substrates' supplementation in NT solution increased LV myocyte contraction and facilitated relaxation from hypertensive rats by increasing $[Ca^{2+}]_i$ transients and reduced myofilament Ca^{2+} sensitivity, despite that myofilament Ca^{2+} sensitivity was reduced prior to NF supplementation. Importantly, the myofilament Ca^{2+} sensitivity was decreased before NF application compared to that of sham, in line with the previous results from our laboratory (Jin CZ et al., 2013). However, NF further decreased myofilament Ca^{2+} sensitivity in HTN. It is possible that serum fatty acids concentrations were enhanced in hypertensive rat (Joel A et al., 1996). Therefore, I detected the serum fatty acid concentrations from sham and HTN using Metabolomics (collaboration with clinical Pharmacology department in Seoul National University). As shown, oleic acid, palmitic acid or linoleic acid concentrations were not changed in sham and HTN. These results suggest that the metabolic substrates are similar for myocytes from sham and hypertensive rats. In addition, supplementation of metabolic substrates potentiates myocyte inotropy and lusitropy by regulating key elements of Ca^{2+} handling processes and myofilament Ca^{2+} sensitivity, albeit different mechanism may apply in HTN. That is because in HTN, diastolic and systolic $[Ca^{2+}]_i$ were greater in HTN than in sham, and facilitated Ca^{2+} reuptake into the SR via SERCA. In addition, NF further increased diastolic and systolic $[Ca^{2+}]_i$. The peak I_{Ca} density was reduced by NF, but the integral of I_{Ca} (total Ca^{2+} influx) was not changed. Accordingly, APD was not changed in NF. These results suggest that $[Ca^{2+}]_i$ elevation with NF may be only due to further decreased myofilament Ca^{2+} sensitivity. As described in Part II, I did experiments using BDM.

The results showed that myofilament Ca^{2+} desensitization with BDM prevented NF-induced increase in the amplitude of $[Ca^{2+}]_i$ in LV myocytes from HTN rat hearts.

Taken together, the preliminary results clearly indicate that metabolic substrates increased myocytes contraction and facilitated the relaxation similar to sham, and further decreased the myofilament Ca^{2+} sensitivity. Intracellular Ca^{2+} homeostasis maybe remodeled in hypertensive LV myocytes. Detailed mechanisms mediating metabolic substrate regulation of myocardial contractile function in diseased hearts need further investigation.

Part IV:

Roles of eNOS and nNOS in metabolic substrate' regulation of cardiac excitation-contraction coupling in LV myocytes from sham and hypertensive rat hearts.

The present study showed that metabolic substrate supplementation in NT solution increased both basal and beta-adrenergic LV myocyte contraction in normal or hypertensive rats. Importantly, insulin signaling is impaired and beta-adrenergic stimulation increased the susceptibility of arrhythmias in the presence of metabolic substrates and this effect was significantly increased in hypertension. nNOS, by controlling basal Ca^{2+} homeostasis, moderate the susceptibility of beta-adrenergic arrhythmias in both normal and hypertension. The activity of Na^{+}-Ca^{2+} exchanger, which increases with ISO (Zhang YH et al., 2009), contributes to the beta-adrenergic arrhythmogenesis.

It has been known for more than half century that fatty acids (FA) are the preferred metabolic substrates for cardiac metabolism (Shipp JC et al., 1961). Accordingly, adding FAs (together with plasma carbohydrate derivatives) significantly improved basal and beta-adrenergic myocyte contraction. The question is whether FAs are indeed responsible for the increment and

whether inhibition of FA-dependent beta-oxidation can prevent greater contraction by NF? To answer these questions, I conducted experiments by supplementing FAs (linoleic acids, palmitic acids and oleic acids, 3FA as shown in Part II). 3FA mimicked the effects of NF and increased basal and ISO-stimulation of myocyte contraction and induced DAC. Interestingly, despite the presence of a FA derivative, carnitine (a substrate for beta-oxidation in mitochondria) which is important in cardiac metabolism and function (Fillmore N et al., 2013), carnitine palmitotransferase-1 (CPT-1) inhibition with ranolazine (10 μM) did not affect greater myocyte contraction in NF and in NF+ISO. Although it is not known whether metabolic substrates other than FA, *e.g*. glucose or pyruvate-dependent oxidation and metabolism may have taken over to maintain the myocyte contraction in the presence of ranolazine (because pyruvate alone also potentiate myocardial contractility (Torres CA et al., 2013), both FAs and other carbohydrate derivate are instrumental in improving cardiac contraction.

Supplementation of metabolic substrates may stimulate oxidative phosphorylation (mitochondrial metabolism) and increased superoxide production from mitochondria may activate protein kinases, such as protein kinase A (Burgoyne JR et al., 2009), which *in turn*, mediates NF enhancement of myocyte contraction. In contrast to this assumption, incubation of LV myocytes with an anti-oxidant, NAC (1 mM) did not affect NF-induced greater myocyte shortening. There was a tendency towards a reduction in the number of contractions and a reduction of myocyte contraction with ISO in NAC-pretreated myocytes. Although ranolazine or NAC did not affect myocyte contraction, the data suggest that LV myocyte contraction is compromised in both normal and hypertensive rats.

My data show that metabolic substrates impaired tyrosine phosphorylation of IRβ and IRS-1 and impaired insulin-dependent moderation of beta-adrenergic inotropy in cardiac myocytes. FAs, saturated FAs in particular, are implicated in insulin resistance in muscles (Kiens B et al.,

2006). Recently, unsaturated FAs, such as oleic acid, have been shown to enhance insulin receptor signaling (at Tyr1185) and facilitates insulin-induced glucose uptake into adipocytes (Tsuchiya A et al., 2014). In addition, linoleic acid restored palmitate-impaired insulin signaling and promoted glucose uptake in C2C12 skeletal muscle cells (Park SY et al., 2014) It is plausible that palmitic acid plays predominant roles in reducing tyrosine phosphorylation of IRβ and IRS-1, despite concomitant "rescuing efforts" by oleic acid and/or linoleic acid. The complex scenario may have been presented by Akt, whose phosphorylation at $Akt^{23/24}$ was increased by insulin in NF. Increased Akt phosphorylation maintains glucose transport and increases cardiac myocyte contraction under these conditions. Importantly, both IRβ and IRS-1 tyrosine phosphorylation were impaired in cardiac myocytes from hypertensive rats before the application of metabolic substrates. This is despite that upregulation of renin angiotensin system (RAS) or Ang II *in vitro* or *in vivo* does not affect FA β-oxidation before the onset of heart failure (Mori J et al., 2012; Pellieux C et al., 2006; Mori J et al., 2013). RAS, oxidative stress or inflammation are involved in the dysregulation of insulin signaling and resistance in hypertension, however, molecular insights in the myocardium are not clearly defined yet.

Impaired insulin signaling in NF was associated with reduced eNOS phosphorylation (at Ser^{1177}) and blunted anti-adrenergic inotropic effect of insulin. This is an interesting finding because it has been controversial whether endogenous eNOS affects contraction in isolated cardiac myocytes and the role of eNOS in basal and beta-adrenergic myocyte contraction *in vitro* (without FAs) has been doubted (Zhang YH et al., 2012). Insulin should be taken into account, at least if eNOS phosphorylation and activity were included in the mechanism of future study. Nevertheless, eNOS phosphorylation by insulin in immunoblotting experiments seem vary: either increase or no effect despite that insulin attenuated ISO-stimulation of myocyte contraction in most of cells studied. I suggest that insulin regulation of beta-adrenergic inotropy

may require intact signaling cascades in spatial compartments that may have been disrupted in immunoblotting conditions. Similarly, insulin signaling is impaired in cardiac myocytes from hypertensive rats even before the application of metabolic substrates. Although not tested, inflammation, reactive oxygen species or mammalian target of rapamycin/p70S6 kinase 1 (mTOR/S6K1) (Kim JA et al., 2012) may affect IRβ and IRS-1 tyrosine phosphorylation and pre-disposes impaired insulin signaling in the presence of FAs. In contrast to eNOS, nNOS does not seem to affect insulin-regulation of myocardial contraction in basal or with ISO. It is possible that nNOS, which is spatially different from eNOS, is not the downstream target of insulin in cardiac myocytes.

However, nNOS plays important roles in beta-adrenergic arrhythmogenesis in the presence of FAs. Intriguingly, this effect was intensified in hypertension, in line with clinical statistics that hypertension is an important precursor of arrhythmias and sudden cardiac death. Indeed, increased metabolic status (in particular, increased serum fatty acids in metabolic syndrome) is often associated with increased coronary artery diseases and sudden cardiac death due to ventricular arrhythmias. Systematic inflammation (e.g. increased plasma cytokines) may underlie the arrhythmogenesis *in vivo*. However, I have shown in the present study that diastolic Ca^{2+} levels are increased by metabolic substrates and Ca^{2+} release *via* ryanodine receptors (RyR) are higher (increasing stimulation frequency from 2Hz to 4 – 8Hz abolished DAC). Interestingly, nNOS inhibition with SMTC significantly increased the incidence of arrhythmias in sham but SMTC significantly reduced arrhythmias in hypertension. We have shown recently that nNOS decreases the amplitude of Ca^{2+} transient in sham LV myocytes but increases it in hypertension (Jin CZ et al., 2013). It is possible that different intracellular Ca^{2+} status may have contributed to the SR Ca^{2+} loading and spontaneous Ca^{2+} release. Beta-adrenergic stimulation further increased Ca^{2+} release, an important precursor of increased spontaneous Ca^{2+} release.

The abnormal rise of cytosolic Ca^{2+} by ISO leads to increased Ca^{2+} removal *via* increased phosphorylation and activity of Na^{+}/Ca^{2+} exchanger (NCX) (Zhang YH et al., 2009), which is fundamental in generating depolarizing current. This depolarizing current, if of sufficient size and occurring at the resting membrane potential, leads to a delayed afterdepolarization (DAD) that can trigger a new action potential and ectopic beat (Tweedie D et al., 2000).

In conclusion, my current study showed that metabolic substrates' supplementation increased basal and beta-adrenergic stimulated myocyte contraction, impaired insulin response and induced arrhythmias in normal and hypertension - an *in vitro* cardiac model of "metabolic syndrome". The effects of metabolic substrates are accompanied by changes in intracellular Ca^{2+} handlings. Detailed mechanisms underlying the phenomenon will facilitate our understandings of cardiac dysfunction that is associated with metabolic syndrome.

References

Ashley CC, Moisescu DG (1977) Effect of changing the composition of the bathing solutions upon the isometric tension-pCa relationship in bundles of crustacean myofibrils. J Physiol 270(3):627–652

Ashley, E.A., et al (2002) Cardiac nitric oxide synthase 1 regulates basal and beta-adrenergic contractility in murine ventricular myocytes. Circulation 105 (25):3011-6.

Altug S, Uzun O, Demiryurek AT, Cakici l, Abacioglu N, Kanzik l (1999) The role of nitric oxide in digoxin-induced arrhythmias in guinea-pigs. Pharmacol Toxicol 84(1):3-8.

Bers, D.M., et al., (2002) Cardiac excitation-contraction coupling. Nature 415 (6868), 198-205.

Eisner, D.A., et al., (2000) Integrative analysis of calcium cycling in cardiac muscle. Circ Res 87 (12), 1087-1094.

Berlin, J.R., et al., (1994) Intrinsic cytosolic calcium buffering properties of single rat cardiac myocytes. Biophys J 67 (4), 1775-1787.

Boden G, Salehi S (2013) Why does obesity increase the risk for cardiovascular disease? Curr Pharm Des 19(32):5678-83.

Briston, S.J., et al., (2014) Balanced changes in Ca buffering by SERCA and troponin contribute to Ca handling during β-adrenergic stimulation in cardiac myocytes. Cardiovasc Res 104 (2), 347-54.

Best PM, Donaldson SK, Kerrick WG (1977) Tension in mechanically disrupted mammalian cardiac cells: effects of magnesium adenosine triphosphate. J Physiol 265(1):1–17.

Burgoyne JR, Eaton P (2009) Transnitrosylating nitric oxide species directly activate type I protein kinase A, providing a novel adenylate cyclase-independent cross-talk to beta-adrenergic-like signaling. J Biol Chem 284(43):29260-8.

BoudinaS, Abel ED (2007) Diabetic cardiomyopathy revisited. Circulation 115(25):3213-23.

Boudina S, Bugger H, Sena S, O'Neill BT, Zaha VG, IIkun O, et al., (2009) Contribution of impaired myocardial insulin signaling to mitochondrial dysfunction and oxidative stress in the ehart. Circulation 119(9):1272-83.

Bers DM (2002) Cardiac excitation-contraction coupling. Nature 415:198-205.

Conti, V. et al., (2013) adrenoceptors and nitric oxide in the cardiovascular system. Front. Physiol.

Cingolani HE, Ennis IL, Aiello EA, Pérez NG (2011) Role of autocrine/paracrine mechanisms in response to myocardial strain. Pflugers Arch 462(1):29–38.

Cort SLM, Hasselbaink DM, Koonen DPY, Willems J, Coumans WA, Chabowski A, et al., (2004) Enhanced sarcolemmal FAT/CD36 content and triacylglycerol storage in cardiac myocytes from obese zucker rats. Diabetes 53(7):1655-63.

Cutler MJ, Jeyaraj D, Rosenbaum DS (2011) Cardiac electrical remodeling in healthy and disease. Trends Pharmacol Sci 32:174-180.

Dessy, C. et al., (2005) Endothelial beta 3-adrenoreceptors mediate nitric oxide-dependent vasorelaxation of generation b-blocker nebivolol. Circulation 23;112(8):1198-205.

Dong F, Zhang X, Ren J (2006) Leptin regulates cardiomyocyte contractile function through endothelin-1 receptor-NADPH oxidase pathway. Hypertension 47(2):222–229.

Danson Ej, Choate JK, Paterson DJ (2005) Cardiac nitric oxide: emerging role for nNOS in regulating physiological function. Pharmacol Ther 106:54-74.

Dirkx E, schwenk RW, Glatz JF, et al., (2011) High fat diet induced diabetic cardiomyopathy. Prostaglandins Leukot Essent fatty Acids 85(50:219-25.

Fabiato A, Fabiato F (1978) Effects of pH on the myofilaments and the sarcoplasmic reticulum of skinned cells from cardiac and skeletal muscles. J Phyisol 276:233–255.

Fillmore N, Lopaschuk GD (2013) Targeting mitochondrial oxidative metabolism as an approach to treat heart failure. Biochim Biophys Acta 1833(4):857-65.

Grynkiewicz, G. et al., (1985) A new generation of Ca^{2+} indicators with greatly improved fluorescence properties. J Biol Chem 260(6):3440-50.

Godt RE (1974) Calcium-activated tension of skinned muscle fibers of the frog. Dependence on magnesium adenosine triphosphate concentration. J Gen Physiol 63(6):722–739.

Gray S, Kim JK (2011) New insights into insulin resistance in the diabetic heart. Trends in endocrinology and metabolism: TEM 22(10):394-403.

Gary DL, John RU, Clifford DL. F, Jagdip SJ, William CS (2010) Myocardial fatty acid metabolism in healthy and disease. Physiol Rev 90:207-258.

Huke S, Knollmann BC (2010) Increased myofilament Ca2+ sensitivity and arrhythmias susceptibility. JMol Cell Cardiol 48(5):824–833.

Huke S, Knollmann BC (2010) Increased myofilament Ca2+ sensitivity and arrhythmias susceptibility. JMol Cell Cardiol 48(5):824–833.

Hemptinne A, Marrannes R, Vanheel B (1983) Influence of organic acids on intracellular pH. Am J Phys 245(3):C178–C183.

Jin CZ, Jang JH, Kim HJ, Wang Y, Hwang IC, Sadayappan S, Park BM, Kim SH, Jin ZH, Seo EY, Kim KH, Kim YJ, Kim SJ, Zhang YH (2013) Myofilament Ca^{2+} desensitization mediates positive lusitropic effect of neuronal nitric oxide synthase in left ventricular myocytes from murine hypertensive heart. J Mol Cell Cardiol 60:107-15.

Johnson AM, Olefsky JM (2013) The origins and drivers of insulin resistance. Cell 152(4):673-84.

Joel A. Simon, Josephine Fong, John T. Bernert (1996) Serum Fatty Acids and Blood Pressure. Hypertension 27:303-307.

Khairallah M, Labarthe F, Bouchard B, Danialou G, Petrof BJ, Des Rosiers C (2004) Profiling substrate fluxes in the isolated working mouse heart using 13C-labeled substrates: focusing on the origin and fate of pyruvate and citrate carbons. Am J Physiol Heart Circ Physiol 286(4):H1461-70.

Kiens B (2006) Skeletal muscle lipid metabolism in exercise and insulin resistance. Physiol Rev 86(1):205-43.

Kim JA, Jang HJ, Martinez-Lemus LA, Sowers JR (2012) Activation of mTOR/p70S6 kinase by ANG II inhibits insulin-stimulated endothelial nitric oxide synthase and vasodilation. Am J Physiol Endocrinol Metab 302(2):E201-8.

Kubota I, Han X, Opel DJ, Zhao YY, Baliga R, Huang P, Fishman MC, Shannon RP, Michel T, Kelly RA (2000) Increased susceptibility to development of triggered activity in myocytes from mice with targeted disruption of endothelial nitric oxide synthase. J Mol Cell Cardiol.

32(7):1239-48.

Khan Sa, Skaf MW, Harrison RW et al (2003) Nitric oxide regulation of myocardial contractility and calcium cycling: independent impact of neuronal and endothelial nitric oxide synthases. Cric Res 92:1322-1329.

Kuzkaya N, Weissmann N, Harrison DG, Dikalov S (2003) Interactions of peroxynitrite, tetrahydrobiopterin, ascorbic acid, and thiols: implications for uncoupling endothelial nitric oxide synthase. J Biol Chem 278:22546–54.

Lopaschuk GD, Ussher JR, Folmes CD, Jaswal JS, Stanley WC (2010) Myocardial fatty acid metabolism in health and disease.Physiol Res 90(1):207–258.

Lopaschuk GD, Ussher JR, Folmes CD, Jaswal JS, Stanley WC (2010) Myocardial fatty acid metabolism in health and disease. Physiol Res 90(1):207–258.

Liou YM, Kuo SC, Hsieh SR (2008) Differential effects of a green tea-derived polyphenol (−)-epigallocatechin-3-gallate on the acidosis-induced decrease in the Ca^{2+} sensitivity of cardiac and skeletal muscle. Pflugers Arch 456(5):787–800.

Laskowski KR, Russell RR, 3rd. (2008) Uncoupling proteins in heart failure. Current heart failure reports 5(2):75-9.

Montagnani M, Ravichandran LV, Chen H, Esposito DL, Quon MJ (2002) Insulin receptor substrate-1 and phosphoinositide-dependent kinase-1 are required for insulin-stimulated production of nitric oxide in endothelial cells. Mol Endocrinol 16(8):1931-42.

Maya Khairallah, François Labarthe, Bertrand Bouchard, Gawiyou Danialou, Basil J. Petrof, Christine Des Rosiers (2004) Profiling substrate fluxes in the isolated working mouse heart

using 13C-labeled substrates: focusing on the origin and fate of pyruvate and citrate carbons. American Journal of Physiology - Heart and Circulatory Physiology Vol. 286 no. 4, H1461-H1470 DOI: 10.1152/ajpheart.00942.

Mori J, Basu R, McLean BA, Das SK, Zhang L, Patel VB, Wagg CS, Kassiri Z, Lopaschuk GD, Oudit GY (2012) Agonist-induced hypertrophy and diastolic dysfunction are associated with selective reduction in glucose oxidation: a metabolic contribution to heart failure with normal ejection fraction. Circ Heart Fail 5:493–503.

Mori J, Zhang L, Oudit GY, Lopaschuk GD (2013) Impact of the renin-angiotensin system on cardiac energy metabolism in heart failure. J Mol Cell Cardiol 63:98-106.

Missiaen, L., et al., (2000) Abnormal intracellular Ca^{2+} homeostasis and disease. Cell Calcium 28 (1):1-21.

Massion PB, Ballgand JL (2007) Relevance of nitric oxide for myocardial remodeling. Curr Heart Fail Rep 4:18-25.

Marx SO, Reiken S, Hisamatsu Y, Jayaraman T, Burkhoff D, Rosemblit N, Marks AR (2000) PKA phosphorylation dissociates FKBP12.6 from the calcium release channel (ryanodine receptor): defective regulation in failing hearts. Cell 101:365-376.

Opie LH (1970) Effect of fatty acids on contractility and rhythm of the heart. Nature 227(5262):1055-6.

Opie LH, Sack MN (2002) Metabolic plasticity and the promotion of cardiac production in ischemia and ischemic preconditioning. J Mol Cell Cardiol 34:1077-89.

Palmiter, K.A., et al., (1997) Molecular mechanisms regulating the myofilament response to

Ca^{2+} implications of mutations causal for familial hypertrophic cardiomyopathy. Basic Res Cardiol 92 (S1), 63-74.

Patel, B.G., Wilder, T., John Solaro, R.J., et al., (2013) Novel control of cardiac myofilament response to calcium by S-glutathionylation at specific sites of myosin binding protein C. Front Physiol 4:336.

Pulakat L, Demarco VG, Whaley-Connell A, Sowers JR (2011) The Impact of Overnutrition on Insulin Metabolic Signaling in the Heart and the Kidney. Cardiorenal Med 1(2):102-112.

Preston, L.C., et al., (2007) Functional effects of the DCM mutant Gly159Asp troponin C in skinned muscle fibres. Pflugers Arch 453 (6):771-776.

Poole RC, Halestrap AP (1993) Transport of lactate and other monocarboxylates across mammalian plasma membranes. Am J Phys 264:C761–C782.

Park SY, Kim MH, Ahn JH, Lee SJ, Lee JH, Eum WS, Choi SY, Kwon HY (2014) The Stimulatory Effect of Essential Fatty Acids on Glucose Uptake Involves Both Akt and AMPK Activation in C2C12 Skeletal Muscle Cells. Korean J Physiol Pharmacol 18(3):255-61.

Pellieux C, Aasum E, Larsen TS, Montessuit C, Papageorgiou I, Pedrazzini T, Lerch R (2006) Overexpression of angiotensinogen in the myocardium induces downregulation of the fatty acid oxidation pathway. J Mol Cell Cardiol 41:459–66.

Pogwizd SM and Bers DM (2004) Cellular basis of triggered arrhythmias in heart failure. Trends Cardovasc Med 14:61-66.

Pogwizd SM, Schlotthauer K, Li L, Yuan W, Bers DM (2001) Arrhythmogenesis and contractile dysfunction in heart failure: Roles of sodium-calcium exchange, inward rectifier

potassium current, and residual beta-adrenergic responsiveness. Circ Res 1159-1167.

Robertson, S.P., et al., (1981) The time-course of Ca^{2+} exchange with calmodulin, troponin, parvalbumin, and myosin in response to transient increases in Ca^{2+}. Biophys J 34 (3):559-569.

Robinson P, Griffiths PJ, Watkins H, Redwood CS (2007) Dilated and hypertrophic cardiomyopathy mutation in troponin and alpha- tropomyosin have opposing effects on the calcium affinity of cardiac thin filaments. Circ Res 101(12):1266–127.

Rowe MJ, Neilson JMM, Oliver MF (1975) Control of ventricular arrhythmias during myocardial infarction by anti-lipolytic treatment using a nicotinic acid analogue. Lancet i:295–302.

Randle PJ, Garland PB, Hales CN, Newsholme EA (1963) The glucose fatty-acid cycle. Its role in insulin sensitivity and the metabolic disturbances of diabetes mellitus. Lancet. 1:785-9.

Sowers JR (1997) Insulin and insulin-like growth factor in normal and pathological cardiovascular physiology. Hypertension 29(3):691-9.

Roe, M.W., Lemasters, J.J., Herman. B., et al., (1990) Assessment of Fura-2 for measurements of cytosolic free calcium. Cell Calcium 11 (2-3):63-73.

Shipp JC, Opie LH, Challoner D (1961) Fatty acid and glucose metabolism in the perfused heart. Nature 189:1018–1019.

Schober, T., et al., (2012) Myofilament Ca^{2+} sensitization increases cytosolic Ca^{2+} binding affinity, alters intracellular Ca^{2+} homeostasis, and causes pause-dependent Ca^{2+}-triggered arrhythmia. Circ Res 112(2), 170-9.

Soloff LA (1970) Arrhythmia following fatty acid infusions. Am Heart J 80:671–4.

Sears CE, Bryant SM, Ashley EA, Lygate CA, Rakovic S, Wallis HL, et al., (2003) Cardiac neuronal nitric oxide synthase isoform regulates myocardial contraction and calcium handling. Circ Res 92:e52-9.

Spurgeon, H.A., et al., (1992) Cytosolic calcium and myofilaments in single rat cardiac myocytes achieve a dynamic equilibrium during twitch relaxation. J Physiol. 447, 83-102.

Sears CE, Bryant SM, Ashley EA et al (2003) Cardiac neuronal nitric oxide synthase isoform regulates myocardial contraction and calcium handling. Circ Res 92:e52-e59.

Steinbusch LK, Luiken JJ, Vlasblom R, et al., (2011) Absence of fatty acid transporter CD36 protects against Western-type diet-related cardiac dysfunction following pressure overload in mice. Am J Physiol Endocrinol Metab 301(40:E618-27.

Shannon TR, Ginsburg KS, Bers DM (2000) Reverse mode of the sarcoplasmic reticulum calcium pumo and load-dependent cytosolic calcium decline in voltage-clamped cardiac ventricular myocytes. Biophys J 78:322-333.

Trafford, A.W., et al., (1999) A novel, rapid and reversible method to measure Ca buffering and time-course of total sarcoplasmic reticulum Ca content in cardiac ventricular myocytes. Pflugers Arch 437 (3), 501-503.

Turner N, Cooney GJ, Kraegen EW, Bruce CR (2014) Fatty acid metabolism, energy expenditure and insulin resistance in muscle. J Endocrinal 220(2):T61-79.

Takahashi R, Shimazaki Y, Endoh M (2001) Decrease in Ca2+-sensitizing effect of UD-CG 212 Cl, a metabolite of pimobendan, under acidotic condition in canine ventricular myocardium. J Pharmacol Exp Ther 298(3):1060–1066.

Torres CA, Varian KD, Canan CH, Davis JP, Janssen PM (2013) The positive inotropic effect of pyruvate involves an increase in myofilament calcium sensitivity. PLoS One 8(5):e63608.

Tweedie D, Harding SE, MacLeod KT (2000) Sarcoplasmic reticulum Ca content, sarcolemmal Ca2+ influx and the genesis of arrhythmias in isolated guinea-pig cardiomyocytes. J Mol Cell Cardiol 32(2):261-72.

Tsuchiya A, Nagaya H, Kanno T, Nishizaki T (2014) Oleic Acid Stimulates Glucose Uptake Into Adipocytes by Enhancing Insulin Receptor Signaling. J Pharmacol Sci [Epub ahead of print].

Takimoto E, Champion HC, Li M, Ren S, Rodriguez ER, Tavazzi B, Lazzarino G, Paolocci N, Gabrielson KL, Wang Y, Kass DA (2005) Oxidant stress from nitric oxide synthase-3 uncoupling stimulates cardiac pathologic remodelling from chronic pressure load. J Clin Invest 115:1221–31.

Thomas D, Kiehn J, Katus HA, Karle CA (2004) Adrenergic regulation of the rapid component of the cardiac delayed rectifier potassium current, I(Kr), and the underlying hERG ion channel. Basic Res Cardiol 99:279-287.

Ussher JR, Koves TR, Jaswal JS, Zhang L, IIkayeva O, Dyck JR, et al., (2009) Insulin-stimulated cardiac glucose oxidation is increased in high-fat diet-induced obese mice lacking malonyl CoA decarboxylase. Diabetes 58(8):1766-75.

Vigouroux C, Caron-Debarle M, Le Dour C, Magré J, Capeau J (2011) Molecular mechanisms of human lipodystrophies: from adipocyte lipid droplet to oxidative stress and lipotoxicity. Int J Biochem Cell Biol 43(6):862-76.

Varro, A., Negretti, N., Hester, S.B. et al., (1993) Pflugers Arch 423:158.

doi:10.1007/BF00374975.

Valdivia HH, Kaplan JH, Elis-Davies GC, Lederer WJ (1995) Rapid adaptation of cardiac ryanodine receptors: modulation by My^{2+} and phosphorylation. Science 267:1997-2000.

Willott, R.H., et al., (2010) Mutations in Troponin that cause HCM, DCM AND RCM: what can we learn about thin filament function? J Mol Cell Cardiol 48 (5):882-892.

Wang Y, Youm JB, Jin CZ, Shin DH, Zhao ZH, Seo EY, Jang JH, Kim SJ, Jin ZH, Zhang YH (2015) Modulation of L-type Ca^{2+} channel activity by neuronal nitric oxide synthase and myofilament Ca^{2+} sensitivity in cardiac myocytes from hypertensive rat. Cell Calcium 58(3):264–274.

Whaley-Connell A, Pulakat L, Demarco VG, Hayden MR, Habibi J, Henriksen EJ, Sowers JR (2011) Overnutrition and the Cardiorenal Syndrome: Use of a Rodent Model to Examine Mechanisms. Cardiorenal Med 1(1):23-30.

Xu KY, Huso DL, Dawson TM et al (1999) Nitric oxide synthase in cardiac sarcoplasmic reticulum. Proc Natl Acad Sci USA 96:657-662.

Xia Y, Dawson VL, Dawson TM, Snyder SH, Zweier JL (1996) Nitric oxide synthase generates superoxide and nitric oxide in argininedepleted cells leading to peroxynitrite-mediated cellular injury. Proc Natl Acad Sci U S A 93:6770–4.

Yu Q, Gao F, Ma XL (2011) Insulin says NO to cardiovascular disease. Cardiovasc Res 15;89(3):516-24.

Yi, L., et al., (2007) "Simultaneously quantitative measurement of comprehensive profiles of esterified and non-esterified fatty acid in plasma of type 2 diabetic patients." Chem Phys Lipids

150(2): 204-216.

Yu QJ, Si R, Zhou N, Zhang HF, Guo WY, Wang HC, Gao F (2008) Insulin inhibits beta-adrenergic action in ischemic/reperfused heart: a novel mechanism of insulin in cardioprotection. Apoptosis 13:305-17.

Yasuda, S.I., et al., (2001) A novel method to study contraction characteristics of a single cardiac myocyte using carbon fibers. Am J Physiol Heart Circ Physiol 281 (3):H1442-6.

Zhang YH, Dingle L, Hall R, Casadei B (2009) The role of nitric oxide and reactive oxygen species in the positive inotropic response to mechanical stretch in the mammalian myocardium. Biochim Biophys Acta 1797(7):811–817.

Zhang L, Ussher JR, Oka T, Cadete VJ, Wagg C, Lopaschuk GD (2011) Cardiac diacylglycerol accumulation in high fat-fed mice is associated with impaired insulin-stimulated glucose oxidation. Cardiovascular research 89(1):148-56.

Zhang, Y.H., et al., (2008) Reduced phospholamban phosphorylation is associated with impaired relaxation in left ventricular myocytes from neuronal NO synthase-deficient mice. Circ Res 102 (2):242-9.

Zhang YH, Dingle L, Hall R, Casadei B (2009) The role of nitric oxide and reactive oxygen species in the positive inotropic response to mechanical stretch in the mammalian myocardium. Biochim Biophys Acta 1797(7):811–817.

Zhang YH, Hancox JC (2009) Regulation of cardiac Na^{+}-Ca^{2+} exchanger activity by protein kinase phosphorylation--still a paradox? Cell Calcium 45(1):1-10.

Zhang YH, Casadei B (2012) Sub-cellular targeting of constitutive NOS in health and disease.

J Mol Cell Cardiol 52(2):341-50.

국문초록

심근 세포의 대사는 정상적인 수축 기능에 중요하다. 최근까지 대부분 심장 생리 실험에서 포도당은 근세포 ATP 합성의 유일한 대사물질로 사용되었다. 그러나 정상 체내에서 심장이 사용하는 주요 대사 물질은 지방산이다. 이러한 지방산 선호는 심부전과 같은 질병 상황에서 포도당 위주의 대사 경향으로 바뀐다고 알려져 있다. 이런 배경 하에, 심근세포 관류에 사용하는 실험 용액에 포도당과 여러 가지 지방산을 포함한 영양충만 (nutrient full, NF) 용액을 사용하면서, 대사기질의 영향을 정상과 안지오텐신(AngII)-유발 고혈압 모델 쥐의 좌심실근세포 수축, 세포 내 칼슘의 변화 및 근섬유의 칼슘민감도를 분석하였다. NF 용액은 정상 심근세포 수축을 증가시키면서 이완 과정도 촉진하였다. 세 가지 지방산 (리놀산. 올레산, 팔미트산)만을 추가한 용액에서도 비슷한 반응을 확인하였다. 그러나 세포 내 베타-산화 과정에 중요한 carnitine-palmitotransferase-1(CPT-1)의 억제제인 ranolazine 은 NF 용액의 심근 수축력 강화에 영향이 없었다. 이는 포도당과 지방산 의존성 대사가 심장 수축에 대하여 상호 보완적임을 시사한다. NF 용액은 이완기 및 수축기에 관련된 세포 내 칼슘농도 ($[Ca^{2+}]_i$) 변화폭을 증가시켰으며, 최대 칼슘농도에서 유지되는 기간을 늘리면서 일단 농도 감소가 시작되면 그 속도는 더 빠르게 하였다. 근장그물 (SR) 의 칼슘 함량은 NF 에 의해 증가되었다. 또한 NF 는 근섬유의 칼슘-민감도를 낮추는 효과가 있었고, 이는 $[Ca^{2+}]_i$ 의 변화폭 증가와 관련될 것으로 해석되었다. 또한 Whole-cell 패치 클램프 실험을 통하여, NF 용액이 L-type Ca^{2+} 채널을 통한 칼슘 유입을 증가시키고 활동 전위 지속 시간 (APD)을 늘리는 것을 보았다. NF 용액은 세포

내 pH (pH_i)을 낮추는 효과도 있었지만, 이는 HCO_3^-/CO_2 으로 완충한 조건에서는 두드러지지 않았다. 중탄산염 완충 조건은 세포 내 칼슘에 대한 조절을 통해 필라멘트의 칼슘 민감도를 다소 높였다. 정리하면, NF 용액은 칼슘채널 및 SR 을 통한 $[Ca^{2+}]_i$ 증가와 함께, pH_i 감소 유도를 통한 근섬유 칼슘 민감도의 저하로 $[Ca^{2+}]_i$ 증가를 더욱 일으키는 것으로 해석되었다.고혈압 모델 백서의 좌심실근 세포에서는 NF 는 칼슘채널 활성에 대한 변화는 없었지만, 근섬유 칼슘 민감도 감소에 따른 $[Ca^{2+}]_i$ 증가가 수축-이완의 진폭은 더 높이는 것이 관찰되었다.

이소프레날린을 이용한 베타수용체 자극은 두 실험군 모두에서 NF 에 의한 심근세포 수축 증가를 더 강화시켰다. 또한, NF 용액에 이소프레날린을 추가하면 지연성수축 (DAD)과 자발적인 Ca^{2+} transient (sCa)를 유도하였으면, 그 빈도는 고혈압군에서 3 배 이상 높았다. 인슐린 수용체 (IR), IR substrate-1 타로신 인산화 및 내피형-NOS (eNOS) 인산화(eNOS-Ser^{1177})가 정상 및 고혈압 모델 심장에서 모두 NF 용액 조건에서 둔화되였으며, 고혈압 군에서는 NF 용액 투여 전에 이미 둔화되었다. 인슐린은 NF 및 NF+ISO 에 대한 수축력의 강화에는 아무런 영향을 미치지 않았다. 또한, NOS 억제제인 L-NAME 을 전처치 하여도 두 그룹 모두에서 NF 에 의한 심근세포 수축에 영향을 주지 못했다. 이러한 결과에서 대사 기질이 보충된 조건에서 좌심실근세포의 인슐린 수용체 및 eNOS-의존성 신호 전달이 오히려 저하되었음을 시사한다.

흥미롭게도, L-NAME 투여는 정상 심근세포에서 DAD 와 sCa 발생을 증가시켰지만 고혈압 군에서는 모두 현저히 감소시켰다. 이러한 효과는 신경형-NOS (nNOS) 억제제인 SMTC 또한 나타내어서 nNOS 의 중요성을 시사한다. nNOS 는 myofilament Ca^{2+} 민감도와 $[Ca^{2+}]_i$ 을 모두 조절하여 심근세포의 표현형에

영향을 준다. Beta-1 차단제 nebivolol 과 cordycepin, nitric oxide-potentiating chemicals 는 정상과 고혈압 모델 백서 두 그룹에서 모두 NF 와 이소프레날린 에 의한 이완기와 수축기의 $[Ca^{2+}]_i$ 를 현저히 감소시켰고 sCa 의 발현을 유의하게 감소시켰다. 또한 Na^+-Ca^{2+} exchanger 억제제인 KB-R7943 은 두 그룹에서 나타나는 자발적인 수축을 현저히 감소시켰다.

본 연구를 통하여 심근에 유리한 대사기질(metabolic substrate)은 세포내 칼슘의 변화에 영향을 주고 근섬유의 칼슘의 민감성을 감소 시킨다는 것을 알수 있다. 또한 손상된 인슐린/NO signaling 은 베타-아드레날린성 자극에 의한 심부전의 생성에 관여하며, 그 작용은 고혈압 모델에서 더욱 강하다는 것을 알수 있다.

본 내용 (I 부분, II 부분)은 *J Vis Exp* 와 *Pflugers Arch* 에 출판 완료된 내용임 (Zhao ZH et al., 2016; Zhao ZH et al., 2016).

주요어: 대사기질, 인슐린, 신경형 산화질소 합성효소, 내피형 산화질소 합성효소, 수축 이완, myofilament Ca^{2+} 감수성, 고혈압, 부정맥.

학번: 2014-30872

.